THE UNIVERSITY
of EDINBURGH

Higher-Order Tensor Decompositions for Muscle Synergy Analysis

Ahmed Mohamed Ebied

Doctor of Philosophy

The University of Edinburgh

November 2018

THE UNIVERSITY *of* EDINBURGH
School of Engineering

Dedication

For my grandmother who believed in me, ***Karima****.*

Ahmed Mohamed Ebied

November 2018

Abstract

This doctoral thesis outlines several methodological advances in the application of higher-order tensor decomposition for muscle synergy analysis estimated from surface Electromyogram (EMG). This entails both assessing current muscle synergy extraction methods and a novel direct approach to estimate useful muscle synergies using higher-order tensor decomposition. The underlying hypothesis is that higher-order tensor decompositions provide advantages in the estimation of temporal profiles and muscle synergies thanks to the consideration of other domains such as spectral, task or repetition information. Moreover, we implement these advances to inspect potential applications of tensor synergies in biomechanical analysis and myoelectric control.

Firstly, we provide an overview of the current mathematical models for the concept of muscle synergies and compare the common matrix factorisation methods for muscle synergy extraction, in addition to second-order blind identification (SOBI), a technique which has not been used for muscle synergy estimation previously. Synthetic and real EMG datasets related to wrist movements from the publicly available Ninapro dataset were used in this evaluation. Results suggest that a sparse synergy model and a higher number of channels would result in better-estimated synergies. SOBI has better performance when a limited number of electrodes is available, but its performance is still poor in that case. Overall, non-negative matrix factorisation (NMF) is the most appropriate method for synergy extraction and, therefore, it is considered as a benchmark in the rest of the thesis.

We then show the benefits of higher-order tensor decompositions of EMG data for muscle synergy analysis, discussing possible 3rd and 4th-order tensors models for EMG data. We explore muscle synergy estimation from 4th-order EMG tensors by taking the spectral profile into account and utilise this model for classification between the wrist's movements in comparison with NMF. The results provide a proof-of-concept for higher-order tensor decomposition as classification accuracy is slightly improved using tensor decomposition over NMF. However, the addition of spectral mode -with time-frequency analysis- increases the

computational cost for tensor synergy estimation.

After the previous proof of concept, we focus on the 3rd -order tensor model for efficient and reliable extraction of meaningful muscle synergies. The most prominent tensor decomposition models (Tucker and PARAFAC) are compared under different constraints. We notice that unconstrained Tucker decomposition cannot extract unique and consistent muscle synergies as it converges into different local minima, while PARAFAC model cannot deal with a higher number of synergies or tasks as the decomposition deviates from the trilinear model. As a result, we introduce a constrained Tucker decomposition model as a framework for muscle synergy analysis. The advantages of this method over NMF are highlighted in the biomechanical application of identifying shared and task-specific muscle synergies. This benefits from the natural multi-way form of the EMG data, which makes higher-order tensor decompositions a better option than applying matrix factorisation repetitively. The constrained Tucker decomposition can successfully identify shared and task-specific synergies and is robust to disarrangement regarding task-repetition information, unlike NMF.

The constrained Tucker model is then used as a framework to extract synergistic information that could be applied to proportional upper limb myoelectric control. The consistency of extracted muscle synergies with the increase of the wrist's task dimensionality into 3 degrees of freedom (DoF) is investigated in comparison with NMF. In the literature, NMF approaches for synergy-based proportional myoelectric control were viable only with a task dimension of 2 DoF. In contrast, the results show that a constrained Tucker model identifies consistent muscle synergies from 3-DoFs dataset directly. Moreover, a tensor-based approach for proportional myoelectric control is introduced and compared against NMF and sparse NMF as state of the art benchmarks.

To sum up, higher-order tensor decomposition had not been utilised in EMG analysis despite the substantial attention it received in biomedical signal processing applications in recent years. This thesis explores higher-order tensor decompositions for synergy extraction to account for the natural multi-way structure of EMG data. We hope that it will pave the way for the development of muscle activity analysis methods based on higher-order techniques in broader applications.

Lay summary

The question of how the brain controls the body movements and posture has been discussed for over a century. One of the most prominent ideas to explain this question is the concept of "muscle synergy". This hypothesis says that the brain controls groups of muscles together to do a movement rather than controlling individual muscles separately. Muscle synergies have been used in several applications such as biomechanical analysis and myoelectric control. Synergies are estimated from the measures of activity of multi-channel surface electromyography (EMG), where the electrical activity of muscles is picked up through several electrodes on the skin. The current approaches for muscle synergy estimation rely on 2^{nd}-order models, where the data are arranged as a table with time and channels as its dimensions. However, in the analysis of muscle activity, the data are naturally in higher-order form. This means that the data can be indexed by additional dimensions, such as repetitions and/or movements. Hence, we propose that higher-order models would be more suitable to find muscle synergies. This is because they provide advantages by incorporating additional information over that of the 2^{nd}-order models.

In this thesis, we will introduce higher-order models for muscle synergy analysis and we will discuss their advantages over the current models. In these models, the data are in tensor form which is an array with three or more dimensions. In addition, we will implement these advances to inspect potential applications of synergies extracted from higher-order tensor models in biomechanical analysis and myoelectric control. We will assess the most prominent methods for muscle synergy extraction based on the 2^{nd}-order models. To do so, we will compare them using synthetic and real EMG datasets. In addition, second-order blind identification (SOBI), a technique which has not been used for muscle synergy estimation before, will be included in the comparison. The aim is to identify the most appropriate 2^{nd}-order model method for synergy extraction to be considered as a benchmark in the rest of the thesis.

In addition, the construction of 3^{rd}- and 4^{th}-order tensors models for EMG data will be discussed. The muscle synergy estimation from 4^{th}-order EMG tensors will be explored. These tensors incorporate frequency information. Then, this model will be utilised for classification

between wrist movements in comparison with 2nd-order model. This experiment would provide a proof-of-concept for higher-order tensor decomposition for EMG data and determine its suitability for muscle synergy extraction.

The 3rd-order tensor model will be discussed in detail with the addition of different repetitions. This model will be used to compare the most prominent higher-order tensor decomposition models. The comparison will be held under different constraints to develop a suitable method for unique and meaningful estimation of muscle synergies. The developed method will be used in the biomechanical application of identifying shared and task-specific muscle synergies.

Finally, based on the previous results, we will implement an approach based on the higher-order tensor model for proportional upper limb myoelectric control. Synergies estimated from the developed higher-order model will be analysed to determine its suitability for this application in comparison with the current techniques.

We hope that this study will pave the way for the development of muscle activity analysis methods based on higher-order techniques in broader applications.

List of Symbols

- x - Scalar
- $\mathbf{x}$ - Vector
- $\mathbf{X}$ - Matrix (2$^{\text{nd}}$-order tensor)
- $\underline{\mathbf{X}}$ - Higher-order tensor
- $\mathbf{m}$ or $\mathbf{m}(t)$ - one channel EMG signal
- $\mathbf{s}$ - muscle synergy
- $\mathbf{w}$ or $\mathbf{w}(t)$ - weighting function vector
- $\mathbf{M}_{(m\times n)}$ - multi-channel EMG with m channels and n samples
- $\mathbf{S}_{(m\times r)}$ - synergy matrix
- $\mathbf{W}_{(r\times n)}$ - weighting function matrix
- r - number of synergies
- $g()$ - Heaviside function
- $\underline{\mathbf{\Lambda}}$ - super diagonal tensor that has 1s across its supra-diagonal and 0s elsewhere (also known as "identity tensor")
- $\times_n$ - multiplication across the n^{th}-mode of higher order tensor
- $\mathbf{X}^T$ - The transpose of matrix $\mathbf{X}$
- $\mathbf{X}^+$ - The Moore–Penrose inverse (also known as pseudo inverse) of Matrix $\mathbf{X}$
- $\|\mathbf{X}\|_F^2$ - The Frobenius norm also known as the Euclidian norm for $\mathbf{X}$
- $\otimes$ - Kronecker product

- $\odot$ - Khatri-Rao product
- $\mathbf{X}^{(n)}$ - Component matrix for the n^{th}-mode
- $\underline{\mathbf{G}}$ - The core tensor in Tucker decomposition

List of Acronyms

ALS Alternating Least Squares

ANOVA Analysis of Variance

BSS Blind Source Separation

CNS Central Nervous System

consTD constrained Tucker decomposition

CORCONDIA Core Consistency Diagnostic

DoF Degree of Freedom

EEG Electroencephalogram

EMG Electromyography

ICA Independent Component Analysis

***k*-NN** k-nearest neighbours

MDL Minimum Description Length

MU motor unit

MUAP motor unit action potential

MUAPT motor unit action potential train

MDL Minimum Description Length

MEG Magnetoencephalogram

NMF Non-negative Matrix Factorisation

PARAFAC Parallel Factor Analysis

PCA Principal Component Analysis

RMS Root-Mean-Square

SNMF Sparse Non-negative Matrix Factorisation

SNR Signal to Noise Ratio

SOBI Second-Order Blind Identification

Glossary

- **Component** - (also known as factor) is a rank-one model for higher-order tensor.
- **consTD** - Constrained Tucker Decomposition: an approach to extract muscle synergies from higher-order tensor by constraining the core tensor and components of the Tucker model.
- **Explained variance** - For a given dataset, it is a measurement of the proportion to which a mathematical model accounts for the variation, its complementary part is called unexplained or residual variation. It equals the squared correlation coefficient R^2.
- **Loss function** - The function defining the optimisation or goodness criterion of a model.
- **Mode** - A matrix has two modes: the row mode and the column mode, hence the mode is the basic entity building for a tensor. A three-way tensor thus has three modes.
- **Model** - An approximation of a set of data including structural model, additional constraints and a loss function.
- **Order** - The order of an tensor is the number of modes; hence a matrix is a second-order tensor, and a three-way tensor a third-order tensor.
- **Shared synergy** - Muscle synergy shared between two or more movements.
- **Task specific synergy** - Muscle synergy assigned to a specific task or movement.
- **Tensor** - An array of data.
- **Tensor synergies** - Muscle synergies extracted via higher-order tensor decomposition.
- **Tensorisation** - Mapping lower-order data to higher-order form.
- **Unfolding** - (also known as matricization) Rearranging of a higher-order tensor into a matrix.

Acknowledgements

This thesis would not have been possible without the guidance and supervision of Dr. Javier Escudero who gave ever generously of his time and care throughout my PhD studentship. I am grateful to Dr. Adam Stokes for his wisdom and guidance as my second supervisor. I would also like to thank all the editors and reviewers for their handling of manuscripts and their patience with my work and corrections. A special mention goes to my colleague Eli Kinney-Lang for our many discussions throughout the years and to Dr. Hamed Azami, Dr. Loukianos Spyrou, Dr. Keith Smith, and many other members of the Institute past and present who helped throughout my study in university of Edinburgh.

Finally, I am grateful to my wife Amy, for all her patience, advice, and unconditional support, and to my kids Mourad and Mila for their smiles that gave me the encouragement and the joy they brought to our lives. This was not possible without you all.

Declaration

I declare that this thesis has been composed solely by myself and that it has not been submitted, either in whole or in part, in any previous application for a degree. Except where otherwise acknowledged, the work presented is entirely my own.

Ahmed Ebied

November 2018

Contents

Chapter 1

Introduction

1.1 Motivation

The work described in this thesis is motivated by the need to understand more about motor control and how the Central Nervous System (CNS) controls body movements and posture effectively, given the complexity and redundancy of multiple muscles, joints and Degree of Freedoms (DoFs). Particularly, the muscle synergy concept [1, 2] was introduced to answer these questions and it has been used in various applications, such as biomechanical analysis and myoelectric control [3–5]. The first step towards this was to study muscle synergy models and explore the state-of-the-art methods for extracting them from surface Electromyography (EMG) datasets. In this exploration, it became clear that muscle synergy analysis relies on different matrix factorisation methods [6]. We identified that there is a potential to extract synergistic information using higher-order tensor decompositions as in many applications data are naturally structured in a multi-way form and repetitive application of matrix factorisation has been required for synergy extraction. In general, tensor decompositions may provide several advantages over classical matrix factorisation such as compactness, uniqueness of decomposition, and generality of the identified components [7]. Thus, this thesis is largely focused on muscle synergy analysis via higher-order tensor models and its potential applications.

Amongst a wide range of problems from which this topic can benefit, one of the more pressing ones is how to achieve non-invasive, intuitive and proportional myoelectric control. The non-invasive commercial prostheses systems either offer sequential or proportional control with limited number of DoFs in addition to the limitations due to sweating and electrodes

re-positioning [8].

Given the relevance of myoelectric control in the field of EMG analysis, we tried to establish and validate higher-order tensor decomposition for muscle synergy analysis. Then, we illustrated how it could be utilised in myoelectric control with a proof-of-concept inspired by shared synergies.

1.2 Objectives and hypotheses

I hypothesised that by introducing higher-order tensor models to muscle activity analysis, we can benefit from tensor decomposition in the area of muscle synergy extraction, especially in the applications where EMG dataset is already in the multi-way form naturally.

I aim to apply these tensor decomposition methods for synergy extraction and uncover new ways to materialise the power of muscle synergy in different applications. In order to achieve this, I define the following partial objectives.

- Study and compare the current methods for muscle synergy extraction.
- Introduce the use of tensor decomposition for muscle activity analysis.
- Develop novel methods for muscle synergy extraction via tensor decomposition.
- Demonstrate the relevance of tensor synergies in biomechanical analysis and myoelectric control applications.

1.3 Contributions

This thesis provides a novel approach for muscle synergy extraction from higher-order tensor models and its applications.

First, I compare the 2^{nd}-order models for muscle synergy extraction. Second-Order Blind Identification (SOBI) was included in the comparison, a method which has not been used for muscle synergy estimation previously. The comparison is held under various settings to determine the factors that affect the quality of estimated synergies [6]. The best matrix factorisation is used as a benchmark for the rest of the thesis.

I then demonstrate synergy extraction from a 4^{th}-order tensor model to provide a proof-of-concept [9]. This is used it to classify wrist movements in comparison with the matrix factorisation benchmark.

I go on to introduce constrained Tucker decomposition (consTD) approach to extract synergies from a 3^{rd}-order model. This was inspired by shared synergy concept and the results compared with most prominent tensor decomposition methods [10].

As for applications, consTD was used to identify shared and task-specific synergies of the wrists' three main DoFs [10] tasks. The consistency of tensor synergies with the increase of task dimensionality was tested to assess its potential application for proportional myoelectric control [11]. Finally, I illustrate the use of tensor synergies in proportional myoelectric control and compare it with the state-of-the-art synergy approaches [12].

1.4 Structure of the rest of the thesis

The remainder of the thesis is organised as follows:

Chapter 2: Review of the field. This Chapter discusses the literature for muscle synergies and motor control, taking a focus on synergy extraction methods from surface EMG. Various considerations which come up in the methodological pipeline are covered including higher-order tensor models and their most common decomposition methods.

Chapter 3: Second-order matrix models for muscle synergy extraction. This is a detailed comparison between the three most prominent matrix factorisation methods for muscle synergy extraction: Principal Component Analysis (PCA), Independent Component Analysis (ICA), Non-negative Matrix Factorisation (NMF); in addition to SOBI. Real and synthetic datasets are used in the comparison with different settings of sparsity, number of channels and Signal to Noise Ratio (SNR). It is shown that the sparse synergy model and a higher number of channels would result in better-estimated synergies. Moreover, NMF is shown to be the benchmark approach for synergy extraction.

Chapter 4: Higher-order tensor decompositions for muscle synergy extraction. Here, the need of higher-order EMG tensor decomposition is discussed in detail. In addition, the possible

ways for EMG tensor construction are outlined. I propose a 3^{rd}-order tensor model by adding a repetition mode of same and/or different tasks. A 4^{th}-order tensor model is also discussed, which incorporates the spectral mode. I explore synergy extraction from 4^{th}-order tensor and compare it with NMF in classifying wrist's 3 main DoFs.

Chapter 5: Constrained Tucker decomposition. I focus on 3^{rd}-order tensor models and compare Parallel Factor Analysis (PARAFAC) and Tucker decompositions for synergy extraction. The consTD is formulated as the most suitable approach for higher-order muscle synergy estimation. I then apply consTD for identification of shared and task-specific synergies for biomechanical analysis and compare it with the current NMF approach.

Chapter 6: Use of Tensor synergies for myoelectric control. The tensor synergies extracted via consTD are utilised for proportional myoelectric control in a proof of concept. The consistency of synergies is assessed with the increase in task dimensionality. Finally, a synergy-based scheme for proportional myoelectric control is proposed and compared with state-of-the-art approaches of NMF and Sparse Non-negative Matrix Factorisation (SNMF).

Chapter 7: Discussion and Future work. The main findings of the thesis are summarised followed by a discussion of limitations and, finally, the scope for future work is presented based on the novel developments herein.

Chapter 2

Review of the field

2.1 Introduction

"How does the Central Nervous System (CNS) control body movements and posture?" This question has been discussed for over a century with no conclusive answer. The coordination of muscles and joints that accompanies movement requires control over multiple Degree of Freedoms (DoFs). This results a high level of complexity and dimensionality [13]. Understanding our body movements would help us in designing more natural prosthesis for the amputees and improve the rehabilitation techniques. Moreover, the human motor control could inspire us in other fields, such as robotics.

Scientist studied and analysed the electrical activity accompanied to muscles contraction (Electromyography (EMG)) to answer this question. A possible explanation to this problem was the notion that CNS constructs a movement as a combination of small groups of muscles (synergies) that act in harmony with each other, thus reducing the dimensionality of the problem. This idea of modularity could be traced to the first decades of the twentieth century [14] and has been formulated and developed through the years [15–17] to reach the Muscle Synergy hypothesis [1, 2, 18].

In this Chapter, the necessary background information for selected key topics are presented to help in understanding the multi-disciplinary ideas of the thesis. In the following Section 2.2, the electrical muscle activity signal is reviewed including the origin and types of EMG in addition to its recording techniques. The concept of Muscle synergy is discussed in detail in Section 2.3. The evidence for muscle synergy hypothesis and the proposed models are

covered, in addition, the current synergy extraction methods based on matrix factorisation are discussed. In section 2.4, higher-order tensor models and their decomposition techniques are reviewed since they introduced as an alternative to the current matrix factorisation method for muscle synergy analysis. Finally, a brief review on myoelectric control systems is presented in Section 2.5 as a synergy-based myoelectric control system is one of the potential applications of tensor synergies.

2.2 Electromyography

EMG is the recording and study of the electrical activity associated with skeletal muscle contraction. The EMG signal represents the electric current generated by the flow of ions through the muscle fibres, which propagates across the interfacing tissues to reach the detection electrode [19].

2.2.1 EMG formation

Some physiological aspects need to be addressed to understand the processes underlying the generation EMG signals. The skeletal muscles consists of anatomical units called muscle fibres. Those fibres are innervated by the motor nerves called motor neurons which convey commands from the brain through the spinal cord [20].

The motor unit (MU) by definition [21] consists of single motor neuron, including its dendrites and axon, and hundreds of muscle fibres which is innervated by this particular motor neuron. The motor unit action potential (MUAP) is the fundamental element of the EMG signal. MUAP is created when action potential propagates down the motor neuron in order to activate all its muscle fibres; then the depolarisation propagates along the fibre generating an electromagnetic field in the vicinity of the muscle fibres [22]. Every MUAP is constructed from the superposition of single fibre action potentials which is innervated by a single motor neuron and fired nearly synchronously, as shown in Figure 2.1. The shape of MUAP is not fixed and depends on several factors such as, muscle fibre size and the position of electrode in relative to muscle fibres and innervation zone [23].

The MUs must be activated repeatedly in order to sustain muscle contraction. This would result

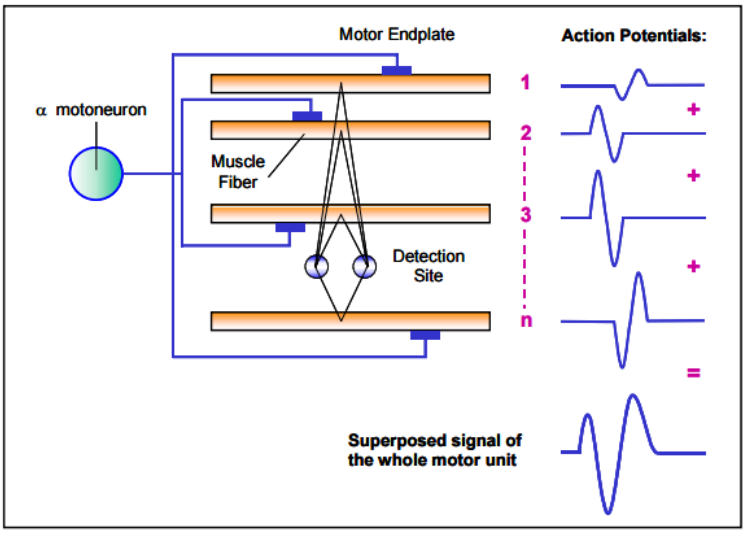

Figure 2.1: Illustration for the generation of motor unit action potential. Figure from [24].

in a sequence of MUAPs called a motor unit action potential train (MUAPT). The wave-form of MUAPs within its MUAPT would not change as long as the geometric relationship between the electrode and the active muscles is unchanged and there are no biochemical changes within the muscle that can affect the conduction velocity or the filtering properties of the muscle tissue. The EMG is considered as the summation of all MUAPTs within the pickup area of the electrode as shown in Figure 2.2.

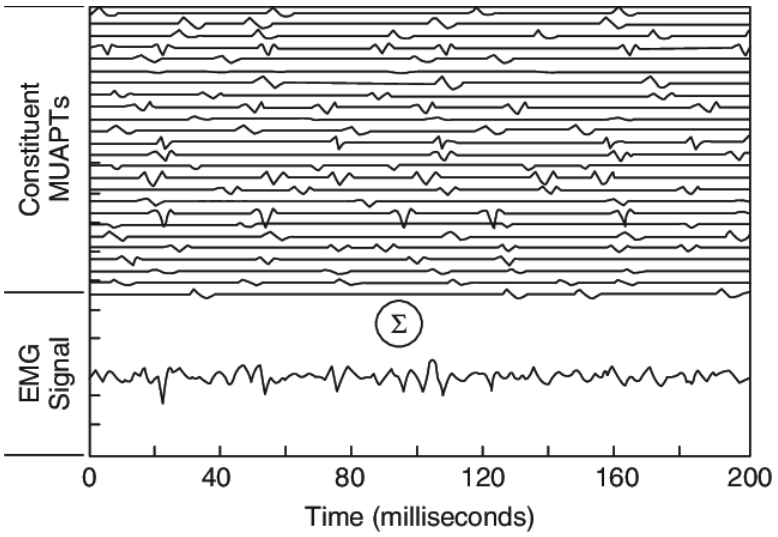

Figure 2.2: An example of EMG generation by summation of 25 MUAPT. Figure from [24].

2.2.2 Types of EMG

Generally, there are two kinds of EMG recordings: intramuscular and surface EMG. The intramuscular EMG is performed using an invasive electrode such as a mono-polar needle electrode. The needle electrode is inserted directly to the muscle under investigation which provide a signal with low level of noise and cross-talk in comparison with surface EMG. On the other hand, surface EMG pick up muscles electrical activity from the skin surface above the muscles using an array of surface electrodes [19, 25].

Surface EMG (also noted as sEMG) had some limitations. For instance, it can be used effectively only with superficial muscles. In addition, recording is affected by cross-talk signals from other adjacent muscles and filtering effect because of the depth of the subcutaneous tissue and skin. For instance, the skin and fatty tissues have an approximate low pass filter effect, while the electrodes will behave like a high pass filter [26]. However, it is preferred over intramuscular EMG in some applications since the latter is invasive and inconvenient. In the case of myoelectric and prostheses control, surface EMG is often used to detect muscle activity since it is far more convenient for the daily user and it contains the needed information regarding the time and magnitude of muscle activation. Therefore, we will be working on surface EMG only and it will be referred to as EMG for the rest of the thesis.

EMG is considered a non-stationary stochastic signal because of MUAPs overlapping and irregular MU discharge. Therefore, EMG signals have frequently been assumed Gaussian distribution with a zero-mean value [27]. Signal amplitude typically range from 0 to 10 mV (peak-to-peak) or 0 to 1.5 mV (Root-Mean-Square (RMS)) while its frequency range from 0 to 500 Hz. However, signal characteristics are extremely dependent on external factors such as, the level and duration of contraction, dynamic or static muscle states, fatigue, and sweat [28]. As a result, EMG signals are usually reported in the form of a linear envelope computed through RMS in most muscle activity studies including muscle synergy analysis [29]. Because of this stochastic nature of EMG signal, every muscular movement produce different EMG patterns since different muscles are activated with different contraction levels.

2.2.3 EMG setup

The EMG signal detected using surface electrodes are strongly influenced by distribution of electrodes, electrode size, and placement. Therefore, the electrode configuration is vital for recording informative and uncontaminated EMG signals. The issue of cross-talk must be considered during electrode placement. A second consideration is the sensitivity of the signal to the architecture of the muscle. It is suggested to place electrodes on the centre of muscle under investigation halfway between the centre of the innervation zone and the further tendon, while one electrode is placed on an electrically quiet location to act as a reference. It is usually placed on bone structures near the detection site [30]. Some additional preparation procedures could help in improving the quality of an EMG measurement such as using a conducting gel or cleansing the skin by alcohol and removing the hair before placing the electrodes [20].

There are two common methods for electrode placement on the upper-limb EMG. The first one is a dense sampling approach [31] where electrodes are placed equally spaced in an array around the limb to provide a spatial information through a multichannel EMG recording. The second method is the precise anatomical positioning strategy [32] as the electrodes are placed on the main activity muscles. Another EMG setup is the high-density EMG method where grids of several closely spaced electrodes are used extract 2D information from muscle activity [33]. This complex setup provides richer information about the recording area that is useful for several applications [34, 35]. However, high-density EMG require high instrumentation and computation demands and challenges that are different from the conventional EMG recording systems [36].

2.2.4 Publicly available datasets

Two datasets from the publicly available Ninapro (Non Invasive Adaptive Prosthetics) database [37, 38] were used in the thesis. The first dataset [39] consists of 27 able-bodied subjects instructed to perform 10 repetitions of 53 hand, wrist and finger movements. In the thesis we worked on a selection of wrist movements and its three DoFs. The dataset includes 10-channel surface EMG signals recorded by a MyoBock 13E200-50 system (Otto-Bock HealthCare GmbH) rectified by RMS and sampled at 100Hz. The hand kinematics were captured using a 22-sensor CyberGloveII (CyberGlove Systems LLC)). The glove returns 8-bit

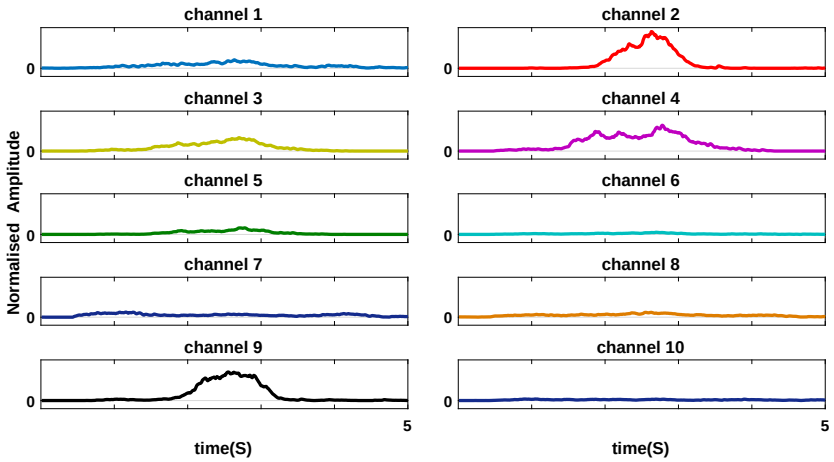

Figure 2.3: Example of 10-channel EMG envelopes recorded during wrist extension movement for 5 seconds of Subject 4/repetition 1 from Ninapro dataset-1 (the amplitude is normalised only in the figure to highlight the differences between channels).

values proportional to joint-angles using a resistive bend-sensing technology with an average resolution of less than one degree depending on the size of subject's hand.

The second dataset [40] consists of 40 able-bodied subjects instructed to perform 6 repetitions of 50 hand, wrist and finger movements. The same wrist tasks investigated in the first dataset were selected from the second one. However, myoelectric activity in this dataset is recorded with 12-channel setup by "Delsys Trigno Wireless System". This different setup allows recording of raw EMG signals sampled at 2 kHz with a baseline noise of less than 750 nV RMS. The EMG data is rectified by RMS in the pre-processing. Hand kinematics were captured using the same 22-sensor CyberGloveII system (CyberGlove Systems LLC)) used in the first dataset.

For both datasets, data synchronisation was performed offline using high-resolution time-stamps [37]. The "stimulus" time series in the Ninapro dataset labelled the start and end of each movement repeated by the subject. This series has been used for dataset segmentation of the training and testing datasets. Figure 2.3 shows an example for EMG segment from dataset-1. The electrodes where placed by combining the two methods: a dense sampling approach and a precise anatomical positioning strategy. For both datasets, two electrodes placed on the main muscle activity spots and the rest (8 for dataset-1 and 10 for dataset-2) were placed uniformly around the forearm. For more details see [37].

2.3 Background on muscle synergies

The muscle synergy concept posits that the CNS achieves any motor control task using a few synergies combined together, rather than controlling individual muscles. Hence, the multichannel EMG signal is considered as a linear mixture of muscle synergies with a weighting function or activation coefficients across time as illustrated in Figure 2.4.

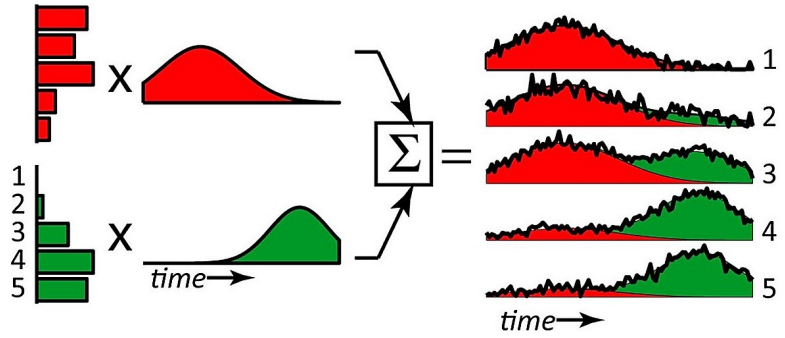

Figure 2.4: A schematic illustration of muscle synergies. Two muscle synergies (red and green) and their weighting function generate 5-channel EMG signal as linear combination. The two colours (red and green) in the EMG recording shows how each synergy contributes to the waveform (black line) of each channel. Figure from [41].

2.3.1 Evidence for muscle synergy

Although the muscle synergy hypothesis is criticised for being very hard to be falsified [42], a repertoire of studies have provided evidence and support for it. Those pieces of research could be categorised into two main categories: direct stimulation and behavioural studies.

The stimulation approaches were conducted by exciting the CNS at different locations to study the resulting activation pattern. Earlier studies focused on the organisation of motor responses evoked by micro-stimulation of the spinal cord of different vertebral species, such as frogs [15–17, 43, 44], rats [45] and cats [46]. They revealed that the responses induced by simultaneous stimulation of different loci in the spinal cord are linear combinations of those induced by separate stimulation of the individual locus. Those findings were supported by another direct stimulation studies where a relatively long period of electric stimulation applied to different sites in the motor cortex resulted in complex movements in rats [47], prosimians [48] and macaques [49,50]. The chemical micro-stimulation has been used through

N-methyl-D-aspartate iontophoresis injected into the spinal cord of frogs which evoked an electromyographic patterns that could be constructed as a linear combination of a smaller group of muscle synergies [18].

Similarly, the behavioural studies rely on recording the electrical activity of the muscles during a specific task (or tasks) or natural behaviour. Then, a number of synergies is extracted from the signals using computational techniques. The identified synergies should be able to describe the recorded signal for the related task or behaviour. Studies have been carried out on cats where four muscle synergies were sufficient to reproduce 95% of postural hind-limb muscles response data [51] and five synergies accounted for 80% of total variability in the data [52]. Similar research on monkeys during grasping activity showed that three muscle synergies accounted for 81% of variability [49]. In humans, muscle synergies were identified from a range of motor behaviours [53, 54] with the ability to describe most of the variability in EMG signals. In addition, other studies show that complex motor outputs such as upper limb reaching movements [55], cycling [56, 57] and human postural control [58] are a result of the combination of a few muscle synergies.

Additional support for the muscle synergy model comes from the common drive concept. This concept, introduced by De Luca *et al.* [59], shows that the pool of MUs of different muscles share common neural drives, as the unique firing patterns of individual MUs are effected, not by separate command signals sent to these units, but by one common drive to which MUs respond differently. This concept backs the muscle synergy hypothesis which suggests that the motor neurons of different muscles share the same common neural drive. This was supported by a study [60] that shows that the common drive exists among MUs from synergistic muscle pair.

However, there are opposing views to the hardwired neural origin of muscle synergy concept. Studies suggest that muscle synergies may also emerge from optimal strategies to achieve high-level task goals within a redundant control space [42, 61]. In the uncontrolled manifold hypothesis [62], a synergy is defined as the shaping of trial-to-trial movement variability along this manifold in any redundant task [63]. While in the optimal feedback control concept [64], it is defined as a minimum intervention strategy that controls only task-relevant DoFs if there is a cost associated with correcting variability. This interpretation of synergy and motor control

has been utilised in several applications including proportional myoelectric control [65, 66].

Despite the debate about the neural origin of muscle synergies [42, 67, 68], they have been proved to be useful for many applications such as clinical studies [69], rehabilitation [70], prosthesis control [4, 71] and biomechanical analysis [3, 72]. In addition, the proposed alternatives to explain the motor control (uncontrolled manifold [62] and an optimal feedback control [64]) have invoked structures that are very similar to muscle synergies [73, 74]. Therefore, the concept of modularity and a combination of muscle synergies could contribute to motor control as proposed by Bizzi *et al.* [68].

Throughout the years researchers determined several characteristics for muscle synergy. For example, it was found that synergies are subject-specific [75]. One of the important observations is shared and task-specific synergies. It implies that shared (common) synergies can be found in diverse motor tasks sharing some mechanical or physical characteristics. On the other hand task-specific (behavioural) synergies are distinctive for one motor task. Support for this idea comes from animal studies (frogs [53, 76] and cats [52]) as well as human studies where shared and task-specific synergies distinctive for one motor task or movement have been investigated across activities such as walking and cycling [77], postural balance positions [75, 78], and normal walking and slipping [3, 72].

2.3.2 Mathematical models for muscle synergies

In all studies, muscle synergies are estimated from the recorded electrical activity of the muscle using the EMG envelope [29]. Therefore, EMG recordings need to be modelled in order to compute the muscle synergies. Two muscle synergy models have been proposed in the literature: the time-invariant or synchronous model [1, 18] and the time-varying or asynchronous model [2, 79].

According to the time-invariant model, the electrical activity for a single muscle or channel or $\mathbf{m}(t)$ is a vector that could be expressed as a combination of synchronous synergies $\mathbf{s}$ (scalar values activated at the same time) multiplied by a set of time-varying coefficients or weighting

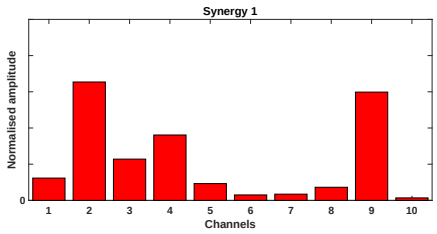

(a) Muscle synergy 1

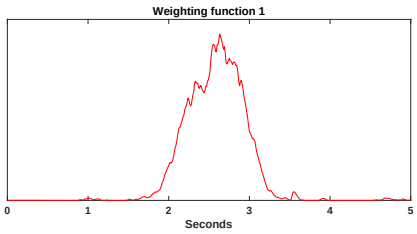

(b) Weighting function 1

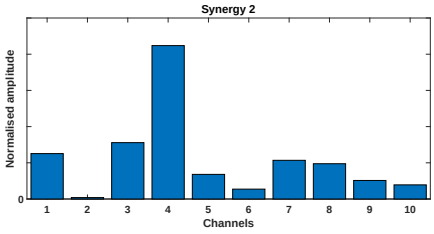

(c) Muscle synergy 2

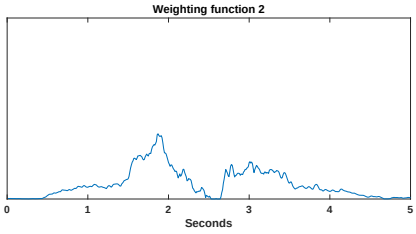

(d) Weighting function 2

Figure 2.5: An example of two component muscle synergy extracted from the EMG segment shown in Fig. 2.3. NMF was used to extract the muscle synergies. The effect of first muscle synergy (Panels 2.5a and 2.5b) can be noticed on channels (2,9) while the second synergy has a noticeable effect on channel 4.

functions $\mathbf{w}$ as shown in Equation 2.1

$$\mathbf{m}(t) = \sum_{i=1}^{i=r} s_i \mathbf{w}_i(t) \tag{2.1}$$

where r is the number of synchronous synergies. Since synergies contribute to each muscle activity pattern with the same weighting function $\mathbf{w}_i(t)$, the synergy model is synchronous without any time variation.

On the other hand, the time-varying synergies are asynchronous as they compromise a collection of scaled and shifted waveforms, each one of them specific for a muscle or channel. Thus, the muscle activity $\mathbf{m}(t)$ can be described according to the asynchronous model with a group of time-varying synergy vectors scaled and shifted in time by c and τ, respectively, as shown in Equation 2.2.

$$\mathbf{m}(t) = \sum_{i=1}^{i=r} c_i \mathbf{s}_i(t - \tau_i). \tag{2.2}$$

In this case, the model is capable of capturing fixed relationships among the muscle activation waveform across muscles and time. By means of comparison, time-invariant synergies can

acquire the spatial structure in the patterns but any fixed temporal relationship can be recovered only indirectly from the weighting functions associated with its synchronous synergy.

Although the time-varying model provides a more parsimonious representation of the muscle activity compared to the time-invariant model, some studies have shown evidence that the muscle synergies are synchronised in time [43, 80]. Therefore, most recent muscle synergies studies adopt the time-invariant model for synergy extraction. This is done by using matrix factorisation techniques on multi-channel EMG activity to estimate the muscle synergies and their weighting functions.

2.3.3 Muscle synergy extraction

Multichannel EMG with *m*-channels is represented as a matrix $\mathbf{M}$. Hence, Equation 2.1 is expanded into matrix form according to the time-invariant synergy model as the following:

$$\mathbf{M}_{(m\times n)} = \mathbf{S}_{(m\times r)} \times \mathbf{W}_{(r\times n)} \tag{2.3}$$

with the number of synergies r being restricted to less than number of channels m and number of samples n ($r \leq m, n$) to impose dimension reduction.

This is considered as a Blind Source Separation (BSS) problem where matrix $\mathbf{M}$ is modelled as a linear mixture of unknown synergies and weighting functions as shown in Equation 2.3 and illustrated in Figure 2.4. In this context, $\mathbf{S}$ is the mixing (synergy) matrix while $\mathbf{W}$ contains the source vectors (weighting functions). The noise is disregarded in Equation 2.3. In order to estimate unique solutions for this problem, matrix factorisation with additional constraints are needed.

Several matrix factorisation methods were proposed to solve this BSS problem and estimate muscle synergies from multichannel EMG data. The most prominent matrix factorisation techniques for synergy extraction are Principal Component Analysis (PCA) [81], Independent Component Analysis (ICA) [82] and Non-negative Matrix Factorisation (NMF) [83]. An example for muscle synergy extracted via matrix factorisation is shown in Figure 2.5.

PCA is one of the oldest and most widely used matrix factorisation techniques. It aims to reduce

the dimensionality of the data while preserving as much variability as possible. PCA constrains the components of the model in Equation 2.3 to be orthogonal, where the first component holds the largest variance and the variance progressively decreases for each component [84]. PCA has been used for synergy extraction in many studies such as [85–87].

Unlike PCA, ICA attempts to extract independent components by whitening the data to remove any correlation. Then, it rotates the pre-whitened data to extract the non-Gaussian components. An example of studies used ICA for muscle synergy extraction is [4] and [88].

Finally, NMF imposes a non-negative constraint on the extracted factors. The algorithm relies on a cost function to quantify the quality of approximation between the data matrix $\mathbf{M}$ and its factorised non-negative matrices $\mathbf{S}$ and $\mathbf{W}$, where $\mathbf{M} \approx \mathbf{SW}$. Values of $\mathbf{S}$ and $\mathbf{W}$ are updated and optimised to find the local minima numerically. Several studies utilised NMF for muscle synergy extraction including [5, 89, 90]. Matrix factorisation will be covered in more detail in Chapter 3.

2.3.4 Number of synergies

Selecting the appropriate number of factors or synergies is instrumental for matrix factorisation. The number of synergies for 2^{nd}-order model extracted via matrix factorisation methods have been determined using two main approaches: a mathematical approach and a functional approach [6].

The mathematical approach relies on the computation of the least number of components that could describe the model [91]. For instance, the Laplacian information criterion and Bartlett's test has been used for subsets PCA components, while likelihood ratios and projected variance has been utilised for ICA components, in addition to Akaike and Bayesian information [92]. Moreover, the explained variance by the model have been used to determine number of synergies by D'Avella *et al.* [55] by identifying the slope change of the explained variance with respect to the number of retained factors. The explained variance accounts for variation of a data set described by given the model. The complementary part of the total variation is called unexplained variation or residuals [93].

On the other hand, the functional approach relies on prior knowledge of the data structure

and myoelectric control requirements to choose the appropriate number of synergies. For example, Muceli *et al.* [94] proposed one synergy for each wrist's DoF, while two synergies were assigned to each wrist's DoF by Jiang *et al.* [95] for proportional myoelectric control.

2.4 Higher order tensor decomposition

Higher-order tensors are the generalisation of vectors (1st-order tensors) and matrices (2nd-order tensors). Tensor decomposition is analogous to matrix factorisation when the data have an order of three or higher. Similarly, higher-order tensors can be decomposed into their main components. Naively, the easiest way to do this is by unfolding the tensor into a matrix and apply a matrix factorisation technique. However, this approach would discard any information from the mutual interactions between the higher dimensions [7] and would not utilise the power of higher-order tensors.

Several tensor decomposition models have been introduced with Tucker and Parallel Factor Analysis (PARAFAC) being the most prominent ones [96]. When analysing higher-order data, tensor decompositions often provide several advantages, such as compactness, uniqueness of decomposition and generality of the identified components, over matrix factorisation [7]. In this section, we will introduce and discuss higher-order tensor and tensor decomposition notations, models and algorithm.

2.4.1 Tensor notations and operations

Higher-order tensors are typically comprised of three or more modes, also called ways or dimensions. Scalars are designated using lowercase italics, x, while vectors are shown in bold lowercase, $\mathbf{x}$. Matrices are shown as bold uppercase, $\mathbf{X}$, and all higher-order tensors (three and above) are designated by bold underlined capitals, $\underline{\mathbf{X}} \in \mathbb{R}^{i_1 \times i_2 \times \ldots i_n}$ where $n \geq 3$. A sub-tensor or sub-array is a subset of the main tensor when one or more indices are fixed. For example, given a three-dimensional tensor $\underline{\mathbf{X}} \in \mathbb{R}^{i_1 \times i_2 \times i_3}$, the mode-1 horizontal slice would be a matrix $\mathbf{X}_{\mathbf{1},:,:} \in \mathbb{R}^{i_1 \times i_2 i_3}$ while a the first fibre of mode-1 would be represented as a vector $x_{:,1,1}$ as illustrated in Figure 2.6.

Higher-order data can be reorganised through concatenation and/or augmentation to change it

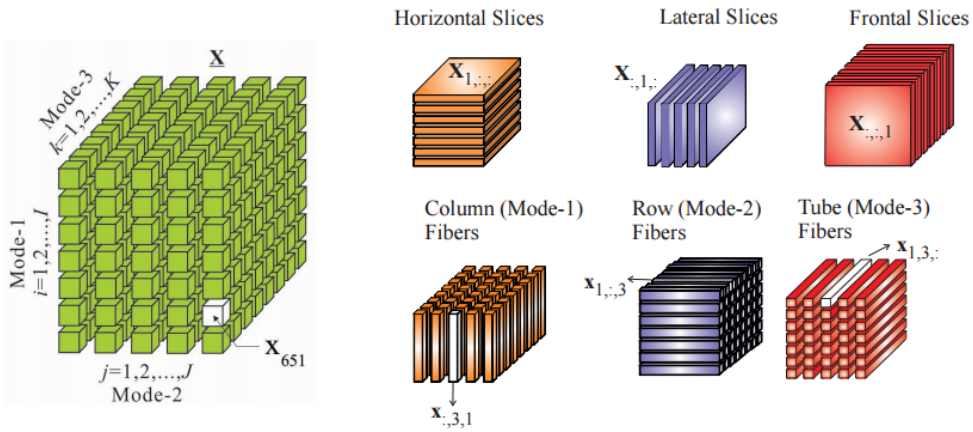

Figure 2.6: 3rd-order tensor $\underline{\mathbf{X}} \in \mathbb{R}^{7\times5\times8}$ with illustration of slices and fibres. Figure from [7].

into a lower or higher order. Unfolding (also known as matricization) is an important concept in higher-order tensor analysis. It is simply a way of rearranging a 3rd-order tensor to a matrix by concatenating its slices matrices for different levels across one mode as shown in Figure 2.7. For example, 3rd-order tensor $\underline{\mathbf{X}}^{(i_1\times i_2\times i_3)}$ can be unfolded across the first mode as $\mathbf{X}^{(i_1\times i_2 i_3)}$ or across its second or third mode as $\mathbf{X}^{(i_2\times i_1 i_3)}$ and $\mathbf{X}^{(i_3\times i_1 i_2)}$ respectively. On the other hand, the opposite process is tensorisation which is constructing higher-order tensor by mapping lower-order data to higher-order data with different techniques. Tensor construction and tensorisation will be covered in more details in Section 4.2.

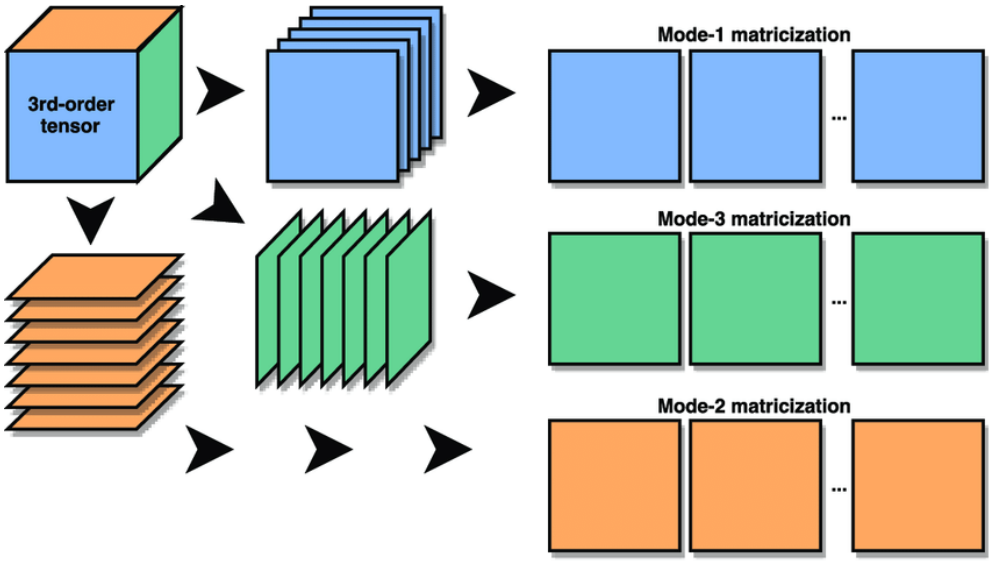

Figure 2.7: 3rd-order tensor unfolded across its three modes.

The Kronecker and Khatri-Rao products [97] are matrix products that will be useful to express

some operations with higher-order tensor models such as direct projection. The Kronecker product is a generalisation of the outer product that can be applied on matrices of arbitrary size. Given matrices $\mathbf{A} \in \mathbb{R}^{i_1 \times i_2}$ and $\mathbf{B} \in \mathbb{R}^{i_3 \times i_4}$ is their Kronecker product would be $\mathbf{A} \otimes \mathbf{B}$ and the result is a matrix $\mathbf{C} \in \mathbb{R}^{i_1 i_3 \times i_2 i_4}$ as:

$$\mathbf{A} \otimes \mathbf{B} = [a_1 \otimes b_1 \; a_1 \otimes b_2 \; a_1 \otimes b_3 \; \ldots a_{i_3} \otimes b_{i_4 - 1} \; a_{i_3} \otimes b_{i_4}] = \mathbf{C} \in \mathbb{R}^{i_1 i_3 \times i_2 i_4} \tag{2.4}$$

The Khatri-Rao is considered as the column-wise Kronecker product. Given two matrices $\mathbf{A} \in \mathbb{R}^{i_1 \times i_3}$ and $\mathbf{B} \in \mathbb{R}^{i_2 \times i_3}$, their Khatri-Rao product is given as $\mathbf{A} \odot \mathbf{B}$ and their result is matrix $\mathbf{c} \in \mathbb{R}^{i_1 i_2 \times i_3}$ This is equivalent to:

$$\mathbf{A} \odot \mathbf{B} = [a_1 \otimes b_1 \; a_2 \otimes b_2 \; \ldots \; a_{i_3} \otimes b_{i_3}] = \mathbf{C} \in \mathbb{R}^{i_1 i_2 \times i_3} \tag{2.5}$$

2.4.2 PARAFAC model

PARAFAC, also known as Canonical Polyadic Decomposition (CPD) [98], is a common tensor decomposition model used to represent higher-order data that can be traced back to the beginning of the 20th century [99]. PARAFAC decomposes a higher-order tensor into the sum of component rank-1 tensors coupled with a supra-diagonal core tensor as shown in Figure 2.8a. The supra-diagonal core tensor (also known as "identity tensor") is a tensor with 1s across its supra-diagonal and 0s elsewhere which limits the interactions in-between components unlike Tucker decomposition which will be discussed in Section 2.4.3.

In general, n^{th}-order tensor $\underline{\mathbf{X}} \in \mathbb{R}^{i_1 \times i_2 \times \ldots i_n}$ can be decomposed into its primary components using r-component PARAFAC model where r is the number of components that is fixed across each mode as the following:

$$\underline{\mathbf{X}} \approx \underline{\mathbf{\Lambda}} \times_1 \mathbf{A}^{(1)} \times_2 \mathbf{A}^{(2)} \cdots \times_n \mathbf{A}^{(n)} \tag{2.6}$$

where $\underline{\mathbf{\Lambda}} \in \mathbb{R}^{r \times r \cdots \times r_n}$ is a super diagonal tensor that have same dimension across each mode and the vector $\boldsymbol{\lambda}$ is across the diagonal of $\underline{\mathbf{\Lambda}}$, while "$\times_n$" is multiplication across the n^{th}-mode [100].

For more clarification, Equation 2.6 can expressed in an element-wise form as:

$$x_{i_1 i_2 \ldots i_n} \approx \sum_{m=1}^{m=r} a_{i_1 m}^{(1)} \, a_{i_2 m}^{(2)} \ldots a_{i_n m}^{(n)} \tag{2.7}$$

or in its matricized form across the first mode using the Khatri-Rao product:

$$\mathbf{X}^{(i_1 \times i_2 i_3 \ldots i_n)} \approx \mathbf{A}^{(1)} \big(\mathbf{A}^{(n)} \odot \mathbf{A}^{(n-1)} \odot \ldots \mathbf{A}^{(3)} \odot \mathbf{A}^{(2)} \big)^T \tag{2.8}$$

From Equation 2.7, PARAFAC decompositions can thus be considered as the multi-linear algebra generalisation of PCA for higher-order tensors. The main difference between PCA and PARAFAC is that in the latter there is no need for requiring orthogonality to identify the mode [101].

The PARAFAC decomposition is unique under very mild conditions such as non-negativity or modularity of components [100]. The uniqueness of PARAFAC model arise from the supra-diagonal core tensor that restricts the interactions between components across different modes in addition to the same number of components in all modes. However, those restriction can affect the quality of decomposition by reducing the ability of components to model the tensor and explain its variance. Therefore, the appropriate choice for number of components is critical for PARAFAC decompositions capturing the underlying structure of the data [102].

Hence, several mathematical approaches have been deployed to determine the appropriate number of components for higher-order tensor decomposition and gauge the quality of the decomposition such as Core Consistency Diagnostic (CORCONDIA) [103] in addition to the traditional method of determining the percentage of the explained variance described by the decomposed model. CORCONDIA is an intuitive direct approach to gauge how well a PARAFAC decomposition is able to model a tensor. In brief, CORCONDIA measures the degree to which a given PARAFAC model deviates from the "ideal" supra-diagonal core. A perfect PARAFAC model would have a pure supra-diagonal core and its CORCONDIA value of 100% while flawed models would deviate significantly and their CORCONDIA value would decrease significantly [103].

2.4.3 Tucker model

On the other hand, the Tucker model [104] is the generalisation of PARAFAC model as the latter is a special case of Tucker with a supra-diagonal core tensor. In Tucker decomposition, the higher-order tensor is decomposed into a smaller core tensor transformed by a matrix across each mode (dimension), where the core tensor is not restricted to be super-diagonal and can have interacting values between multiple components across domains. Consequently, the number of components can be different in each mode unlike PARAFAC where all modes have the same number of components [100]. The differences between both models are represented in Figure 2.8.

An n^{th}-order tensor $\underline{\mathbf{X}} \in \mathbb{R}^{i_1 \times i_2 \times \ldots . i_n}$ can be modelled according to the Tucker model as follows:

$$\underline{\mathbf{X}} \approx \underline{\mathbf{G}} \times_1 \mathbf{B}^{(1)} \times_2 \mathbf{B}^{(2)} \cdots \times_n \mathbf{B}^{(n)} \tag{2.9}$$

where $\underline{\mathbf{G}} \in \mathbb{R}^{j_1 \times j_2 \cdots \times j_n}$ is the core tensor and $\mathbf{B}^{(n)} \in \mathbb{R}^{i_n \times j_n}$ are the components matrices transformed across each mode. The core tensor $\underline{\mathbf{G}}$ is flexible to have different dimensions across each mode as long as it is smaller than the tensor being factored, $\underline{\mathbf{X}}$, so that $j_n \leq i_n$.

Two important variants for the Tucker decomposition models are worth noting, Tucker1 and Tucker2 can be seen as a special case of Tucker model where only one and two modes are estimated respectively. In both models, the additional modes are set to be identity matrices and absorbed into the core tensor [105]. As a result, Tucker1 model is equivalent to the ordinary two-dimensional PCA, while The Tucker2 is a model of intermediate complexity as compared with the Tucker1 and the standard Tucker model [100].

Tucker decomposition can be expressed in an element-wise form as the following:

$$x_{i_1 i_2 \ldots i_n} \approx \sum_{m_1=1}^{m_1=j_1} \sum_{m_2=1}^{m=j_2} \cdots \sum_{m_n=1}^{m_n=j_n} g_{m_1 m_2 \ldots m_n} b^{(1)}_{i_1 m_1} b^{(2)}_{i_2 m_2} \ldots b^{(n)}_{i_n m_n} \tag{2.10}$$

where $j_1, j_2 \cdots \times j_n$ are the number of components (i.e., columns) in the mode matrices $\mathbf{B}^{(1)}, \mathbf{B}^{(2)} \ldots \mathbf{B}^{(n)}$ respectively. $g_{m_1 m_2 \ldots m_n}$ is the corresponding element of a core tensor $\underline{\mathbf{G}} \in \mathbb{R}^{j_1 \times j_2 \cdots \times j_n}$. Here, the core tensor ($\underline{\mathbf{G}}$) defines the level of interaction between the

different components as illustrated in Figure 2.8b.

In the case of Tucker decomposition, the matricized form will use the Kronecker product as the following example across the first mode:

$$\mathbf{X}^{(i_1 \times i_2 i_3 \ldots i_n)} \approx \mathbf{B}^{(1)} \mathbf{G}^{(j_1 \times j_2 j_3 \ldots j_n)} \big(\mathbf{B}^{(n)} \otimes \mathbf{B}^{(n-1)} \otimes \ldots \mathbf{B}^{(3)} \otimes \mathbf{B}^{(2)}\big)^T \tag{2.11}$$

Unlike PARAFAC models, the Tucker model is flexible in determining the number of components for each mode and the interaction between components because of the flexible core tensor ($\underline{\mathbf{G}}$). However, because of this flexibility, Tucker decomposition generally does not provide unique solutions [106]. Therefore, imposing constraints on the model is essential to reduce the possibility of numerical degeneracy and to find a unique solution to the model in practice [100].

2.4.4 Alternating least squares algorithm

Both Tucker and PARAFAC usually employ the Alternating Least Squares (ALS) algorithm to estimate their component matrices (and core tensor in the case of Tucker decomposition) [101]. ALS has two main phases. The first one is initialisation, where the components and core tensor are estimated either randomly [107] or by certain criteria such as singular value decomposition or direct trilinear decomposition [108]. The second phase is iteration or updating which minimise the loss function between the original data and its model by breaking down this complex non-convex problem into a series of simpler, convex problems which are tackled in succession [109]. This is done by fixing all the component matrices to be estimated except for those corresponding to one of the modes and alternate iteratively between all the components to solve each convex problem until convergence [102]. For example, the least squares loss function across the first mode for 3$^{\text{rd}}$-order Tucker decomposition is:

$$argmin_{\mathbf{B}^{(1)},\mathbf{B}^{(2)},\mathbf{B}^{(3)},\underline{\mathbf{G}}} \|\underline{\mathbf{X}} - \mathbf{B}^{(1)} \underline{\mathbf{G}} (\mathbf{B}^{(3)} \otimes \mathbf{B}^{(2)})^T\|_F^2 \tag{2.12}$$

where $\otimes$ is Kronecker product and $\|.\|_F^2$ is the Frobenius norm. This function is solved by fixing the two factors from $(\mathbf{B}^{(1)}, \mathbf{B}^{(2)}, \mathbf{B}^{(3)})$ and computing the third unfixed factor alternatively.

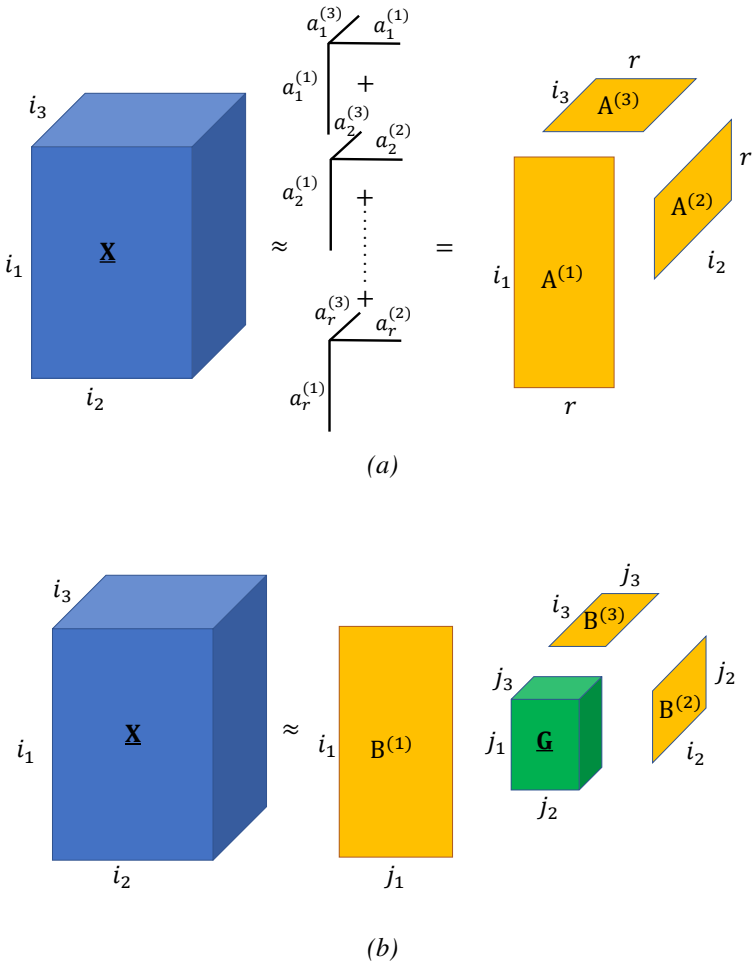

Figure 2.8: Illustration of PARAFAC (Panel 2.8a) and Tucker (Panel 2.8b) decomposition for 3^{rd}-order tensor $\underline{\mathbf{X}}$.

The ALS algorithm has several advantages such as simplicity compared to the simultaneous approaches. However, its main drawback is that it cannot guarantee convergence to a stationary point as the problem could have several local minima. This can be solved by applying multiple constraints on the initialisation and iteration phases [108] to improve the estimation. Moreover, constraining the tensor models has several benefits including: improving the uniqueness of the solution, more interpretable results that do not contradict *a priori* knowledge, avoiding degeneracy and numerical problems, and speeding up the algorithm [100]. Although constraints may lead to poorer fit for the data compared to the unconstrained model, the advantages outweigh the decrease in the fit for most cases [7]. The decomposition models are constrained through their ALS algorithm in the initialisation and/or iteration phases. For example, a non-negativity constraint is one of the most commonly used ones due to the illogical meaning for negative components in many cases. The non-negativity constraint is implemented in the iteration phase by setting the negative values of computed components to zero by the end of each iteration to force the algorithm to converge into a non-negative solution. In the case of muscle synergy extraction, non-negativity would add more information to the decomposition by taking into account the additive nature of muscle synergies.

2.5 Myoelectric control system

Although this thesis is focused on muscle activity signals analysis, myoelectric control is one of the potential applications that could benefit from muscle synergies estimated via tensor decomposition. Therefore, different approaches for myoelectric control systems are briefly reviewed in this section. Myoelectric prosthetic control system consists of three main parts [28, 35]:

- The EMG instrument where the EMG signals are recorded, amplified, filtered and digitised.
- EMG signal processing to extract useful control signal and commands to an external device.
- The external prosthetic device.

Here, we are concerned with the second step of processing EMG signals since this thesis

is mainly focused on muscle activity analysis. Three signal processing approaches will be discussed in this section: Conventional, pattern recognition and muscle synergy approaches.

2.5.1 Conventional approach and commercial application

The direct relation between the power of the EMG and the activation level of the muscle has been used since the first clinically viable myoelectric prosthesis [110] six decades ago. Surprisingly, the same concept is still used nowadays in many upper-limb myoelectric commercial systems due to the need for robustness. These systems rely on comparing the EMG amplitude to a predefined threshold that actuates a matching function. The earlier generations of the myoelectric control systems offer an on/off approach where one specific prosthetic function is assigned to one EMG channel. Multi-function prostheses systems were introduced [111], where level coding was applied as an alternative approach. The EMG signal amplitude is divided into several segments from the predefined threshold to the maximum amplitude and each prosthetic function is assigned to a specific segment [112].

The next generation of the myoelectric control systems include state machines, large-scale threshold control and adjustment of muscle contraction rate. However, they continue to rely on the same concept as before. This principle was used in recent myoelectric prosthetic devices like the Michelangelo Hand[1] and iLimb ultra[2].

In addition to the unnatural switching procedure, the main limitations to those approaches are: 1) EMG cross-talk between muscles, which reduces the control of the device; 2) EMG signal amplitude variability, which acts like the noise in the EMG signal.

2.5.2 Pattern recognition-based myoelectric control systems

Pattern recognition based methods are based on the assumption that each task is characterised by a dependable muscle activation that could be described by a set of features, which could be reproducible across trials of the same task and differentiated from other tasks. Therefore, the direct relation between the features and the neural activity is not strictly relevant. Any reliable information (peripheral or neural) extracted from the EMG could be classified.

[1] https://www.ottobockus.com/prosthetics/upper-limb-prosthetics/solution-overview/michelangelo-prosthetic-hand/
[2] http://touchbionics.com/products/active-prostheses/i-limb-ultra

Correspondingly, cross-talk is not an issue, and may be it could be a source of information if it is consistent across trials [28].

The pattern recognition methods were able to achieve a very high classification accuracy (95%) for a range of motions (10 classes) in the last two decades [113–115], and recently have been implemented into a commercial system[3]. However, the control in the pattern recognition systems is digital and not proportional which means that any error may lead to a completely undesired motion that compromise the whole task. Moreover, most of the proposed methods are not simultaneous and only provide sequential control schemes [35].

In addition to those key limitations, there are some practical limitations that face both pattern recognition and direct-control approaches, such as the abrupt change of the EMG signal from electrode shift [116, 117] or the change in the skin-electrode impedance [27] due to sweating and other factors.

2.5.3 Synergy-based myoelectric control systems

Despite the efforts in the pattern recognition-based myoelectric control system, the intrinsic limitation of the sequential control makes the pattern recognition paradigm very different from natural movement which needs a simultaneous and proportional control of multiple DoFs. Recently, alternative approaches have been proposed for extracting neural control signals from the EMG signal to support more intuitive, simultaneous and proportional myoelectric control systems. Some of these approaches are biologically inspired by the muscle synergy concept.

In general, the proposed synergy-based myoelectric control systems extract muscle synergies from multichannel EMG recording for specific tasks or DoFs using matrix factorisation techniques such as NMF [5, 89, 118] PCA [71] or ICA [4]. Afterwards, the extracted synergistic information is used as training data to either predict the testing tasks and postures by discrete classification [4, 89] or extracting a proportional control signal that could be used in the myoelectric control system [5, 119]. In addition to the practical limitations, the first classification approach does not offer proportional control similar to pattern recognition techniques. On the other hand, the regression approach uses muscle synergies to estimate control signals that are proportional to the movement for simultaneous and proportional

[3] https://www.coaptengineering.com/

myoelectric control. The limited number of DoFs is the main drawback that faces the second regression approach, both studies [5, 119] introduce two DoFs only and when a 3rd DoF was added, the performance of the system was significantly degraded. The proportional and simultaneous synergy-based approach and its limitations will be discussed in more detail in Chapter 6.

2.6 Conclusions

This chapter provided background information necessary to understanding key multi-disciplinary topics fundamental to the thesis. The common methodology used throughout the thesis was described, and general examples were provided for essential concepts like higher-order tensor decomposition. Relevant physiological context for the thesis was also covered in addition to a brief introduction to the upper-limb myoelectric control systems.

Chapter 3

Second-order matrix models for muscle synergy extraction

The contributions of this Chapter were published in Medical Engineering & Physics in April, 2018 [6].

3.1 Introduction

The estimation of muscle synergies (spatial profile) and their weighting functions (temporal profile) from a multi-channel EMG signal is a BSS problem. This problem is approached with matrix factorisation techniques to estimate the set of basis vectors (synergies) able to represent most of the data variability. Various matrix factorisation algorithms have been applied based on different constraints. The most commonly used factorisation techniques to extract synergies for myoelectric control and clinical purposes are PCA [81], which was applied in [87]; ICA [82], which was used in [4] and [88]; and NMF, [83] which have been used in [5, 89] and [90].

In this Chapter, these three techniques are compared among themselves and to Second-Order Blind Identification (SOBI) [120], a technique which has not been used for muscle synergy estimation previously. A first evaluation of the matrix factorisation algorithms for muscle synergy extraction was reported in 2006 [121] where the algorithms were tested with simulated data and real data. They demonstrated the ability of several factorisation algorithms to robustly identify the muscle synergies. However, the algorithms performance was very similar. A more recent study [122] used joint motion data to evaluate kinematics and muscle synergies estimated by PCA, ICA and NMF using the quality of reconstructing the data by synergies as a metric for evaluation. Both PCA and NMF had comparable performance on muscle and kinematic

synergies and both outperformed ICA.

Here, we are concerned with the nature and number of muscle synergies and the factors that affect their quality which have not been discussed by other comparison studies [121, 122]. The sparsity of synergies is investigated where synthetic sparse and non-sparse synergies are compared to study their effect on the matrix factorisations. Moreover, the ratio between the number of channels and synergies (dimension reduction ratio) is studied. Those comparisons are carried out under different noise levels to show the robustness of factorisation methods to noise. In addition, a synthetic dataset is used to assess the ability of the Minimum Description Length (MDL) method to calculate the appropriate number of synergies. Finally, synergies extracted from a real dataset by the four matrix factorisation techniques were used to classify between wrist movements. The classification accuracy was used as a metric in the factorisation methods comparison.

We aim to compare current matrix factorisation techniques in addition to SOBI and investigate the factors that affect the quality of their extracted synergies. Hence, we could select the best matrix factorisation method as a benchmark for the proposed higher-order tensor decomposition approaches, and achieve better understanding of the nature of the muscle synergy model.

3.2 Methods

3.2.1 Matrix factorisation algorithms

According to the time-invariant model of muscle synergy [1], a multichannel EMG signal matrix $\mathbf{M}$ is modelled as a linear mixture of synergies $\mathbf{S}$ and its weighting functions $\mathbf{W}$ as follows:

$$\mathbf{M} = \mathbf{SW} \tag{3.1}$$

Hence, this is BSS problem, and to extract muscle synergies, matrix factorisation methods with additional constraints are needed. Muscle synergies are extracted with three of the most common matrix factorisation methods (PCA, ICA and NMF) and compared among themselves and to SOBI.

Here, PCA has been performed using the "pca" Matlab function (version 2016a). For ICA, the fixed-point algorithm introduced by Hyvärinen [123] has been used. The Matlab function "nnmf" (version 2016a) was used to perform the NMF based on the work by Berry *et al.* [124].

SOBI [120] has not been applied to extract muscle synergies before. However, it is included in this comparison because SOBI utilises the joint diagonalisation of time delayed covariance matrices to estimate the unknown components. Thus, SOBI leads to components that are uncorrelated at those time delays and, therefore, it is sometimes considered an alternative to ICA, which is based on higher order statistics. As a result, SOBI could reveal more information about the temporal profile of the EMG activity. Here, SOBI was performed using the default 4 diagonalised covariance matrices with the function "sobi" in the ICALAB package [125].

3.2.2 Synthetic dataset

The performance of each matrix factorisation algorithm was tested using synthetic datasets as ground truth. Since the studies [43, 80] showed evidence that the muscle synergies are synchronised in time, the data was generated according to the time-invariant model [1] in which EMG activity for j^{th}-channel is the summation of its coefficients in each synergy (s_{ij}), weighted by the respective weighting function ($\mathbf{w}_i$), as the following:

$$\mathbf{m}_j = \sum_{i=1}^{i=r} s_{ij}\mathbf{w}_i + g(\epsilon) \tag{3.2}$$

where $\mathbf{m}_j$ is the simulated EMG data over channel j, while ϵ is a Gaussian noise vector and $g(x)$ is the Heaviside function used to enforce non-negativity. For m-channel data, this model could be expanded into its matrix form. In this case, the synthetic EMG data $\mathbf{M}$ is a matrix with dimensions (m channels $\times$ n samples) as

$$\mathbf{M}_{(m\times n)} = \mathbf{S}_{(m\times r)} \times \mathbf{W}_{(r\times n)} + g(\mathbf{E}_{(m\times n)}) \tag{3.3}$$

where r is the number of synergies ($r<m$) and $\mathbf{E}$ is the matrix form of the Gaussian noise vector ϵ for all channels. $\mathbf{S}_{(m\times r)}$ and $\mathbf{W}_{(r\times n)}$ are the synergy matrix and weighting function matrix form, respectively.

In order to generate a synthetic EMG signal that mimics the real EMG data and carries the

synergistic information, the three elements in Equation 3.3 should be designed so that they reflect real activities under diverse assumptions. The synergy matrix $\mathbf{S}_{(m\times r)}$ was assigned a non-negative random values between [0,1] to retain the additive nature of synergies, while each weighting (activation) function $\mathbf{W}_{(r\times n)}$ is a real EMG envelope randomly assigned from the Ninapro first dataset from different subjects and movements to impose independence. This approach based on real data was chosen to ensure that the generated signal retains the statistical properties of the EMG signal rather than assigning randomly generated signals for the weighting function as done in the past [121]. Finally, the non-negative part of the Gaussian noise is applied to the mixture by the Heaviside function $g(\mathbf{E})$. An example of the generated synthetic EMG signal is shown in Figure 3.1.

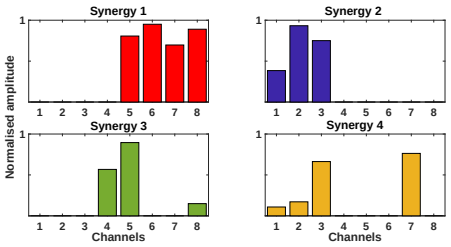

(a) Synthetic sparse synergies

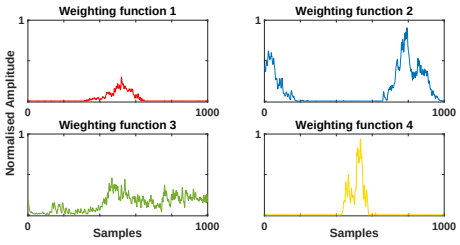

(b) Weighting functions

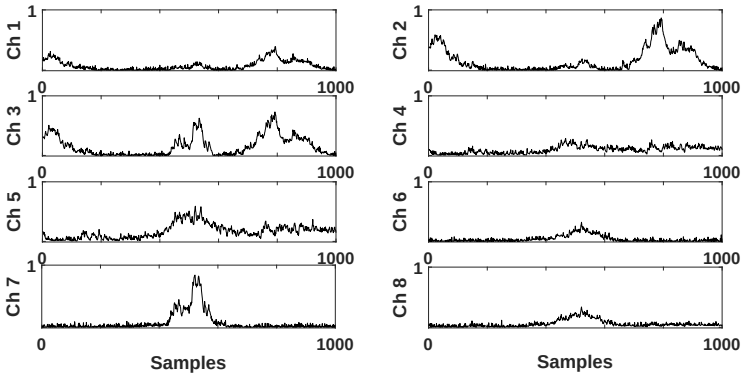

(c) The resulting synthetic EMG dataset (after adding the noise).

Figure 3.1: An example of 8-channel synthetic EMG signal (Panel 3.1c) creation using four sparse synergies (Panel 3.1a) and their respecting weighting functions (Panel 3.1b) which is a randomly selected real EMG segments with 15 dB SNR.

The synthetic signals were generated with different settings to compare the factorisation methods under various conditions. In all settings, the number of synergies (r) was fixed to four synergies. This choice was based on the fact that the number of synergies used in previous studies varied from one or two synergies [5] to six synergies [126] according to the application

requirements.

Three criteria were investigated: the sparsity of synergy matrix, the number of channels, and the added noise level. The sparsity of the synergy matrix $\mathbf{S}_{(m\times r)}$ is investigated since all muscles (channels) may be not activated during a specific movement at the same time. The sparse synergies were created by constraining each channel to a 40% sparsity level (i.e., a maximum of four channels being active in each synergy) to ensure that each channel has at least one non-zero value in the four synergies. This approach would typically avoid having channels that are inactive in all 4 synergies as shown in Figure 3.1a, as an example of sparse synthetic synergies. In comparison, the non-sparse synergies are non-negative random values between [0,1]. Secondly, the effect of dimension reduction between the generated signal and synergies (basis vectors) is examined. The number of synergies is fixed to 4 in all settings while the number of channels are 4 (no dimension reduction), 8 or 12 channels. Finally, the effect of additive signal to noise ratio (Signal to Noise Ratio (SNR)) is compared at three levels: 10, 15 and 20 dB. In total, 10 synthetic datasets are generated, each containing 1000 separate trials for each setting.

3.2.3 Synthetic dataset comparison

The comparison between the four matrix factorisation techniques relies on the similarity between estimated and true synergies using the correlation coefficient on the basis of full identification of true synergies (which is the ability of the algorithm to identify all four synergies) and similarity level between them (based on correlation coefficient values). The sequence of this process is shown in Figure 3.2.

The first step is to match each of the extracted synergies with the true ones by calculating Pearson's correlation coefficients between them. True and estimated synergies with the highest correlation value are matched together. This matching is done freely and unconstrained. In other words, without forcing a full match (all four estimated synergies matched with all four true synergies) because in some cases two or more estimated synergies have the maximum correlation with the same true synergy. In those cases, the factorisation is not successful since the extracted synergies failed to fully represent all true synergies. Hence, the "fully matched" criterion is the ability of the factorisation method to estimate fully distinctive synergies that

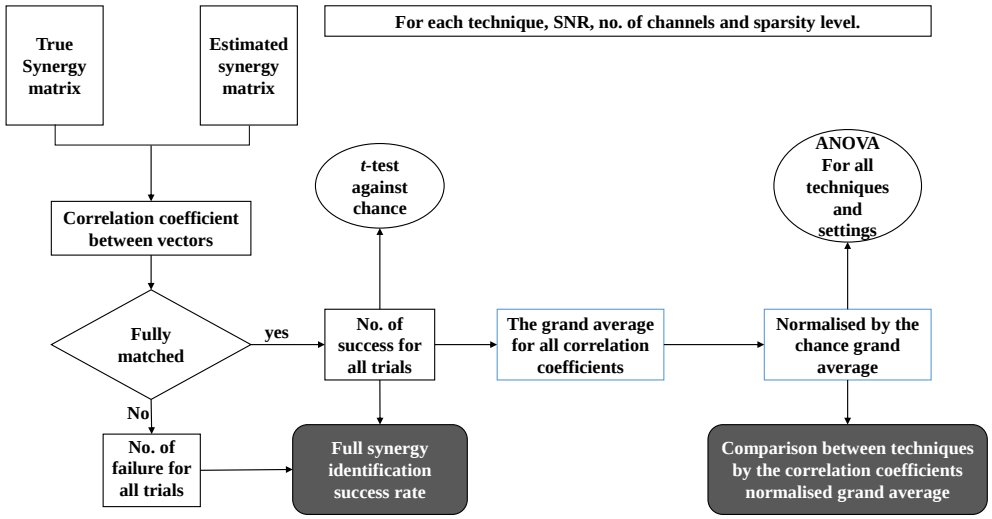

Figure 3.2: Block diagram for the comparison between matrix factorisation techniques.

match all true synergies without duplication. The success rate for a "fully matched" is computed across the 10 generated datasets. It is used as a metric to judge the ability of extracted synergies to fully represent all the true synergies, since a good factorisation would represent all of them.

In order to account to the chance that synergies may be randomly paired, the correlation coefficients between the true synergies and a set of randomly generated synergies are computed and the pairing rates are compared against for each factorisation method using a two-sample t-test with significance level set up at ($p < 0.05$).

Secondly, the correlation coefficient values for fully identified synergies are averaged for each trial. The grand average is computed for 10,000 trials (1,000 epochs$\times$ 10 datasets) of each setting combination. Then, it is normalised by the random synergy's correlation coefficients (chance grand average) as baseline removal as the following:

$$Normalised\ grand\ average = \frac{(grand\ average - chance\ grand\ average)}{(1 - chance\ grand\ average)} \tag{3.4}$$

The normalised grand average of the correlation coefficients between estimated and true synergies is computed for each matrix factorisation method with all different combination of

the 3 settings (SNR levels, number of channels and sparsity). This criterion is an indicator of general factorisation quality. Therefore, we statistically analyse it to compare the factorisation techniques and the effect of all three settings using the two-way Analysis of Variance (ANOVA) method with the significance level at ($p < 0.05$).

3.2.4 Real dataset comparison

For the real data comparison, three wrist DoFs are investigated. Wrist flexion and extension (DoF1), wrist radial and ulnar deviation (DoF2), and wrist supination and pronation (DoF3) are the main DoFs for wrist movement. Wrist movement through these three degrees of freedom are essential for prosthetic control [35]. Thus, they may be representative of application of muscle synergies in myoelectric control.

Since there is no ground truth for real data comparison of synergies extracted by each technique, we compared the techniques regarding their application for prosthesis control. In several studies [119, 127], muscle synergy is used as a feature to classify different hand and wrist movements. Therefore, the factorisation techniques are assessed according to their classification accuracy for the three main wrists DoFs.

To this end, the Ninapro first dataset is divided into training and testing sets with 60% (six repetitions of each task) of the data assigned to training for each subject. For each factorisation technique, synergies are estimated from training repetitions for each task. Those synergies are used to train k-nearest neighbours (k-NN) classifier (k=3 for simplicity). Four classifiers are trained using the training synergies, three of them to classify between two tasks of each wrist DoF while the fourth classifier is trained to classify between all six tasks. The number of synergies extracted was one for each repetition (two for each DoF) as in [5] to avoid permutation issues. The testing dataset - which contains the other four repetitions of each task - is used to test those classifiers. One synergy is estimated directly from each task repetition in the test set using the four factorisation methods and used to predict the task through the trained classifiers. The classification error count for each DoF is used to evaluate the factorisation techniques.

3.2.5 Number of synergies

In the literature, there are two main approaches to determine the appropriate number of synergies: the functional and the mathematical. The functional approach determines the number of synergies according to the application requirements such as myoelectric control when two synergies are assigned for each DoF [94, 95]. On the other hand, the mathematical approach relies on explained variance using tests such as scree plot or the likelihood criteria such as Akaike information criteria and MDL [92].

Since the number of underlying synergies of the generated synthetic dataset was known to be four, it was also used to test the ability of MDL to determine the number of synergies. MDL was chosen as an alternative to the explained variance methods as the latter is biased towards PCA since it relies on maximising the explained variance on the first components. The MDL method determines the number of synergies that could minimise the MDL. For more details, please, see Appendix **A**.

The MDL method was tested across various settings (sparsity, noise and channel to synergy ratio). Since four true synergies are used, only the 8 and 12 channels datasets were investigated as the MDL boundary cannot estimate number of synergies when it is equal to channels. This is not a problem in practical applications since the muscle synergy hypothesis implies the concept of dimension reduction. In addition, three level of SNR (10, 15 and 20 dB) of sparse and non-sparse datasets were explored with 1,000 trials for each combination. The result for correct estimation of synergies number is analysed via ANOVA and multiple comparison of results.

For the classification accuracy comparison using real datasets, the functional approach to determine number of synergies was chosen. Two synergies are assigned for each DoF (one synergy per task) as in [94, 95]. On the other hand, for the synthetic dataset comparison, the number of underlying synergies was known to be four as mentioned above.

3.3 Results

3.3.1 Number of synergies

The model selection method based on MDL was examined with the synthetic EMG data where the number of synergies are known (four synergies). The MDL method was tested on 1,000 trials for each combination of sparsity, three levels of noise and two sets of channels (8 and 12 channels).

The ANOVA shows that sparsity has no significant effect on the estimation of the correct number of synergies (p>0.05), while number of channels has a significant effect with $[F(1,11) = 19.94, p = 0.003]$ as 12-channel datasets perform better than 8-channel signals (shown in Figure 3.3). As for the level of noise, 10 dB SNR had a significantly worse performance than 15 and 20 dB SNR with the effect of noise significant at $[F(2,11) = 24.22, p = 0.007]$ by one-way ANOVA. This indicates that, the MDL method for estimating the correct number of synergies performs better with lower noise and more available channels, as expected.

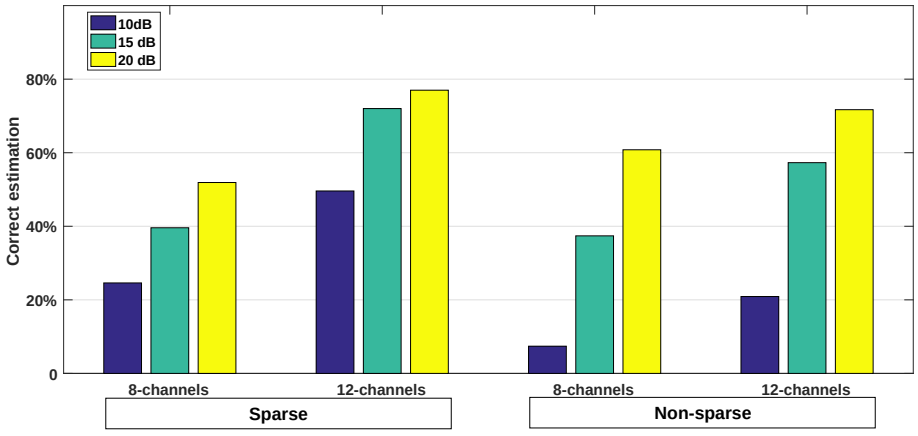

Figure 3.3: Percentage of correct synergy number estimation using the MDL method across the three settings (noise, number of channels and sparsity).

3.3.2 Synthetic dataset comparison

The four matrix factorisation methods were compared on the basis of two criteria: synergy full identification success rate, and the normalised grand average of correlation coefficients for the fully identified synergies. The comparison was done on 10,000 trials (10 datasets of 1,000 trials) for each combination of the three settings (sparsity, SNR and number of channels). An example of one setting of non-sparse, 12-channel with 15 dB SNR is shown in Figure 3.4. All the four factorisation techniques had converged for all trials except for ICA which failed to converge in 1.48% of them.

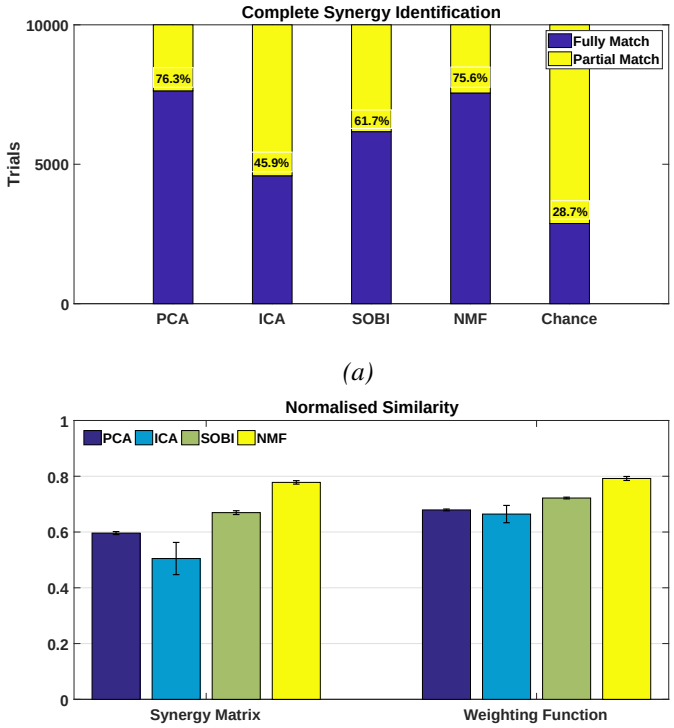

Figure 3.4: The results for non-sparse, 12 channels dataset with 15dB SNR. Panel 3.4a, the success ratio for the factorisation techniques to fully match the true synergies is shown. Panel 3.4b, the normalised similarity values for each technique single trial with the same settings. Error bars indicate standard deviation.

The four factorisation methods were assessed by their ability to fully identify all four true synergies by matching them according to their Pearson's correlation coefficients values. In order to rule out any statistical chance from it, a two-sample *t*-test was conducted to compare the success rate of each technique and the randomly generated synergies. All the techniques

succeeded to reject the null hypothesis ($p < 0.05$) for all the settings. Hence, there is a significant difference between the matching success rate for each of the matrix factorisation methods and the randomly generated synergies. An example of the success rate for one of the settings is shown in Figure 3.4a, while the average success rate to fully identify the true synergies for all settings is represented in Figure 3.5. NMF and PCA have the highest success rates to fully identify synergies.

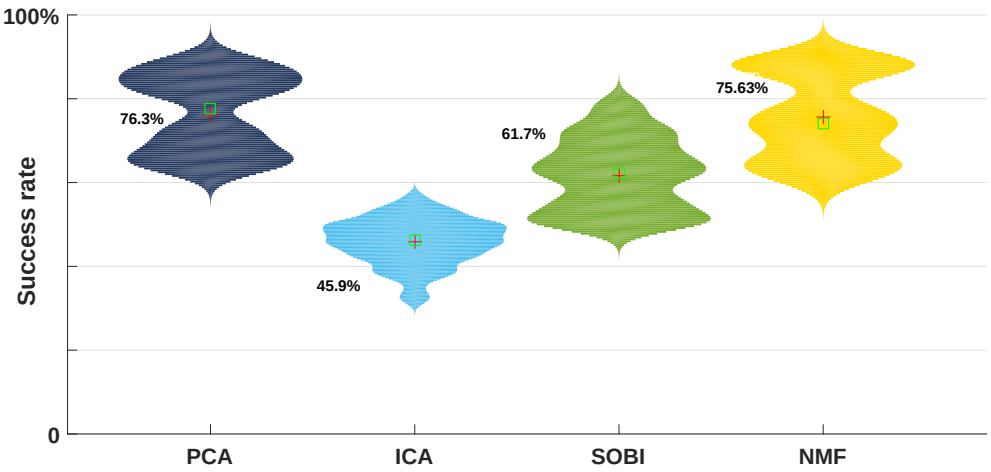

Figure 3.5: Violin graph for the success rate of full synergy identification for each method across all settings. The mean and median are represented in the Figure as red crosses and green squares respectively.

The correlation coefficients of the matched synergies normalised by random synergy correlation coefficients using Equation 3.4 is shown in Figure 3.4b. Then the normalised correlation coefficient of synergies (synergy matrix) were averaged across trials. The grand average for each factorisation method was normalised by the chance's grand average. In Figure 3.6, the normalised grand average (similarity metric) for the four matrix factorisation methods is plotted for all different settings (sparsity, number of channels and noise level). It is worth mentioning that NMF has the highest similarity for all settings except for the four channel case (the results for the sparse, four-channel setting for NMF are mostly negative). Moreover, all four algorithms perform worse with four channels (no dimension reduction) with SOBI being the best algorithm in this case.

In order to explore the significance of those settings the two-way ANOVA was performed with a post-hoc multiple comparison test. The result shows that number of channels and sparsity

had a significant effect on the grand normalised average at $[F(2, 688) = 1364.5, p \leq 0.001]$ and $[F(1, 400) = 7.35, p = 0.007]$ respectively. The multiple comparison test shows that sparse synergies and the higher number of channels show better similarity levels. On the other hand, the noise level fails to reject the null hypothesis. This means that the level of noise used in these experiments did not affect the quality of estimated synergies significantly unlike the sparsity or number of channels. In addition, this was supported by the interaction results, where factorisation methods and the number of channels interaction showed a significant effect on the grand normalised average, as well as the factorisation method and sparsity interaction. On the contrary, the noise level and factorisation techniques interaction has no significance on the grand normalised average.

The computational efficiency was compared after each technique ran for 100 times on Matlab 2017B with Intel core i7 processor (2.4 GHz, 12 GB RAM) and the median value for the running times were computed. PCA and SOBI were the fastest with (0.0012 s and 0.0015 s) respectively followed by NMF with 0.0063 s while ICA was significantly slower by 0.6419 s.

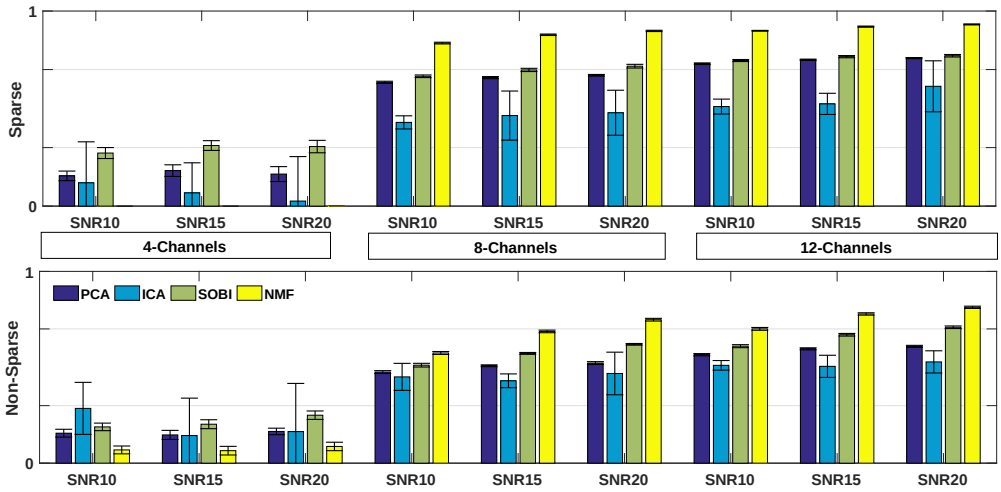

Figure 3.6: The normalised grand average of correlation coefficients for the fully identified synergies compared across all 3 settings (sparsity, SNR and number of channels) for the 4 matrix factorisation methods. Error bars indicate standard deviation.

3.3.3 Real dataset comparison

As an illustration, the four matrix factorisation methods (PCA, ICA, SOBI and NMF) were used to estimate two synergy model from a real 10-channel EMG epoch as shown in Figure 3.7. The number of synergies needed in this example was chosen to be two according to the MDL

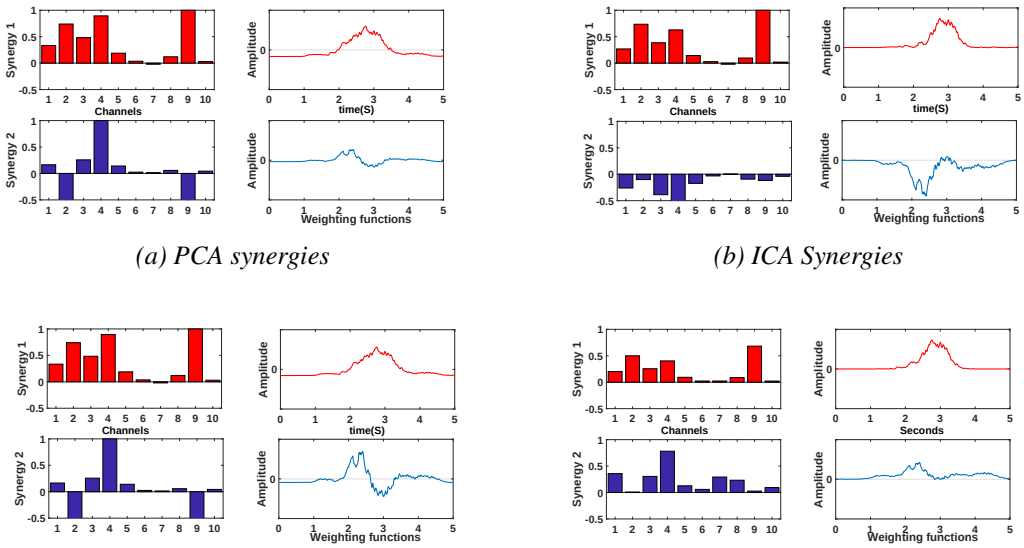

(a) PCA synergies

(b) ICA Synergies

(c) SOBI synergies

(d) NMF synergies

Figure 3.7: Two-component muscle synergy extracted via the four matrix factorisation methods for the 10-channel EMG signal recorded during wrist extension movement for 5 seconds (Subject 4 / repetition 1)

method.

In addition, to compare between the matrix factorisation techniques, a one-component synergy was used to train a k-NN classifier (k=3) in order to classify between two antagonistic movements (one DoF) for each technique. This was calculated for the three wrist DoFs separately as shown in Table 3.1. In addition, the same synergies were used to classify between all six movements (three DoFs). The average classification error rate and its standard deviation for the 27 subjects is also represented in Table 3.1.

3.4 Discussion and conclusions

We compared the most common matrix factorisation techniques (PCA, ICA and NMF) for muscle synergy estimation alongside SOBI, a BSS method that had not been applied for synergy extraction yet. Many studies rely on muscle synergy concept such as myoelectric control and biomechanical research. However, only two studies [121, 122] compared various factorisation methods (excluding SOBI) for synergy estimation without investigating the factors that affect the factorisation quality - except for noise.

Herein, the comparison was performed on real data and synthetic signals generated with known synergies and under different settings. Using the synthetic data we studied the effect of those settings on the muscle synergy extraction for each technique. The sparsity nature of synergies and level of noise was investigated in addition to the number of channels needed to extract the four synthetic synergies. The ability of the four factorisation methods to extract synergies from synthetic data was judged according to two metrics: success rate to fully identify synergies (Figure 3.5) and the correlation coefficients between true and estimated synergies (Figure 3.6). Moreover, the synthetic data was used to assess the MDL method to determine number of synergies needed under those three settings.

For the real datasets, since there is no ground truth against which to compare synergies estimated, we compared the factorisation methods according to the ability of their extracted synergies to classify wrist movements (Table 3.1) as a proof of concept for prosthesis control [4, 89]. PCA and NMF had the best classification accuracy followed by SOBI, while ICA had the lowest accuracy.

On the other hand, the synthetic datasets results showed that NMF and PCA had a better success rate to fully identify the four true synergies than SOBI and ICA. However, NMF and SOBI had the best normalised grand average of correlation coefficients (similarity level) between estimated and true synergies followed by PCA then ICA. Notably, NMF performed poorly with four-channel datasets when there was not any dimension reduction. In general, all algorithms

Table 3.1: The classification error count and (error percentage) for each wrist's DoF (Sample size=216) and all 3 DoFs (sample size=648) across 27 subjects

	PCA	**ICA**	**SOBI**	**NMF**
DoF1 (wrist flexion and extension)	1 (0.46%)	28 (12.96%)	8 (3.70%)	1 (0.46%)
DoF2 (wrist radial and ulnar deviation)	12 (5.56%)	29 (13.43%)	19 (8.80%)	1 (0.46%)
DoF3 (wrist supination and pronation)	7 (3.24%)	31 (14.35%)	18 (8.33%)	5 (2.31%)
All 3 DoFs (all 6 movements)	43 (6.64%)	122 (18.83%)	65 (10.03%)	41 (6.33%)

perform better with a higher number of channels compared to synergies, where SOBI was the best algorithm when there is no dimension reduction. Therefore, SOBI would be a relevant algorithm in situations with limited number of electrodes as it is preferable to minimise the number of electrodes for practical prosthesis control [128, 129].

The two-way ANOVA showed that the tested range of SNR has no significant effect on the factorisation performance, although it is noted that ICA was the most unaffected method to noise according to the multiple comparison test. On the other hand, sparsity had a significant effect ($p< 0.05$) on the correlation between true and estimated synergies. According to the multiple comparison test, the sparse synergies are easier to estimate by all factorisation methods. Moreover, the number of channels shows a significant effect ($p< 0.05$) on the correlation between estimated synergies and true ones. In addition, a higher number of channels to number of synergies ratio provides better synergy extraction.

Regarding the estimation of the number of synergies, the multichannel EMG signal is reduced into a lower subspace for the purpose of synergy extraction. The estimation of this subspace's dimension or, in other words, the number of synergies is crucial for the factorisation process. In the literature, the number of synergies are determine according to the requirement of the application (functional approach) or determined mathematically relying on variance explained tests or likelihood criteria. Here, we explored the MDL as an alternative for variance explained methods using the synthetic dataset. The results show that MDL performs better with higher channel to synergy ratio. This supports the current challenges for effective synergy identification with a limited number of electrodes. However, further investigation is needed to compare between different methods to estimate number of synergies using synthetic datasets with various settings.

Other limitations are worth noting. The results may be biased towards NMF due to the non-negative nature of the simulated synergies. However, this choice is supported by previous studies [89] which suggested the usefulness of NMF due to the additive nature of the synergies. In addition, further examination is needed if the setting of EMG acquisition changes dramatically (really bad SNR, much higher number of channels, etc.) to evaluate the validity of our conclusions in those settings. Finally, since various studies employ the muscle synergy in prosthesis control, a simple approach (k-NN classifier) was used in this paper as an

example to guide synergy application and to support the synthetic results. We treated this part of the study as a proof of concept. Additional work is needed with more advanced techniques and variety of tasks and movements.

In conclusion, we compared matrix factorisation algorithms for muscle synergy extraction and the factors that affect the quality of estimated synergies. Our findings suggest that the presence of sparse synergies and higher number of channels would improve the quality of extracted synergies. When the number of channels equal to synergies (no dimension reduction), SOBI performed better than other methods although the performance was still poor in this case. Otherwise, NMF is the best solution for robust synergy extraction when number of channels/muscles is higher than the required muscle synergies.

Therefore, NMF is used a benchmark for synergy extraction via matrix factorisation and will be compared with the proposed higher-order tensor decomposition methods in the following Chapters. Moreover, the results for the sparse synergy model have been supported with a recent study [130] that found evidence of sparsity in grasping tasks. In addition, Sparse Non-negative Matrix Factorisation (SNMF) was introduced as a novel approach for a synergy-based myoelectric control system in a recent study [118].

Chapter 4

Higher-order tensor decompositions for muscle synergy extraction

The work in this Chapter introduces tensor factorisation for EMG analysis and extends the work published in IEEE Proceedings of the EMBC 2016 [9]. The extension provides a general framework within which the methods of this publication are framed, and explores higher-order EMG tensor construction.

4.1 Introduction

Recently, higher-order tensor decompositions have received substantial attention in biomedical signal processing applications. For instance, they have been utilised in brain activity analysis [131]. Some applications include analysing Electroencephalogram (EEG) data to classify epileptic patients [132] and analysis of Magnetoencephalogram (MEG) activity in Alzheimer's disease [133]. Surprisingly, tensor factorisation had hardly been used in EMG analysis [9]. To the best of our knowledge, just one study used Tucker decomposition for feature extraction from a 2-channel EMG for classification [134]. Moreover, Delis *el al.* [135] proposed a space-by-time decomposition model to extract concurrent spatial and temporal components from single-trial EMG recordings, using a Sample-Based Non-negative Matrix Trifactorization algorithm that resembles a Tucker2 tensor decomposition model [136]. However, a detailed evaluation of the potential of tensor factorisation models for EMG analysis is lacking.

Multichannel EMG data are most often represented in matrix form with $time$ and $channels$ as indices along each mode (dimension) so that two-way signal processing methods (i.e., matrix factorisations) are used for muscle activity analysis. However, in most EMG studies, data are

naturally structured with more modes than the $temporal$ $(time)$ and $spatial$ $(channels)$ indices. For instance, the EMG datasets usually includes repetition of subjects and/or movements. This means that the muscle activity naturally fits into a higher-order tensor model including additional modes to the $temporal$ and $spatial$ ones. This is what the seminal studies [134] illustrated and show that current 2^{nd}-order approaches do not take advantage of such data structure. This means that some information about the interaction between modes may be lost in those approaches. In addition, although the EMG data was not tensorised into a higher order form in Delis *el al.* [135, 137], these studies supported the need for concurrent spatial and temporal components extraction for better synergy analysis. Thus, we hypothesise that higher-order tensor decomposition will be beneficial for muscle activity analysis by adding more depth and domains to improve the extracted synergistic information.

This would be carried out by taking into account aspects other than the spatial profile of the synergies. An obvious candidate to consider is the spectral profile, which could provide a model that is robust to frequency changes due to fatigue and channel cross-talk. Consequently, in this chapter, we expand the current muscle synergy model into a higher order one where synergies are estimated through tensor decomposition rather than matrix (2^{nd}-order tensor) factorisation. We discuss the possible ways to construct higher-order tensors for muscle activity. In addition, a 4^{th}-order tensor muscle synergy model is introduced, which expands the current model into 4 modes by adding $spectral$ and $repetition$ modes onto the $spatial$ and $temporal$ modes. Finally, a comparison of the models is done to classify the wrist movements. This study presents a proof-of-concept for the use of tensor factorisations for the extraction of muscle synergies.

4.2 Tensor construction

Tensors are a higher-order generalisation of vectors (1^{st}-order) and matrices (2^{nd}-order). The first step to create a higher-order synergy model is to prepare the data in a higher order form. This process of transformation or mapping lower-order data to higher-order data is known as "tensorisation". Several stochastic and deterministic techniques have been used for tensorisation [138].

"Segmentation" is one of the deterministic techniques where lower-order tensors are reshaped

into higher-order form by extracting small segments from it and stacking them beside each other. For example, the segmentation of a vector $\mathbf{v} = \{1, 2, 3, 4, 5, 6\} \in \mathbb{R}^n$ into a matrix $\mathbf{S} \in \mathbb{R}^{i \times j}$ where $n = i \times j$ as $\mathbf{S} = \begin{bmatrix} 1 & 4 \\ 2 & 5 \\ 3 & 6 \end{bmatrix}$.

In this thesis, we use choose the segmentation method to create 3rd and 4th-order EMG tensors from multichannel EMG datasets.

4.2.1 Third-order tensor

To create a 3rd-order tensor for an EMG dataset, the multichannel EMG recordings of several movements and/or tasks can be represented as a matrix with *time* and *channels* are its dimensions or modes. This matrix is segmented into equal epochs where each epoch contains one or more repetitions of one movement or task. By stacking these epochs across the new *repetition* mode, a 3rd-order tensor is created with modes $spatial \times temporal \times repetition$.

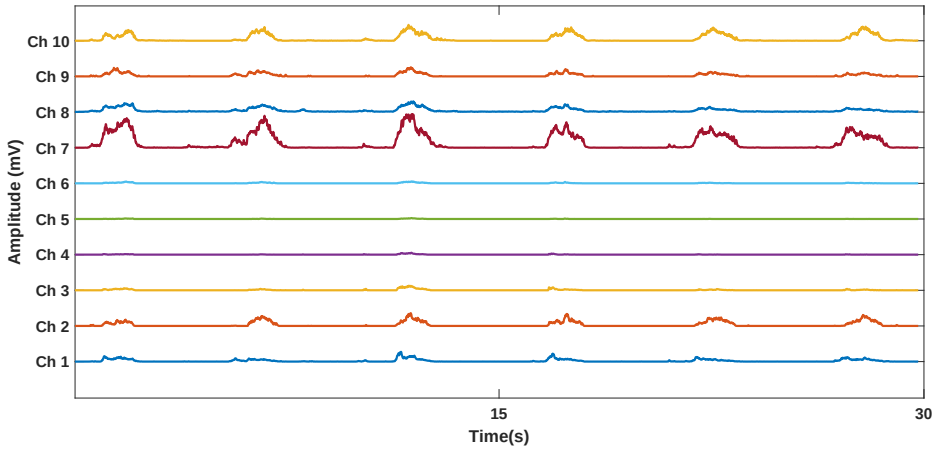

Figure 4.1: An example of 10-channel EMG recording for 6 repetitions of wrist flexion movement.

For example, Figure 4.1 is a 10-channel EMG signals of six repetitions of wrist flexion movement from the Ninapro dataset [37]. According to the "segmentation" approach for tensorisation, the EMG recording is divided into equal segments each of them consists of one repetition of the wrist flexion movement. The start and end of each movement is determined by high-resolution time-stamps provided by the Ninapro dataset [37]. The 3rd-order tensor is

constructed by stacking these repetition segments across the new $repetition$ mode as shown in Figure 4.2.

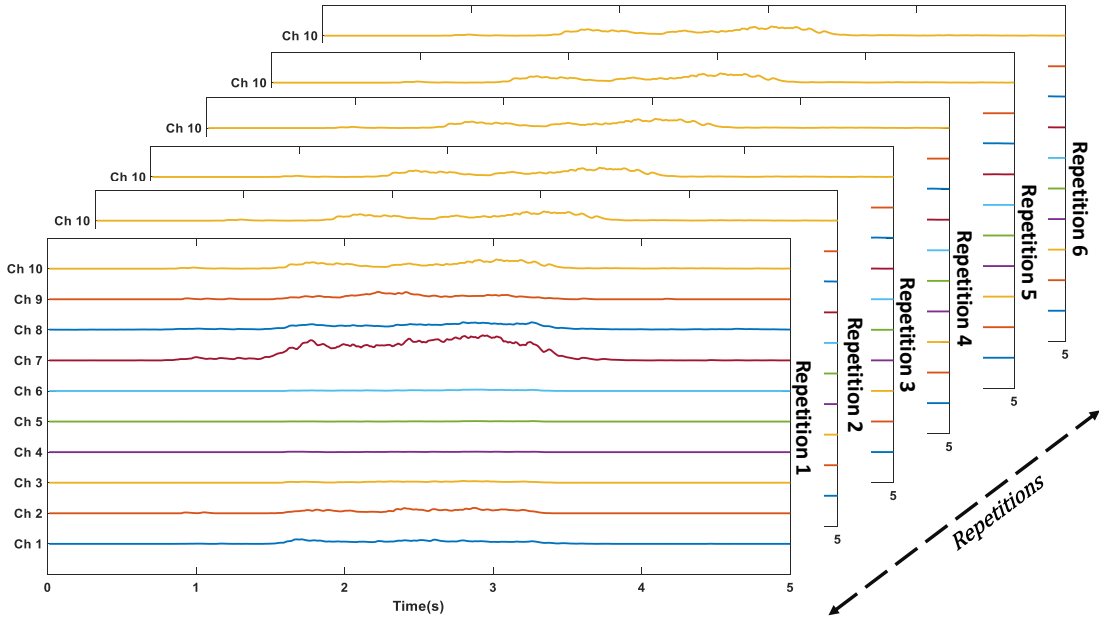

Figure 4.2: An example of 3rd-order tensor constructed via segmentation of the EMG recording shown in Fig. 4.1.

4.2.2 Fourth-order tensor

In this study, a 4$^{\text{th}}$-order EMG tensor is created by adding a $spectral$ mode to the $spatial$, $temporal$ and $repetition$ modes of 3$^{\text{rd}}$-order EMG tensor. This is based on the hypothesis that spectral information would be beneficial for synergy extraction because of the stochastic nature of an EMG signal (for more details see Section 2.2.2). We postulate that synergies have distinct spectral components since the motor unit action potential firing rate relies on the muscle's force modulation [139].

Therefore, a time-frequency analysis technique is used to estimate the spectral components from each signal (single channel activity). Wavelet analysis is applied to each EMG channel activity using the Log-normal wavelet as the mother wavelet. Since it has a logarithmic frequency resolution, the Log-normal wavelet provides increased frequency resolution compared to linear wavelets [140].

This converts a multichannel EMG epoch of a single repetition into 3rd-order tensor with

modes $spatial \times temporal \times spectral$ as shown in Figure 4.3 . Each slice of this tensor is the wavelet transform for the respective channel. Then, by concatenating these 3^{rd}-order tensors of different repetitions, a 4^{th}-order tensor $\underline{\mathbf{X}} \in \mathbb{R}^{i_1 \times i_2 \times i_3 \times i_4}$ is constructed with modes $spatial \times temporal \times spectral \times repetition$.

4.3 Muscle synergy extraction from fourth-order tensor

For the rest of the Chapter, we will work on 4th-order EMG tensors while 3rd-order tensors will be discussed in details in the following chapter. In this study, a 4th-order tensor is created for each DoF of the wrist's three main DoFs: ulnar and radial deviation (DoF1); wrist extension/flexion (DoF2); and wrist supination/pronation (DoF3) where the repetition mode consists of repetitions from positive and negative movements of that DoF. The 5-second repetition epochs are decomposed via a Log-normal wavelet into 282 frequency-bins between 0 to 50 Hz to create a 4th-order tensor for each DoFs with dimensions (500 samples$\times$10 channels$\times$282 frequency bins$\times$20 repetitions).

4.3.1 Methods

4.3.1.1 Dataset

In this study, the datasets were selected from the Ninapro first database [37, 38]. The selected dataset include EMG recordings for six wrist movements collected from 27 healthy subjects. For each subject, the dataset is divided into training and testing sets where 60% of the data (6 repetitions of each movement) have been assigned to training and 40% are testing. The data is tensorised to form separate training and testing 4th-order tensors with modes $spatial \times temporal \times spectral \times repetitions$ as discussed in Section 4.2.2. For each DoF, a training 4th-order tensor is constructed with with 12 repetitions in the $repetition$ mode divided between the positive and negative movements of each DoF, and a separate testing 4th-order tensor with 8 repetitions in the $repetition$ mode.

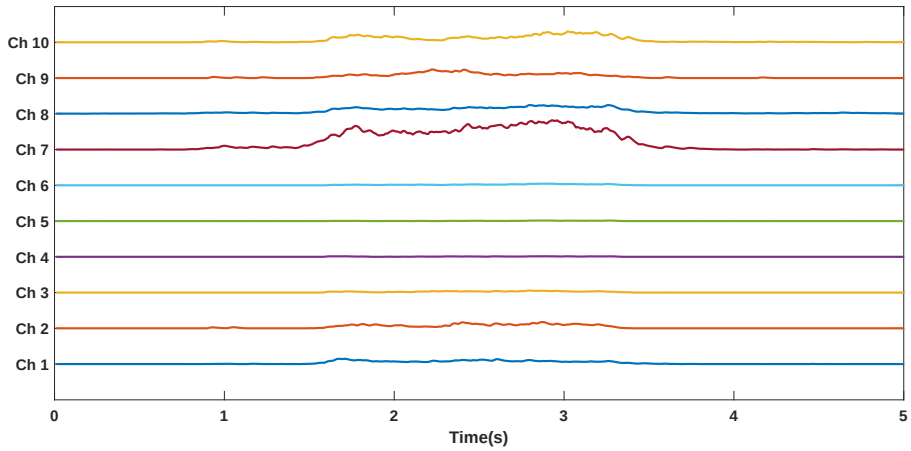

(a) 5 seconds epoch of 10-channel EMG signal for a single repetition of wrist flexion movement (also a slice of the tensor shown in Fig. 4.2).

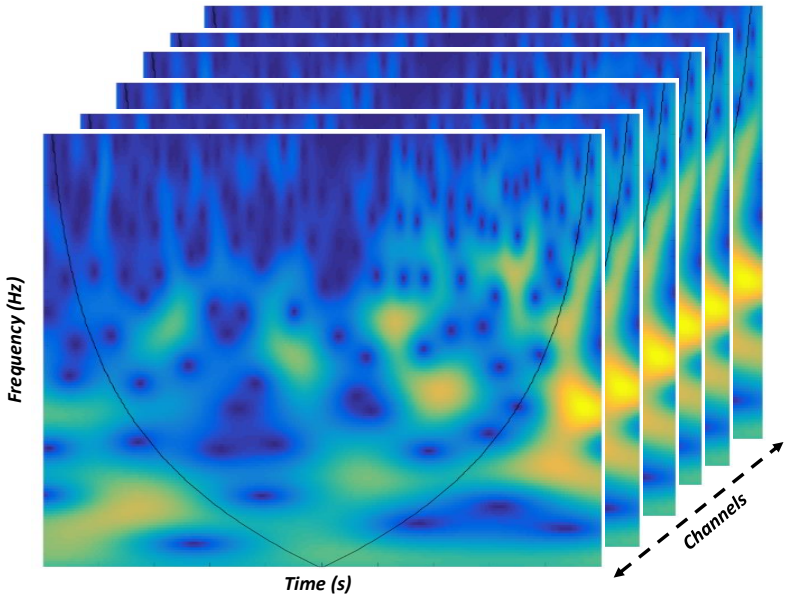

(b) A 3rd-order tensor of (10 channels × 5 seconds × 282 frequency bins) is created by applying wavelet transform on each channel activity for the segment shown in Panel 4.3a.

Figure 4.3: An EMG epoch for a single repetition (Panel 4.3a) is converted to a 3rd-order tensor with wavelet analysis (Panel 4.3b). 4th-order tensor with dimensions ($time \times channels \times spectral \times repetitions$) is constructed by concatenating these tensors for different repetitions.

4.3.1.2 Tucker decomposition for muscle synergy extraction

Several tensor decomposition models have been introduced to decompose higher-order tensors into their main components [100]. The Tucker model [136] is one of the most prominent models for higher-order tensor decomposition. In the Tucker model, the tensor is decomposed into a core tensor multiplied (transformed) by a matrix along each mode. For example, a 4$^{\text{th}}$-order tensor $\underline{\mathbf{X}} \in \mathbb{R}^{i_1 \times i_2 \times i_3 \times i_4}$ can be decomposed into smaller core tensor $\underline{\mathbf{G}} \in \mathbb{R}^{j_1 \times j_2 \times j_3 \times j_4}$ and four factor matrices of $\mathbf{B}^{(n)} \in \mathbb{R}^{i_n \times j_n}$ where $n = 1, 2, 3, 4$ as the following:

$$\underline{\mathbf{X}} \approx \underline{\mathbf{G}} \times_1 \mathbf{B}^{(1)} \times_2 \mathbf{B}^{(2)} \times_3 \mathbf{B}^{(3)} \times_4 \mathbf{B}^{(4)} \tag{4.1}$$

while "$\times_n$" is multiplication across the n^{th}-mode [141].

In general, the Tucker model is flexible in terms of number of components and permutations of each mode. Therefore, adding constraints to the Tucker model is important to reduce the possibility of numerical degeneracy [100]. In the case of muscle synergy extraction, non-negative constraints would be appropriate due to the physiological significance and the additive nature of synergies.

The non-negativity constraint would add more information to the decomposition by taking into account the additive nature of muscle synergies. It was implemented in the iteration phase of the ALS algorithm by setting the negative values of computed components to zero by the end of each iteration to force the algorithm to converge into a non-negative solution for these modes.

In order to investigate the use of tensor factorisation in muscle activity analysis, the 4$^{\text{th}}$-order EMG tensor was decomposed using the Tucker model with different settings and compared against each other. The first model was an unconstrained $\{2, 2, 2, 2\}$ Tucker model. The second model was also a $\{2, 2, 2, 2\}$ Tucker model but with a non-negativity constraint on all modes except for the $repetition$ mode. The third and final Tucker model used was a $\{3, 3, 3, 3\}$ with non-negativity constraint on the same first three modes ($spatial, temporal$ and $spectral$). The three Tucker model were applied on the DoF1 tensor for the 27 subjects. The explained variance and execution time were recorded for each decomposition.

4.3.1.3 Movement classification using Tucker decomposition

The Tucker decomposition was used to classify between the movements of each DoF. The $\{2, 2, 2, 2\}$ Tucker model was applied on the training 4^{th}-order tensors with non-negativity constraints on the first three modes ($spatial$, $temporal$ and $spectral$). The number of components were chosen to be two for each mode, since each tensor consists of repetitions of two movements. In addition, the preliminary results showed subtle differences with the change in number of components.

The $repetition$ mode was unconstrained since it will be used for movement classification. The values of training $repetition$ mode components are used to train a *k*-NN classifier (*k*=3) to classify between positive and negative movements of each DoF.

For testing, the $repetition$ mode components were estimated through direct projection of the testing tensor onto the other training components (core tensor and $spatial$, $temporal$ and $spectral$ modes). According to Equation 4.1, the testing $repetition$ mode components ($\mathbf{B}_{test}^{(4)}$) is projected as:

$$\mathbf{B}_{test}^{(4)} = \underline{\mathbf{X}}_{test}^{(i_4 \times i_1 i_2 i_3)} [\underline{\mathbf{G}}_{tr}^{(j_4 \times j_3 j_2 j_1)} (\mathbf{B}_{tr}^{(3)} \otimes \mathbf{B}_{tr}^{(2)} \otimes \mathbf{B}_{tr}^{(1)})^T]^+ \tag{4.2}$$

where $[.]^+$ is the Moore–Penrose inverse, while $\mathbf{B}^{(1)}$, $\mathbf{B}^{(2)}$ and $\mathbf{B}^{(3)}$ are the $spatial$, $temporal$ and $spectral$ modes calculated from the training dataset respectively. While $\underline{\mathbf{G}}_{tr}^{(j_4 \times j_3 j_2 j_1)}$ is the training core tensor unfolded across the $repetition$ mode (j_4).

The testing $repetition$ mode components are used as a predictor to the *k*-NN classifier trained by the training $repetition$ mode components. This has been carried out for the 27 healthy subjects. The 3 DoFs of the wrist were investigated where each DoF consists of two movements (positive and negative) and the classification accuracy was calculated for each DoF.

4.3.1.4 Movement classification using NMF

As a benchmark, the same *k*-NN classifier scheme has been trained by the synergy matrices extracted from the training dataset using NMF. According to the 2^{nd}-order model, the multichannel EMG signals are represented as a matrix $\mathbf{X}$ with dimensions (*m* channels $\times$ *n*

samples). According to this model, the multichannel EMG recordings are factorised into two lower rank matrices. The synergy matrix $\mathbf{B}^{(1)}$, which holds the channel (spatial) profile and the weighting matrix $\mathbf{B}^{(2)}$ with the temporal profile as shown in Equation 4.3.

$$\mathbf{X}_{(m\times n)} = \mathbf{B}^{(1)}_{(m\times r)} \times \mathbf{B}^{(2)^T}_{(n\times r)} \tag{4.3}$$

where r is the number of synergies or components.

In this study, the number of NMF synergies was chosen to be one synergy for each movement (two for each DoF) as in [5] and to have the same number of factors (components) as the Tucker method. NMF was applied on the testing dataset to estimate the synergy matrices which have used as a predictor to the *k*-NN classifier trained by the synergies extracted from the training dataset. The classification accuracy was calculated for each of the three wrist's DoFs for the 27 subjects.

4.3.2 Results

4.3.2.1 Tucker decomposition for muscle synergy extraction

4$^{\text{th}}$-order DoF tensors were decomposed using three Tucker models to extract synergistic information and classify between the two movements of that DoF. An unconstrained $\{2, 2, 2, 2\}$ Tucker model was used to decompose the tensor as shown in Figure 4.4. A similar $\{2, 2, 2, 2\}$ Tucker model was used but all modes except for $repetition$ constrained to be non-negative as illustrated in Figure 4.5. The third model was $\{3, 3, 3, 3\}$ Tucker model with non-negative constraints imposed on the first three modes as well as shown in Figure 4.6.

The explained variance and execution time for each decomposition were recorded across the 27 subjects for comparison. The median values were calculated and summarised in Table 4.1.

4.3.2.2 Movement classification using Tucker decomposition and NMF

The non-negative $\{2, 2, 2, 2]$ Tucker decomposition shown in Figure 4.5 was used to classify between movements of each DoF. For comparison, the $spatial$ and $temporal$ modes (synergy matrix and weighting function) were estimated from the same training data (Subject 4/ DoF1)

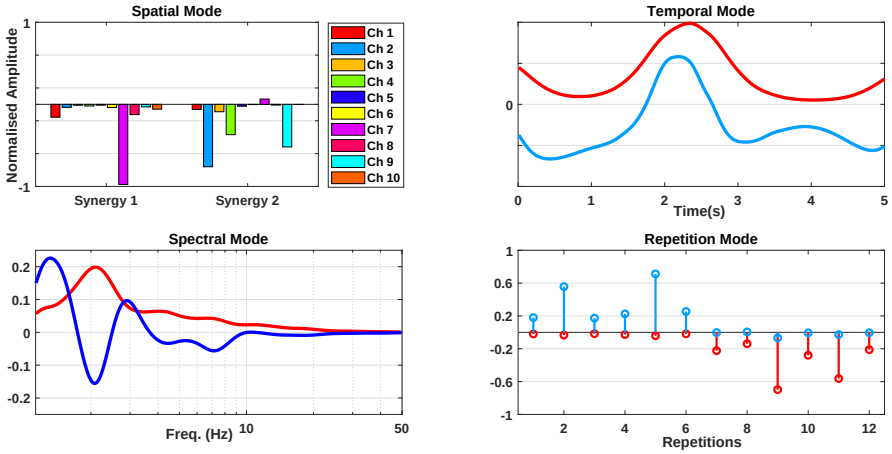

Figure 4.4: The components of unconstrained $\{2, 2, 2, 2\}$ Tucker decomposition for the 4^{th}-order EMG tensor for DoF1 (subject 4).

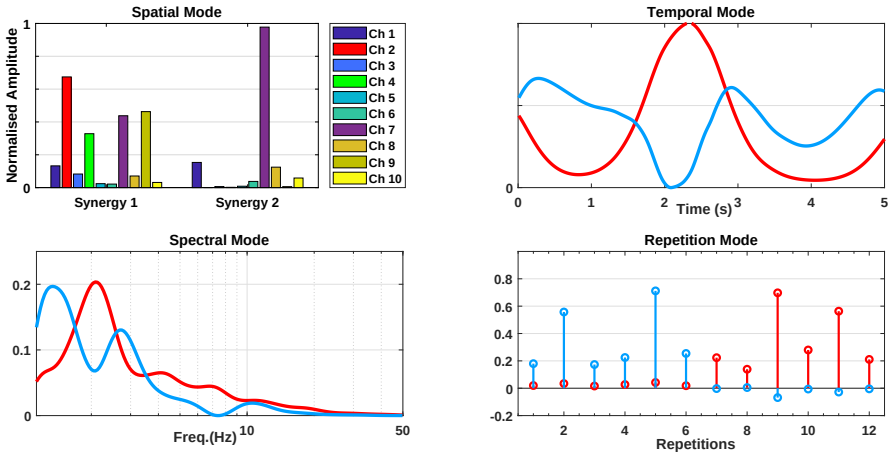

Figure 4.5: The components extracted via a $\{2, 2, 2, 2\}$ Tucker decomposition of the 4^{th}-order tensor for DoF1 (subject 4) with the $spatial, temporal$ and $spectral$ modes are restricted to be non-negative. The repetition mode components showed the difference between the two movements where the blue component has a higher values for the wrist flexion repetitions (1-6) while the red was higher in the wrist extension repetitions (6-12).

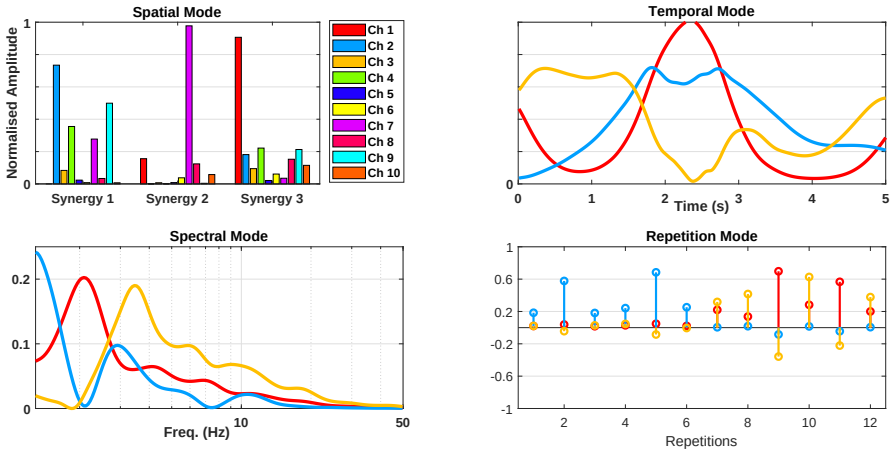

Figure 4.6: The components of $\{3, 3, 3, 3\}$ *Tucker decomposition for the* 4^{th}*-order EMG tensor for DoF1 (subject 4) with the* $spatial, temporal$ *and* $spectral$ *modes are restricted to be non-negative.*

via NMF. The extracted muscle synergies and their weighting functions were averaged across repetitions and illustrated in Figure 4.7.

Tucker decomposition and NMF were utilised to classify between two movements of the same DoF. The $repetition$ mode components extracted from the training and testing tensors were used to train and test a k-NN classifier. On the other hand, the same classifier was trained and tested with NMF synergies extracted from training and testing datasets. The classification accuracy was calculated for each DoF across the 27 subjects and the results is summarised in Table 4.2.

Table 4.1: The median explained variance and execution time for Tucker decomposition under different settings.

	Explained Variance	Time (s)
$\{2, 2, 2, 2\}$ unconstrained	62.9%	305.76
$\{2, 2, 2, 2\}$ Non-negative	60.12%	716.57
$\{3, 3, 3, 3\}$ Non-negative	69.7%	769.78

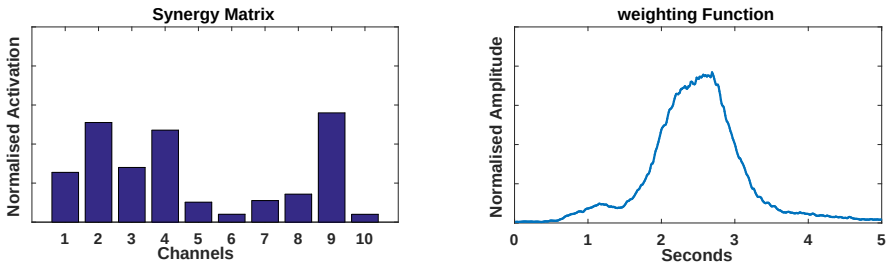

(a) Wrist flexion (Positive DoF) NMF

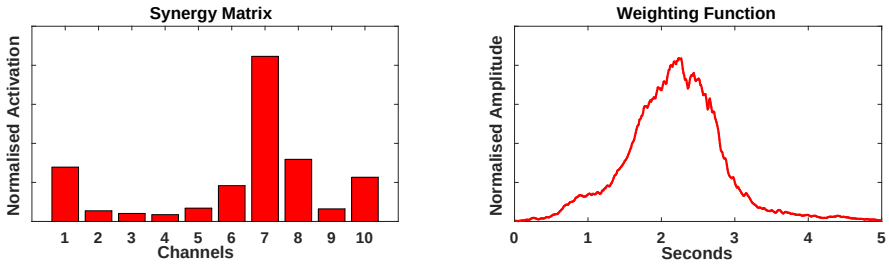

(b) Wrist extension (Negative DoF) NMF

Figure 4.7: The average synergy matrices (spatial profile) and weighting functions (temporal profile) estimated by one component NMF for DoF1 training dataset (subject 4).

4.3.3 Discussion

The comparison between the three Tucker model showed the importance of non-negative constraint to estimate comprehensible synergistic information. However, the non-negativity constraint increased the execution time and slightly decreases the explained variance. The $\{3, 3, 3, 3\}$ model increases the explained variance due to the additional component in each mode, but the computational cost increases in comparison with the non-negative $\{2, 2, 2, 2\}$ Tucker model. Therefore, we were encouraged to use the non-negative $\{2, 2, 2, 2\}$ Tucker

Table 4.2: Average classification error rate across the 27 subjects.

	Tucker	NMF
DoF1 (wrist flexion and extension)	0%	0.463%
DoF2 (radial and ulnar deviation)	0%	0.463 %
DoF3 (wrist supination and pronation)	0%	2.315%

model for movement classification as its $repetition$ mode components were consistent to differentiate between movements and provided meaningful muscle synergies can be compared with NMF synergies.

There are differences and similarities between the estimated components and synergies from both 2nd- and higher-order models. If we compare the common modes ($spatial$ and $temporal$) from Tucker and NMF, we notice two points. Firstly, there is a similarity between spatial components (synergy matrices) for each separate movement as shown in Figures 4.5 and 4.7. Although the Tucker components do not have to be directly associated with the movements due to its flexible nature, the $spatial$ mode estimated the two components (synergies) with each strongly linked to one movement in comparison with NMF.

Secondly, unlike the $spatial$ mode, the two components of the $temporal$ mode in the Tucker model are not linked directly to movements. In comparison with NMF (Figure 4.7), the weighting functions for each movement are similar since they capture the main motor activity. Thus, the first temporal component (red) in the Tucker model (Figure 4.5) represents both weighting functions while the second component (blue) expresses other activities in this time window. The same concept could be applied on the $spectral$ mode where the two components represent the lower and higher frequency elements in the data. This suggests that the tensor decompositions are better able to reveal patterns in the EMG envelope than matrix factorisation. However, this Tucker model may be unable to directly link each component in the mentioned modes to a specific movement.

Regarding the classification performance, the Tucker decomposition approach exhibited a slight improvement in classification accuracy over NMF as shown in Table 4.2. This suggests a potentially greater usefulness of higher-order tensor models also taking into account that such models can provide more descriptive information. However, this improvement in classification accuracy came at a price, as the Tucker decomposition algorithm was much more complex and computationally expensive in comparison with NMF. In addition, these results are limited by the use of off-line data and the small number of movements and DoFs.

After all, this study provides a proof-of-concept for higher-order tensor muscle synergy models. The complexity of these models could increase the computational cost but the additional modes

offer a new range of possibilities to incorporate more information.

4.4 Conclusions

The current muscle synergy model relies only on the spatial information from the synergy matrices to deduce motor control. This approach is vulnerable to many factors such as electrode re-positioning, sweat and fatigue [142]. Therefore, other factors and variables should be taken into account. The higher-order tensor muscle synergy models provide the opportunity to alleviate the effect of those factors by incorporating a more complex description of the data and its dependencies. The results suggest that tensor factorisation models can be a useful tool for muscle synergies extraction. In addition, it is encouraging to explore the potential of higher-order tensor muscle synergy model in future work.

In conclusion, we introduced and discussed the higher-order tensor models for muscle activity in this chapter. Two models were proposed for EMG data tensor construction: a 3$^{\text{rd}}$-order tensor model with $spatial \times temporal \times repetition$ modes and a 4$^{\text{th}}$-order tensor model that adds a $spectral$ mode through time-frequency analysis to the other three modes.

In addition, we conducted our first study on muscle activity analysis a via higher-order tensor model. The Tucker models were used used to decompose a 4$^{\text{th}}$-order EMG tensor and were compared to NMF model components. The results were encouraging and provided a proof-of-concept for higher-order tensor muscle synergy models.

However, the computational needs for 4$^{\text{th}}$-order tensor decomposition is high due to the time-frequency analysis and the high number of modes. This computational need may not be suitable for some applications such as myoelectric control. Moreover, it was noted that the Tucker model was unable to link its components to a specific movement especially for $temporal$ and $spectral$ modes where one of the components captured irrelevant information. The additional component in the $\{3, 3, 3, 3\}$ Tucker model improved the explained variance but with an additional increase in the computational cost.

Hence, the spectral mode is dropped from further analysis, and we will focus on the 3$^{\text{rd}}$-order model in the next chapters since synergy-based myoelectric control is one of our objectives. Using the knowledge we gained from this Chapter, we aim to improve the synergistic

information extracted from higher-order EMG tensors and decrease the computational time. We postulate that this could be achieved by constraining the Tucker model or using less flexible model (such as PARAFAC) which will be discussed in detail in the following chapter.

Chapter 5

Constrained Tucker decomposition

The work in this chapter covers the work puplished in IEEE Access in January 2019 [10].

5.1 Introduction

The results from Chapter 4 showed the potential of higher-order tensor decomposition for muscle synergy extraction. However, the addition of spectral mode to the tensor using time-frequency analysis increases the computational cost of 4^{th}-order tensor decomposition. Therefore, we focused on 3^{rd}-order tensor decomposition for muscle synergy analysis.

In this chapter, we investigate the use of higher-order tensor decomposition in muscle activity analysis and its possible application and benefits over matrix factorisation. We propose a constrained Tucker decomposition (consTD) model for muscle synergy analysis and compare it with the most prominent tensor decomposition models (PARAFAC and Tucker). Hence, we formulate an appropriate and efficient approach for consistent and meaningful muscle synergy extraction. Then we devise the consTD method to take advantage of the multi-way structure in EMG activity to extract shared and task-specific muscle synergies. The consTD method will be compared against the current traditional method that uses a 2^{nd}-order analysis model (NMF) for the the decomposition of wrist movements. This will be an illustration for advantages of higher-order tensor decomposition in muscle synergy extraction.

5.1.1 Shared and task-specific muscle synergies

To demonstrate the use of consTD of higher-order EMG tensors, a relevant problem is shared and task-specific muscle synergies identification. This problem has been addressed in a number

of biomechanical analysis studies [75, 77, 78].

The muscle synergies extracted from EMG signals recorded during one motor task can be divided into two groups. The first one is shared, or common, synergies that could be found in another motor tasks sharing some mechanical or physical characteristics with the current one. The other group is task-specific, or behavioural, synergies that are distinctive for that motor task. The existence of these two types of synergies has been observed across species, including frogs [53, 76], cats [52] and humans where different tasks were investigated to identify shared synergies such as walking and cycling [77], postural balance positions [75, 78] and normal walking and slipping [3, 72].

The current approach to estimate the shared and task-specific synergies is to apply NMF on the multi-channel EMG signals recorded during the tasks in question. This is done for several repetitions of each task and usually for a number of different subjects. Then, the synergies are rearranged across tasks, repetitions and subjects (in some cases) in order to maximise the similarity between a set of synergies, which is assumed to be shared across tasks and/or subjects. Most of the shared synergies studies rely only on correlation coefficients as a similarity metric to differentiate between shared and task-specific synergies. Nonetheless, this approach is limited by the fact that the rearrangement of synergies would have a significant effect and impact on this metric [3, 72, 77].

In addition, the natural structure of data under investigation is not taken advantage of since the procedure involves a repetitive application of analysis steps using a 2^{nd}-order model (NMF). Therefore, a higher-order model for muscle synergy would represent the data in a more natural way and will not rely on the similarity via correlation coefficients since the rearrangement process will be skipped. In this case, the data from different repetitions of tasks and subjects would benefit from structuring in a 3^{rd}-order tensor form in order to capture the (shared) synergies between movements or tasks.

5.2 Constrained Tucker decomposition

In this section, the consTD method is discussed in detail, including the number of components and different constraints imposed to improve muscle synergy extraction.

Imposing constraints on the tensor decomposition model has several benefits [7] as discussed in Section 2.4.4. Therefore, in order to extract consistent and meaningful muscle synergies, a consTD model is proposed for muscle synergy analysis. We hypothesise that this model would benefit from the flexibility and versatility of the Tucker model in comparison with PARAFAC decomposition while retaining the high explained variance. In addition, the additional constraints would result in a unique and consistent synergy extraction. This approach was inspired by the shared-synergy concept [53,76] by including additional components to account for any shared variability across movements, tasks or DoFs.

5.2.1 Number of components

In this setup, one $temporal$ component is assigned for each DoF instead of two components. Hence, information will not be segmented in multiple components as in PARAFAC since we are concerned with extracting the main muscle activity for each DoF.

For the $spatial$ and $repetition$ modes two components are assigned to each DoF to estimate a task-specific synergy for each movement. In addition, an additional component (shared) was assigned in these two modes in order to improve the data fit and account for any common variability.

5.2.2 Additional constraints

In this chapter, we propose four constraints on the Tucker model to facilitate the muscle synergy identification. Two constraints are imposed in the initialisation phase on the core tensor and $repetition$ mode components, while the other two are applied during the iteration phase of the ALS algorithm.

The core tensor is initialised to link each of the components in the $temporal$ and $repetition$ modes into their respective $spatial$ components (synergy). The core tensor is initialised and fixed (does not update with each iteration) to a value of 1 between each spatial synergy and its respective components in the other modes and 0 otherwise. This ensures that every spatial synergy is assigned to only one $repetition$ component and avoids any cross interaction. The values of the core tensor are chosen to be 1 to account for all the variability in the mode components.

In addition, since we know that each repetition in the 3rd-order tensor belongs to a known movement, we use this information in tensor decomposition by constraining the $repetition$ mode. The components of the $repetition$ mode are initialised and divided into "task-specific" and "shared" components. The task-specific components are initialised to 1 for a repetition of the considered movement or task and 0 otherwise, while the shared component is initialised by a value of 0.5 for all repetitions. Unlike the core tensor the update of this mode is not fixed to account for the variability and differences between repetitions of the same movement, alternatively, a controlled averaging constraint is used during the iteration phase.

The other two constraints on updating components in Tucker's ALS algorithm are the non-negativity on $temporal$ and $spatial$ modes and the controlled averaging on the initialised $repetition$ mode. The non-negativity constraint are imposed in order to have meaningful components (synergies) [9, 89] as discussed in Section 2.4.4.

The controlled averaging constraint aims to allow some variability within each $repetition$ component whether it is shared or task-specific. This approach will hold the structure of $repetition$ factors that was initialised without fixing it through iterations and take the differences between repetitions into account. This is implemented by modifying the iteration phase in the ALS algorithm. The estimated components are averaged after each iteration by a moving average function with window length $k = 3$. This constraint would lead to higher explained variance in the consTD model compared to fixed factors, thereby improving identification of muscle synergies.

5.3 Muscle synergy extraction from a third-order tensor

In this section, the two most widespread tensor decomposition models (PARAFAC and Tucker) are compared against the proposed consTD method for muscle synergy analysis. Synergies are extracted from 3rd-order tensors of the wrist's three main DoFs.

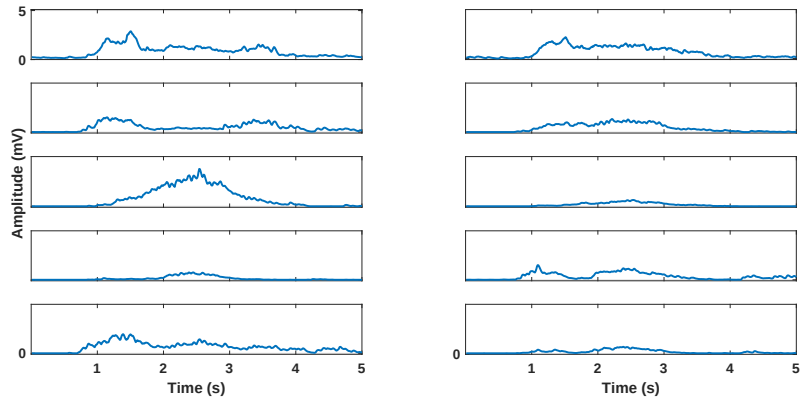

(a) 1-repetition of ulnar deviation

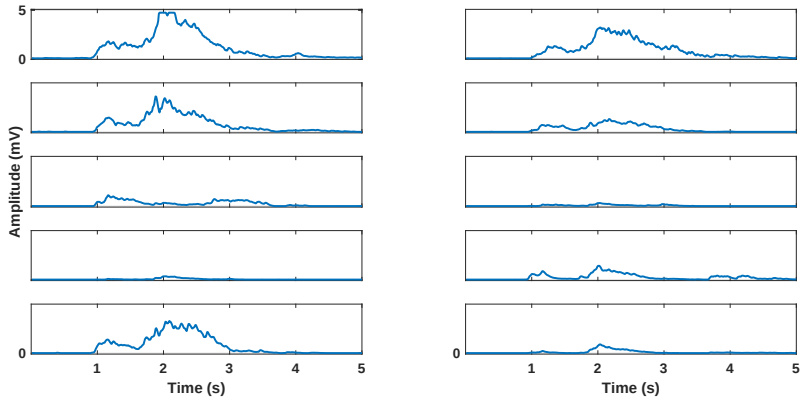

(b) 1-repetition of radial deviation

Figure 5.1: 10-channel EMG recordings of Ninapro first database for subject (1). The recording is for 1 repetition of ulnar (5.1a) and radial deviation (5.1b) movements (DoF1).

5.3.1 Methods

5.3.1.1 Tensor setup

The repetition segments from the Ninapro dataset can naturally be arranged in the form of three-way tensors with modes $(time \times channels \times repetitions)$ as discussed in details in Section 4.2. A given wrist's DoF tensor is constructed by stacking repetitions of wrist movements. For example, a 1-DoF tensor is created using ulnar (Fig. 5.1a) and radial (Fig. 5.1b) deviation movements repetitions to form a 3rd-order tensor as shown in Figure 5.2. The 2-DoFs tensor consists of 4 wrist movements repetitions; the ulnar and radial deviation in addition to wrist extension and flexion movements. Both tensors are used in the comparison

between tensor decomposition models. However, only the 1-DoF tensors are used for shared and task-specific synergies comparison against NMF for simplicity, as we introduce this application as a proof of concept.

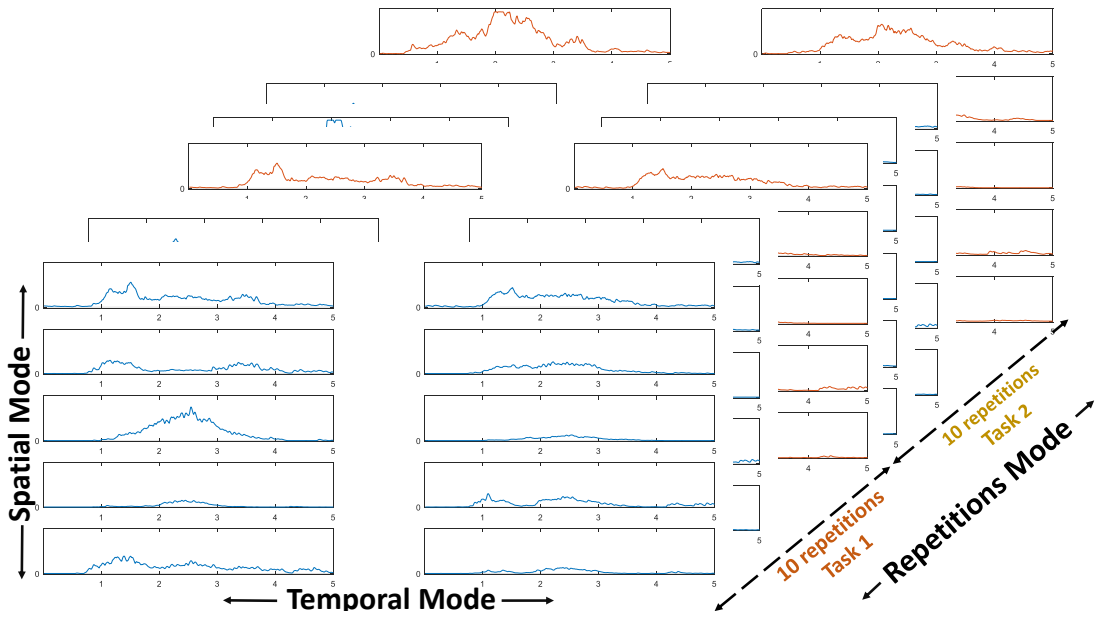

Figure 5.2: An example for tensor construction by stacking repetitions for radial and ulnar deviations movements (Fig. 5.1). 3^{rd}-order tensor is constructed with modes [10-channels× 500-samples (5-seconds) × 20-repetitions (10 repetitions for each movement)] for DoF1.

5.3.1.2 Number of components for PARAFAC and Tucker decomposition

Selecting the appropriate number of components (including synergies in $spatial$ mode) for higher-order tensor models is vital for capturing the underlying structure of the data [102]. Several mathematical approaches have been deployed to determine the appropriate number of components for higher-order tensor decomposition such as CORCONDIA [103], heuristic and approximating [143] techniques.

On the other hand, the number of synergies for the 2^{nd}-order model extracted via matrix factorisation methods have been determined using two main approaches: a functional approach, and a mathematical approach [6] as discussed in Chapter 3.

Here, the prior knowledge of the data structure (*i.e.,* number of movements) had been used to choose the number of components for PARAFAC and Tucker models. In addition, the mathematical criteria (CORCONDIA and explained variance) was used to test and compare

different numbers of components for PARAFAC and Tucker decomposition, respectively. Both the 1-DoF and 2-DoFs tensors were decomposed using PARAFAC with a set number of components (2, 3 and 4 components). This helped to guarantee each movement was identified by at least one muscle synergy. Similarly, $\{2, 2, 2\}$, $\{3, 3, 3\}$ and $\{4, 4, 4\}$ Tucker models were used to decompose both tensors since we aim to estimate at least one synergy for each movement and the number of movements are 2 and 4 in the 1-DoF and 2-DoFs tensors respectively. In order to compare both models (Tucker and PARAFAC), the number of components for the Tucker model is fixed for all modes as the PARAFAC model.

5.3.1.3 Tucker and PARAFAC models for synergy extraction

In order to examine the use of Tucker decomposition for muscle synergy extraction, both tensors (1-DoF and 2-DoFs) were decomposed with a non-negative Tucker decomposition. Three models were applied on the 3rd-order tensors with different numbers of components; $\{2, 2, 2\}$, $\{3, 3, 3\}$ and $\{4, 4, 4\}$. The time for algorithm execution is recorded for every run across the 27 subjects as well as the explained variance percentage as a metrics to compare tensor decomposition models.

On the other hand, to highlight the differences between Tucker and PARAFAC models in muscle activity analysis, 2-, 3- and 4-component PARAFAC models with non-negativity constraints are applied on the same wrist's tensors. The execution time for each run as well as CORCONDIA were recorded to compare between tensor decomposition for synergy analysis. The number of components for both methods were chosen according to the criteria discussed in Section 5.3.1.2.

5.3.1.4 Constrained Tucker decomposition for synergy extraction

The proposed consTD method is applied to the 1- and 2-DoFs tensors for muscle synergy analysis. The consTD aims to extract one synergy for each movement (task-specific synergy) in addition to a shared synergy across all movements. The number of components for consTD were $\{1, 3, 3\}$ for 1-DoF tensors and $\{2, 5, 5\}$ for 2-DoFs tensors according to the criteria discussed in Section 5.2.1.

Therefore, two components in the $spatial$ and $repetition$ modes were assigned to each DoF

in addition to an additional "shared" component in these two modes. Only one $temporal$ component is assigned for each DoF since we do not need to segment main temporal activity. Thus, a $\{1, 3, 3\}$ consTD is developed to estimate interpretable components from 1-DoF tensors, while a $\{2, 5, 5\}$ model was used for the 2-DoFs tensors.

Table 5.1: Core tensor intialisation for consTD models.

$\{1, 3, 3\}$		$\{2, 5, 5\}$	
$g_{1,n,n} = 1$	$n \in \{1, 2, 3\}$	$g_{1,n,n} = 1$	$n \in \{1, 2, 5\}$
		$g_{2,n,n} = 1$	$n \in \{3, 4, 5\}$
$g = 0$	$otherwise$	$g = 0$	$otherwise$

The core tensor is initialised and fixed for both consTD models accordingly as shown in Table 5.1. The $repetition$ mode is initialised as discussed in Section 5.2 where the task-specific components are initialised to 1 for a repetitions of the considered movement and 0 otherwise and the shared component is initialised by a value to 0.5 for all repetitions. The $repetition$ mode is constrained in the iteration phase through controlled averaging while the non-negativity constraint is imposed on the $temporal$ and $spatial$ modes.

5.3.1.5 Experimental settings

In order to compare the proposed consTD model for muscle synergy analysis with non-negative Tucker and PARAFAC models. The three algorithms were run 10 times in order to examine the uniqueness of solution by testing the ability of algorithms to converge to the same point with similar resulting components. For each run, the time of execution and explained variance were recorded for both Tucker decomposition models while CORCONDIA and execution times were recorded for PARAFAC. All decomposition models are performed using Matlab 2018A with Intel core i7 processor (2.4 GHz, 12 GB RAM).

5.3.2 Results

5.3.2.1 Tucker and PARAFAC models for synergy extraction

Three non-negative Tucker decomposition models with $\{2, 2, 2\}$, $\{3, 3, 3\}$ and $\{4, 4, 4\}$ components were applied on 1- and 2-DoFs tensors for muscle synergy extraction. Each decomposition was performed 10 times to test the ability of the algorithm to converge to the

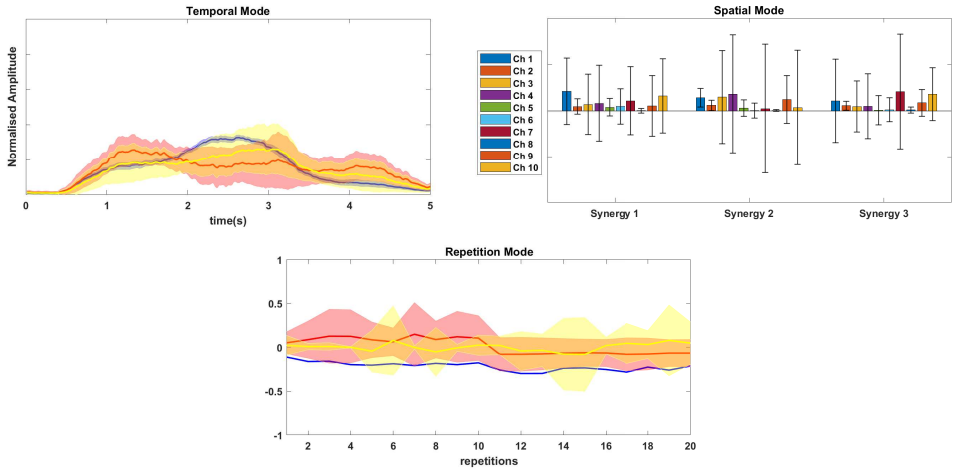

(a) The average and standard deviation for 10 runs of non-negative $\{3, 3, 3\}$ Tucker decomposition for 1-DoF tensor.

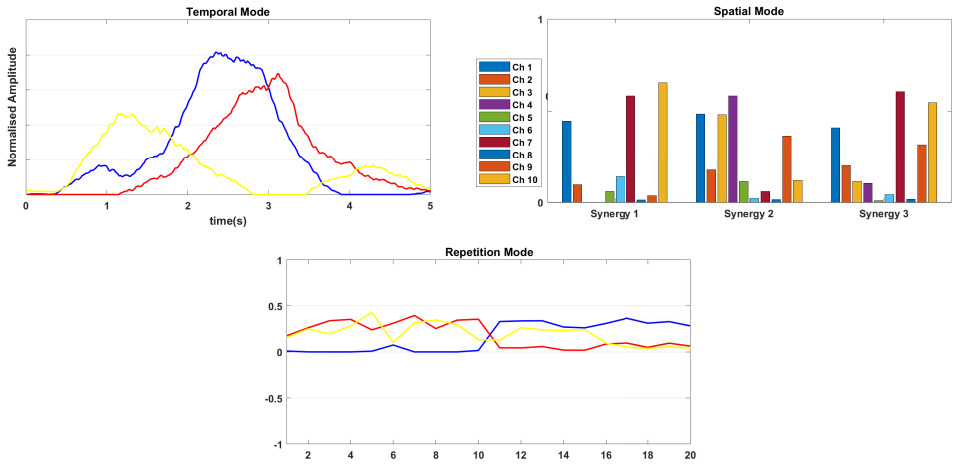

(b) The average and standard deviation for 10 runs of non-negative 3-components PARAFAC decomposition for 1-DoF tensor.

Figure 5.3: The average (solid line) and standard deviations (shaded areas) for 10 runs of non-negative Tucker (Panel 5.3a) and PARAFAC (Panel 5.3b) applied on the 3^{rd}-order tensor. Because of the uniqueness of PARAFAC solution, its standard deviation is zero as shown in Panel 5.3b. On the other hand, only one component (blue) in Tucker seems to be unique in the $temporal$ and $repetition$ mode as shown in Panel 5.3a.

same point. An example of the 10 runs of the $\{3, 3, 3\}$ Tucker decomposition for 1-DoF tensor is shown in Figure 5.3a. The explained variance and the algorithm execution time were recorded for each decomposition and the median values across the 27 subjects are summarised in Table 5.2.

The PARAFAC decomposition model was applied on both 1- and 2-DoFs tensors of wrist

horizontal and vertical DoFs. The number of components explored were 2, 3 and 4 where a non-negativity constraint was applied on all components and the algorithm run for 10 times to examine the uniqueness of solution. An example of 3-component PARAFAC decomposition on 2-DoFs tensor is shown in Figure 5.3b. The time of execution for PARAFAC algorithm as well as CORCONDIA were recorded across the 27 subjects are summarised in Table 5.3.

An example of unconstrained $\{3, 3, 3\}$ Tucker decomposition and 3-component PARAFAC is illustrated in Figure 5.4 to show the effect of non-negativity constraint on tensor synergy extraction.

5.3.2.2 Constrained Tucker decomposition for synergy extraction

The consTD models described in Section 5.2 were applied to 1- and 2-DoFs tensors for muscle synergy estimation for 10 runs across the 27 subjects. The 1-DoF tensor was decomposed using $\{1, 3, 3\}$ consTD method while the 2-DoFs tensor was decomposed using $\{2, 5, 5\}$ consTD model. The number of components is chosen to have one synergy for each movement in addition to a shared synergy between them. An example of $\{1, 3, 3\}$ consTD method for Tensor shown in Figure 5.2 is illustrated in Figure 5.5. Explained variance and execution time were recorded and the median values are shown in Table 5.4.

5.3.3 Discussion

The comparison between Tucker, PARAFAC and consTD models for muscle synergy analysis showed that Tucker decomposition can provide a good fit for the data as shown by the high explained variance percentage in Table 5.2. However, the estimated synergies via non-negative

Table 5.2: Median explained variance and execution time for the non-negative Tucker decomposition of the 27 subjects.

	1-DoF Tensor		**2-DoFs Tensor**	
No. of components	Explained Variance	Time(s)	Explained Variance	Time(s)
{**2,2,2**}	87.8%	12.5	77.5%	24.9
{**3,3,3**}	92.2%	25.7	86.4%	59.7
{**4,4,4**}	94.3%	73	89.8%	75.2

Table 5.3: The median core consistency and time of execution for the PARAFAC decomposition across the 27 subjects.

	1-DoF Tensor		**2-DoFs Tensor**	
No. of components	Core consistency	Time(s)	Core consistency	Time(s)
2	95.2%	0.39	91.1%	0.58
3	30%	0.60	64.6%	0.72
4	6%	0.91	29.3%	1.13

Table 5.4: The median explained variance and time for execution for the consTD across the 27 Subjects.

	1-DoF Tensor	**2-DoF Tensor**
No. of components	$\{1, 3, 3\}$	$\{2, 5, 5\}$
Explained Variance	78.28%	73.21%
Time(s)	0.26	0.65

Tucker decomposition were inconsistent as shown in Figure 5.3a. This also agrees with the fact that the algorithm took more iterations to converge and consequently a longer execution time as represented in Table 5.2. Despite the increase in explained variance percentage with the additional number of components, the execution time increased as well, since the algorithm could not converge easily.

On the other hand, PARAFAC was significantly faster as seen in Table 5.3, since it converged to the same local minima most of the time due to its extreme constrained structure. PARAFAC with non-negativity constraints was capable of estimating estimate muscle synergies from the 1-DoF tensor as shown in Figure 5.3b. However, PARAFAC could not deal with 2-DoFs tensors or a higher number of synergies as the decomposition deviates from the trilinear model and PARAFAC is not effective. This is illustrated with low CORCONDIA as shown in Table 5.3. In addition, synergy estimation is affected by inflexibility of the PARAFAC model as the number of components are fixed across modes. Therefore, the information of each task in the $temporal$ mode is segmented between components.

In addition to the non-negative PARAFAC and Tucker decomposition, both methods were applied on the 3rd-order tensor shown in Figure 5.2 without any constraints. The unconstrained

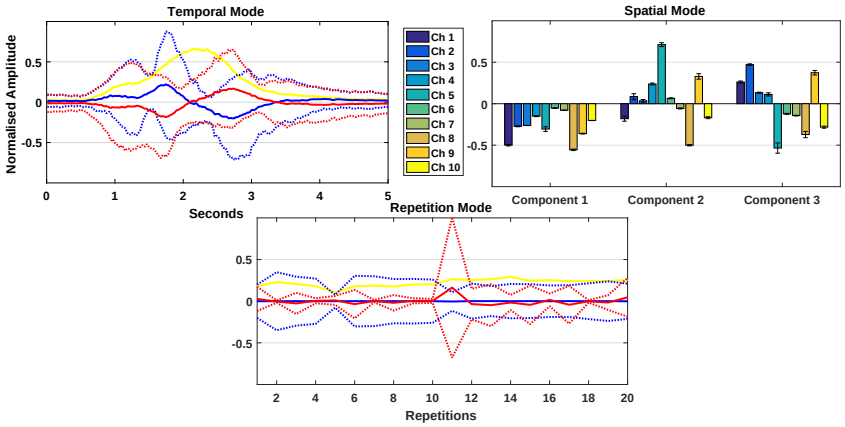

(a) The average and standard deviation for 10 runs of unconstrained $\{3, 3, 3\}$ *Tucker decomposition for DoF1 tensor.*

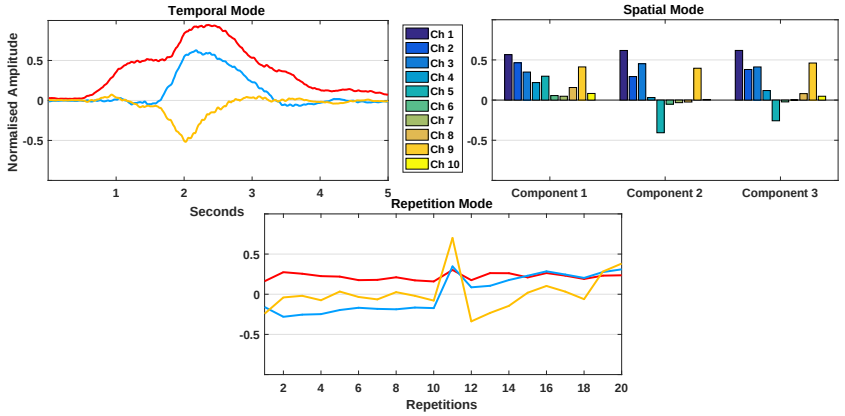

(b) The average and standard deviation for 10 runs of unconstrained 3*-components PARAFAC decomposition for DoF1 tensor.*

Figure 5.4: The average (solid line) and standard deviations (dotted lines) for 10 runs of unconstrained Tucker (5.4a) and PARAFAC (5.4b) applied on the 3^{rd}*-order tensor in Fig. 5.2.*

Tucker and PARAFAC is shown in Figure 5.4. Since the PARAFAC decomposition usually converges into the same point and its solution is unique, the standard deviation values were nearly zero for 10 runs of the algorithm as shown in Panel 5.4b. On the other hand, despite the higher explained variance of Tucker, the solution (including the core tensor) was different each run except for one factor (yellow) in the temporal and repetition modes as shown in Panel 5.4a.

Two consTD models ($\{1, 3, 3\}$ and $\{2, 5, 5\}$) were proposed to decompose the 1-DoF and 2-DoFs tensors respectively. They were able to achieve over 70% explained variance and decrease the execution time by about 10-fold compared to the non-negative Tucker model as shown in Table 5.4. Moreover, the resulting synergies were consistent over the runs as shown

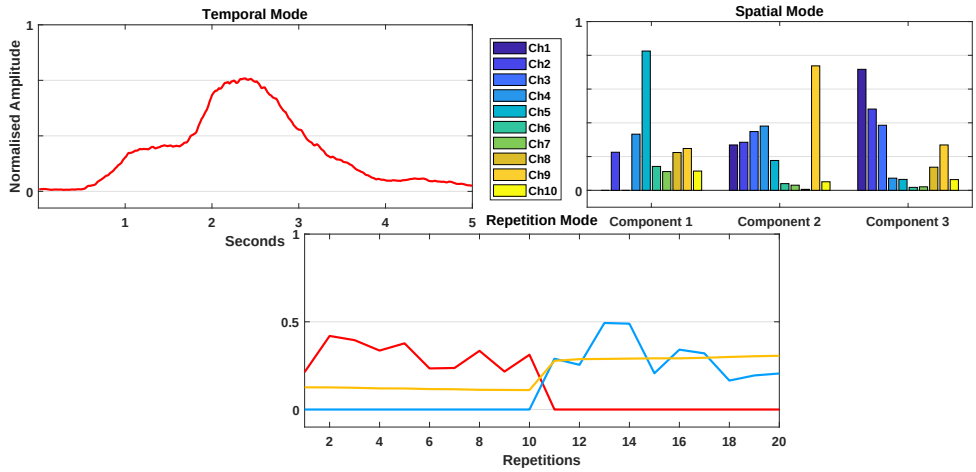

Figure 5.5: Constrained $\{1, 3, 3\}$ *Tucker decomposition for the 3*rd*-order tensor in Figure 5.2. The* $spatial$ *mode had 3 components, the first 2 components are muscle synergies specified for the ulnar and radial deviation movements while the third synergy represents the shared synergy between them.*

in Figure 5.5 unlike Tucker model. The consTD approach allocates one synergy for each movement and additional "shared" synergy to account for variability inspired by the shared synergy concept. This additional shared synergy improved the explained variance compared to $\{1, 2, 2\}$ constrained Tucker model where the median explained variance was 59.3% in the preliminary results.

Moreover, the total number of components in consTD may be greater than or equal to the number of components in traditional Tucker decomposition. However, the total number of elements for consTD is significantly less than the Tucker model. For example, the 1-DoF tensor ($500sample \times 10channels \times 20repetitions$) with the number of elements=$100,000$ is decomposed via $\{2, 2, 2\}$ unconstrained Tucker decomposition into 1060 elements in addition to 8 elements in the core tensor. On the other hand, a $\{1, 3, 3\}$ consTD can decompose the same tensor into 590 elements in addition to 9 elements in its sparse core tensor. Hence, the proposed consTD for synergy extraction is more efficient in comparison to the unconstrained Tucker model.

Hence, we conclude that the proposed consTD method is a promising solution to obtain unique and interpretable synergies from 3rd-order tensor decomposition. The non-negativity constraint is essential because of the additive nature of synergies. Moreover, the fixed core tensor is

pivotal, as we can directly relate synergies (in the $spatial$ mode) to other specific components in $temporal$ and $repetition$ modes. This is contrary to the unconstrained core tensor in Tucker model, which allows for interactions between all components in each mode. Due to these interactions, it becomes difficult to achieve a unique solution for Tucker decomposition. This increases the computational time dramatically.

5.4 Shared muscle synergy identification

In this section, the consTD method is utilised as a direct novel approach for shared and task-specific synergy estimation. This method is compared with the current standard approach of repetitive application of NMF and computation of the correlation coefficient. In addition, the consTD is tested against disarrangement of repetitions with regard to task-repetition information.

5.4.1 Methods

5.4.1.1 NMF as benchmark

NMF [3, 76, 77, 144] is used here as a comparative benchmark for shared synergy extraction. NMF processes the multi-channel EMG recording as a matrix $\mathbf{X}$ with dimensions ($channel \times time$). NMF decomposes EMG recordings into two lower dimension matrices (factors). The first component holds the temporal information (also known as weighting function) $\mathbf{B}^{(1)}$ while the other is the muscle synergy holding the spatial information $\mathbf{B}^{(2)}$ as shown in Equation 4.3 where both $\mathbf{B}^{(1)}$and $\mathbf{B}^{(2)}$ are constrained to be non-negative. For details see [145].

Since the dataset had 10 repetitions for each task, NMF was applied on each of them. The number of synergies was chosen by variance accounted for (VAF) as a metric [4]. The first step to identify the shared and task-specific synergies would be finding the reference synergy [3,77] from the 10 repetitions of that task. This is done by calculating the inter-correlation between the 10 repetitions. Since number of synergies are two, 200 correlation processes are needed to identify the reference repetition which is achieves the highest average correlation coefficient between repetitions.

The second step is to use this reference to arrange synergies within each repetition [77]. Finally, the arranged synergies are averaged to compute the first and second mean synergies for the task. Then, to identify the shared synergy of one DoF, the mentioned method is applied on the two tasks forming the DoF in question, the correlation coefficients between the resulting four mean synergies (two for each task) are calculated so that the highly correlated synergies between the two tasks are identified as shared, while the other two are considered as task-specific [3, 75, 144].

5.4.1.2 Constrained Tucker and NMF shared synergy comparison

We compared shared and task-specific synergies identified using the consTD method with those identified by using the traditional NMF and correlation method. This comparison is held since there is no ground truth about the shared and task-specific synergies. Therefore, for each wrist's DoF, three synergies are identified by Tucker (two task-specific and one shared synergy) while four mean synergies (two for each task in the DoF) are estimated using NMF. The correlation coefficient between Tucker and NMF synergies are calculated and averaged across all 27 subjects. The comparison is held between the main three wrist's DoFs: ulnar and radial deviation (DoF1); wrist extension/flexion (DoF2); and wrist supination/pronation (DoF3).

5.4.1.3 Validation with randomised repetitions

In order to provide further validation to the approach of shared synergy identification using consTD, the $repetition$ mode in the 3$^{\text{rd}}$-order tensor of each DoF was randomly shuffled to destroy any task-repetition information. The same consTD algorithm is applied on the tensor to identify the shared synergy between the two tasks. The two task-specific synergies will be corrupted since information about the tasks are missing. However, this experiment tests the ability of consTD method to identify the shared synergies without any data arrangement, something that cannot be achieved using the traditional NMF and correlation method. The shared synergies identified from the shuffled 3$^{\text{rd}}$-order tensors are compared against the shared synergies estimated from uncorrupted ones by calculating the correlation coefficients between them. The comparison is done using 15 shuffled tensors for each DoF of the main 3 wrist's DoF and the average correlation is computed.

5.4.2 Results

5.4.2.1 NMF synergies

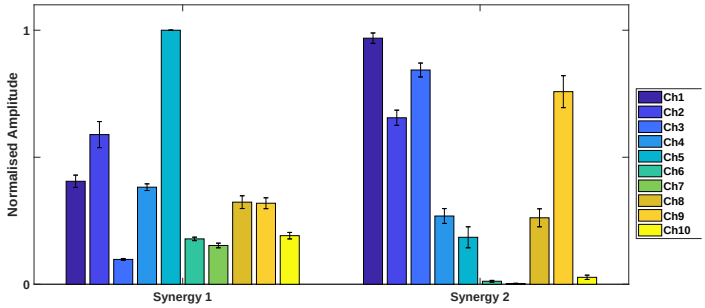

(a)

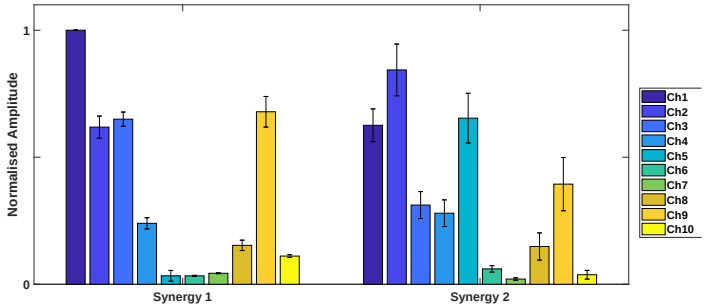

(b)

Figure 5.6: Two-component NMF for the ulnar (Panel 5.6a) and radial (Panel 5.6b) deviations movements of subject "1" averaged across 10 repetitions for each task. The second component of ulnar deviation is highly correlated with the first component of radial deviation suggesting that these are the shared synergies between those tasks.

A number of wrist tasks were selected and 10-channel EMG recording was decomposed using NMF to extract two synergies for each task. Our analysis found that two synergies could account for over 90% of the variability in data for all repetitions. For each task, NMF was applied on each of the 10 repetitions and the estimated synergies were rearranged using mutual correlation coefficients then averaged across repetitions to result in two muscle synergies for each movement. An example of the averaged synergies are shown in Figure 5.6 for the ulnar and radial deviation movements (DoF1) of subject "1".

Shared synergies are determined through correlation. As shown in Figure 5.6, the second synergy of ulnar deviation (Fig. 5.6a) is highly correlated with the first component of radial

deviation (Fig. 5.6b) with correlation coffiecent average$= 0.91$. Therefore, according to the standard NMF approach the average of these two synergies is considered as a shared synergy between the ulnar and radial deviation tasks while the remaining synergies are task-specific.

5.4.2.2 Shared synergies comparison

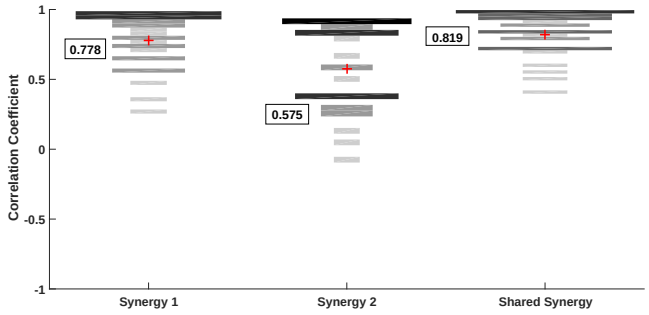

(a)

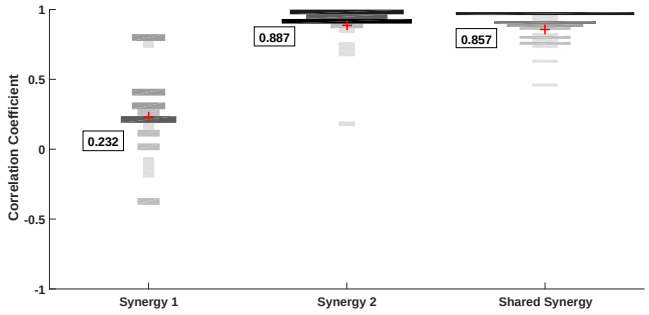

(b)

Figure 5.7: Visualisation of the histogram and mean values (red cross) for the correlation coefficients between synergies extracted by consTD method and NMF averaged synergies for ulnar (Panel 5.7a) and radial (Panel 5.7b) deviation (DoF1) for all 27 subjects.

Synergies extracted from consTD (Fig. 5.5) are compared against NMF (Fig. 5.6) synergies to test the ability of this method to identify shared and task-specific synergies. The correlation coefficients between Tucker and NMF synergies are used as a metric. This was done for three pairs of tasks (DoFs) for the wrist movements. The average correlations are summarised in Table 5.5. This was done for the 27 subjects in the dataset, where the three synergies from Tucker decomposition are compared against each averaged NMF synergies of each task. For example, the correlation coefficients between the estimated tensor synergies and NMF synergies of ulnar and radial deviation for the 27 subjects are represented in Figure 5.7.

Table 5.5: Average correlation coefficients between Tucker and NMF synergies for the 3 Main DoFs of wrist.

		Synergy 1	Synergy 2	Synergy 3
DOF 1	Ulnar deviation	0.778	0.575	0.819
	Radial deviation	0.232	0.887	0.857
DOF 2	Wrist extension	0.729	0.337	0.868
	Wrist flexion	0.408	0.776	0.880
DOF 3	Wrist supination	0.911	0.481	0.879
	Wrist pronation	0.104	0.920	0.792

The third (shared) synergy is highly correlated with both tasks as the average correlation coefficients for ulnar and radial deviation are 0.819 and 0.857, respectively. Each of the other two task-specific synergies are correlated with its respective task. For ulnar deviation, the first synergy has correlation coefficient of 0.778 compared to 0.575 for the second synergy, while for the radial deviation the second synergy has an average correlation coefficient of 0.887 compared to 0.232 with the first synergy. Similar results are found with other movements such as wrist extension/flexion and wrist supination/pronation as shown in Table 5.5.

5.4.2.3 Validation with randomised repetitions

In order to validate the approach of shared synergy identification and to show that it is robust to any repetitions disarrangement, the 3$^{\text{rd}}$-order tensor in Figure 5.2 was randomly shuffled across the $repetition$ mode to destroy the task-repetition information. The consTD was applied on the randomly shuffled tensor to identify shared synergy as shown in Figure 5.8. In comparison with the normal tensor decomposition (Fig. 5.5), we noticed that the task-specific components were different as expected since the information was destroyed. On the other hand, the shared synergy in the $spatial$ mode were very similar. The average correlation coefficients between shared synergies identified from 15 shuffled tensors and from arranged ones were found to be 0.89. This shows the ability of the algorithm to identify the shared synergy despite the corruption in the task-repetition information during the tensor construction.

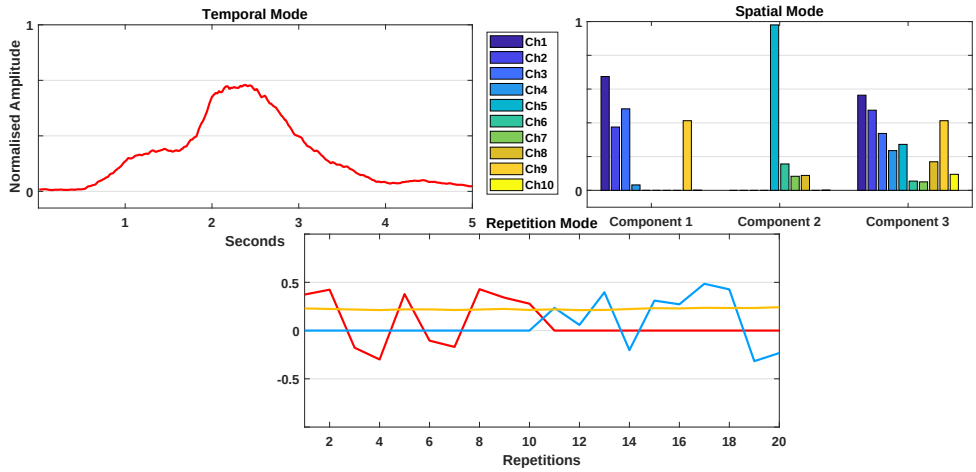

Figure 5.8: consTD for the DoF1 tensor in Panel 5.2 but with shuffled $repetition$ mode. The algorithm was able to identify the same shared synergy (third $spatial$ component) as the decomposition of the regular tensor (Fig. 5.5) even without any task-repetition information.

5.4.3 Discussion

We showed that higher-order tensor decomposition models can achieve direct identification of shared synergies without relying on any similarity metric such as correlation coefficient. This is in contrast with the current approaches for shared synergy estimation [3, 72, 77, 78, 144] which apply NMF repetitively on multi-channel EMG recordings of different repetitions and then rely on maximising the correlation coefficients between the estimated synergies with regard to a reference one. Then, shared and task-specific synergies are identified through the correlation coefficient threshold. This was illustrated in Figure 5.5 of consTD model, where component 1 and 2 in the $spatial$ mode are task-specific for the two task forming the tensor while component 3 is the shared synergy between them.

Synergies identified via consTD were compared against synergies extracted using NMF for the 27 subjects. In spite of the potential drawbacks of NMF shared synergies, we used NMF as the benchmark since there is no ground truth for shared synergies to compare both methods against. In addition, the wrist movements included in the study are limited since shared synergies are easier to identify as only two NMF synergies could explain over 90% of variance. Hence, the errors of disarrangement is minimised. This was done for 3 pairs of tasks (DoFs) for the wrist movements (Table 5.5).

The shared synergies identified by Tucker (third synergy in Figure 5.5) were highly correlated with both tasks while each of the other two tasks correlated with one task as a task-specific synergy. This highlights the ability of consTD to identify task-specific and shared synergies directly from the multi-way datasets. Further validation was performed by applying the consTD on randomly shuffled tensors without any task-repetition information. The proposed algorithm was able to estimate nearly the same shared synergy as the ordered tensor (Fig. 5.8), which indicated robustness of the method. In addition, the standard NMF approaches for shared and task-specific synergies identification are vulnerable to errors and biases since they depend on the particular arrangement of the data, the choice of the reference synergy, and the correlation coefficient threshold. This is not the case for the consTD approach where it was able to identify the shared synergy even with a shuffled tensor as shown in Figure 5.8. In addition, it is a more direct and faster alternative since there is no need to apply repetitive NMF and correlation.

5.5 Conclusions

Usually, the shared and task-specific synergies are identified in a study of complex multi-joint movements such as gait and posture analysis [3, 72, 77]. However, we chose simple wrist movements for a few reasons. Firstly, this is a first study to show how higher-order tensors could be beneficial for muscle synergy analysis. Secondly, wrist movements are simple tasks that can be described by two synergies as mentioned before. Therefore, shared synergies can be identified easily with minimum disarrangement errors for good comparison and validation for our proposed tensor approach. Finally, we are interested in upper-limb myoelectric control and looking to the shared synergy concept as an inspiration for proportional myoelectric control based on muscle synergies in the future.

Moreover, the main aim for this is study is to highlight the potential of a higher-order tensor model for muscle activity analysis especially extracting muscle synergies. Hence, consTD could be extended to various applications by converting the information we have into the right set of constraints. For example, this approach could be extended to estimate the shared synergies across subjects to explore the subject-specific synergies [75]. In addition, and in relation to the point above, different sets of constraints could help to develop a myoelectric control based on muscle synergies as in [146].

We conclude that constraints play an important role in achieving effective muscle synergy analysis. For instance, the identification of shared and task-specific synergies is not viable with PARAFAC despite having a unique solution as purely trilinear model would be too strict. Unconstrained Tucker has higher explained variance but it is not suitable since its solutions are not unique and hard to interpret. Therefore, a consTD model is a more appropriate model for this application. In this sense, identifying the shared and task-specific synergies across tasks are a good example for utilising tensor decompositions to benefit from the multi-way structure of EMG datasets.

In summary, we introduced tensor decomposition models (PARAFAC and Tucker) for muscle synergy extraction and compared their use in EMG analysis to extract meaningful muscle synergies with a proposed consTD model. The developed method was the best approach for muscle synergy estimation by providing unique and interpretable synergies with high explained variance and short execution time. The proposed consTD model can be used to identify shared and task-specific synergies. The results were compared against the standard NMF approach using data from the publicly available Ninapro dataset. The consTD method was more suitable to the multi-way nature of the datasets without relying on similarity metrics or synergies arrangements. Furthermore, it provided more direct and data-driven estimations of the synergies in comparison with NMF-based approaches, making our approach more robust to disarrangement of repetitions and the loss of task-repetition information.

Thus, we expect that this study will pave the way for the development of muscle activity processing and analysis methods based on higher-order techniques. For instance, in the next chapter we will provide the consTD method with different set of constraints to utilise it in a proof of concept for synergy-based myoelectric control application.

Chapter 6

The use of tensor synergies for myoelectric control

The work in this chapter has been reported in IEEE/EMBC conference on Neural Engineering (NER 2019) [11] and in [12] currently under preparation.

6.1 Introduction

EMG has been used for decades to control prostheses [147]. In addition to the conventional direct control approach, the current state-of-the-art methods for prosthetic upper-limb are usually based on pattern recognition techniques [148] which has been successful in achieving high classification accuracy for a range of motions (10 classes) [115] (for more details see Section 2.5). Moreover, pattern recognition-based systems recently found their way into commercial products such as "Complete Control" [1].

However, pattern recognition systems generally provide sequential control schemes [35] and natural limb movements consist in the simultaneous and proportional activation of multiple DoFs [149]. In the recent years, muscle synergies have been utilised in prosthesis control to achieve a simultaneous and proportional myoelectric control across multiple DoFs [5, 118]. Most approaches for upper-limb synergy-based myoelectric control [89, 95, 119] rely on a matrix factorisation algorithm (usually NMF) to extract muscle synergies from a training multichannel EMG dataset. Then, the extracted synergies are used to estimate continuous control signals from a testing dataset for proportional and simultaneous myoelectric control.

[1] https://www.coaptengineering.com/

Synergy-based myoelectric control schemes need to identify the muscle synergies and their weighting functions associated with a single-DoF. In this way, a control signal which corresponds to this DoF can be estimated through matrix factorisation. However, NMF is unable to extract the specified DoF synergies without further conditions imposed on the protocol. To tackle this problem Choi and Kim [89] chose a completely supervised approach using a joint synergy matrix. Jiang *et al.* [95] proposed a semi-supervised approach named "divide and conquer" method, which was used in a number of studies [5, 119]. This was done by designing an experimental protocol to estimate muscle synergies and their respective weighting function for a single DoF at a time. This method limits the factorisation into a few possible solutions, which allows simultaneous and proportional EMG control without multi-DOF training data. Recently, Lin *et al.* [118] introduced a SNMF algorithm since the lack of sparseness in the solution is one of the notable drawbacks for NMF [83, 150]. In addition, some recent studies suggest the sparse nature of muscle synergies [6, 130]. The SNMF algorithm was utilised to identify control signals from two DoFs training datasets where synergies are assigned to their respective DoF after matrix factorisation which makes it a quasi-supervised approach.

The performance of proportional myoelectric control based on NMF synergies degrades significantly with the increase of the task-space dimension into 3 DoFs of movement [5, 119]. In addition, the current approaches assign two synergies to each DoF (1 synergy per movement). Thus, the number of synergies needed for control increases with the number of tasks [142].

We hypothesise that tensor decompositions could help to solve this problem by incorporating the movement and DoF information into the decomposition process. Hence, control signals for each DoF can be extracted directly with an appropriate tensor decomposition method.

In this chapter, we will discuss and explore the potential application of higher-order tensor decomposition in myoelectric control. We will propose a consTD model for muscle synergy extraction that can be used for synergy-based myoelectric control. It will be compared with the current matrix factorisation models for synergy extraction. First, in Section 6.2, we will discuss the consistency of tensor Synergies with the increase of task dimensionality and compare it to NMF. We hypothesise that, in order for the tensor synergies to be useful in proportional

myoelectric control, they need to be consistent when extracted from different numbers of DoF. Then in Section 6.3, the consTD model will be used to estimate DoF control signals that can be utilised for proportional myoelectric control. It will be compared against the state-of-the-art synergy extraction techniques that have been used in synergy-based myoelectric control in the recent years.

6.2 Consistency of tensor synergies over the increase of task dimensionality

In this section, the potential use of tensor synergies in proportional myoelectric control is explored by first analysing their consistency. We hypothesise that, in order for tensor synergies to be useful in proportional myoelectric control, they need to be consistent when extracted from different numbers of DoF. Thus, we investigate the ability of a proposed consTD method to extract muscle synergies from 3-DoFs (6 movements) tensors. The 3^{rd}-order tensors will be constructed by repetitions of the six movements (tasks) that form the main three wrist's DoFs. Synergies estimated from this 3-DoFs tensors will be compared with synergies identified by decomposition of 1-DoF tensors to test if they are consistent when increasing the task dimensionality from 1 to 3 DoFs.

6.2.1 Methods

6.2.1.1 Data and tensor construction

In this study, six movements were selected from the publicly available Ninapro first data-set [38]. The wrist motion and its three DoFs wrist flexion and extension (DoF1), wrist radial and ulnar deviation (DoF2); and wrist supination and pronation (DoF3); are investigated since they are essential for myoelectric control [5]. Each movement has 10 repetitions from 27 able-bodied subjects.

3^{rd}-order tensors are created by stacking 10 repetitions of the 10-channel EMG segments as discussed in Section 4.2.1. Two types of tensors were used in this study. The first is a larger 3-DoFs tensor which consists of repetitions from the six wrist movements stacked together. On

the other hand, a smaller tensor for a single DoF (1-DoF) is created from repetitions of the 2 movements of that DoF.

6.2.1.2 Constrained Tucker decomposition

As we concluded from Chapter 5, consTD is a promising approach for meaningful synergy extraction. In this study, a similar consTD was used to extract task-specific synergies and one shared synergy for each DoF. Since the significance of shared synergies and the ability of tensor synergies to identify them was established in Chapter 5, the constraints on the consTD are modified accordingly to improve its performance with a larger tensor of multiple DoFs. A detailed comparison is made between both approaches in Appendix **B** which showed how the approach improved the explained variance and execution time. The new set of constraints and number of components of the proposed consTD are described in this section.

The number of components were designed to be the same as the number of movements (tasks) (n_{mov}) for the $temporal$ and $repetition$ modes. On the other hand, the number of spatial components (synergies) would be the sum of the number of task-specific and shared DoF synergies, that is, $1.5n_{mov}$ since we assume one shared synergy for each DoF (2 movements).

Three constraints have been imposed on this $\{n_{mov}, 1.5n_{mov}, n_{mov}\}$ Tucker model. Two of them were used during the initialisation phase and one constraint was implemented in the iteration phase of ALS.

Both core tensor and $repetition$ mode were initialised and fixed to identify the $spatial$ mode components (synergies). Since each component is linked to one movement, each component in $repetition$ mode was designed to have a value of 1 for a repetition of the considered movement and 0 otherwise.

The second constraint is the initialisation of the core tensor into a value of 1 between each component in the interaction between ($temporal \backslash repetition$) modes and its respective spatial synergy (either task-specific or shared) and 0 otherwise. The task-specific synergies are linked to one component in the $temporal$ and $repetition$ modes while the shared synergies are linked to the two components that form the desired DoF. This core set-up that does not update with every iteration avoids undesired cross interactions between spatial components (synergies) and

other mode's components. The values of the core tensor are chosen to be 1 in order to hold any variability in components rather than in the core tensor.

For the iteration phase, only the non-negativity constraint has been imposed on $temporal$ and $spatial$ modes because of the additive nature of synergies [6]. According to this setup, the shared DoF synergies are identified by the core tensor link with its respective components in the $temporal$ and $repetition$ mode, unlike the consTD proposed in Chapter 5 where shared synergies were identified by the moving average constraint on the additional repetition component. This would help when the 3$^{\text{rd}}$-order tensor consists of multiple DoFs and more than one shared synergy is needed to be identified as in our case.

6.2.1.3 Comparison between single and 3-DoFs tensors synergies

The $\{n_{mov}, 1.5n_{mov}, n_{mov}\}$ consTD was applied to both single (1-DoF) and 3-DoFs 3$^{\text{rd}}$-order tensors described in Section 6.2.1.1. The 1-DoF tensor is decomposed into $\{2, 3, 2\}$ components giving three muscle synergies, two of which are task-specific and one shared across the DoF. On the other hand, the 3-DoFs tensor is decomposed into $\{6, 9, 6\}$ components, with nine synergies (six task-specific and three shared).

For each subject, synergies are extracted from both tensors, then compared against each other to test the consistency of the estimated synergies with the increase of task-dimensionality from 1-DoF to 3-DoFs. Two similarity indices (Pearson Correlation coefficient and cosine of angles) were computed between each synergy estimated from single DoF tensors and its respective synergy from the 3-DoF tensor for the 27 subjects. The mean values for correlation coefficients of synergies are calculated across subjects.

6.2.1.4 NMF as a benchmark

The same approach for comparing synergies extracted from the data of one and three DoFs was applied using NMF as a benchmark for the proposed consTD method. Six muscle synergies were extracted from one epoch consisting of the EMG recordings for the three wrist's DoFs (six movements). Those synergies were compared against synergies extracted from EMG epochs for each DoF individually. The number of synergies were chosen to be two and six for the 1-DoF epochs and the 3-DoFs epoch respectively to assign each movement to one synergy.

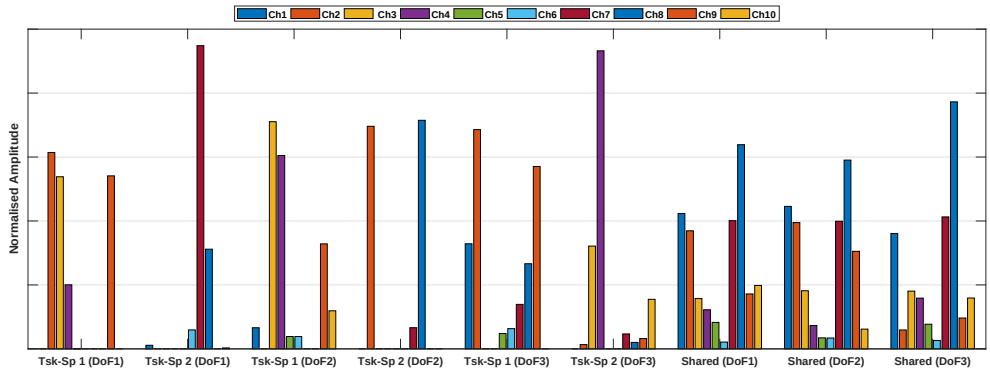

(a) Synergies extracted from a tensor with all 3 DoFs.

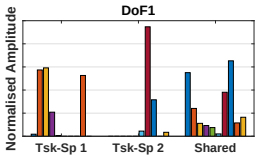

(b) from the DoF1 tensor.

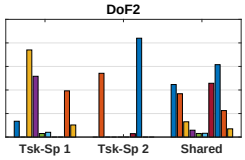

(c) from the DoF2 tensor.

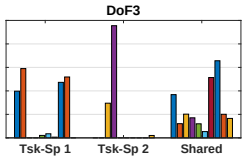

(d) from the DoF3 tensor.

Figure 6.1: The spatial mode (synergies) estimated via consTD method from a 3^{rd}-order tensor of all three wrist DoFs (Panel 6.1a) and synergies estimated separately from 3^{rd}-order tensor of DoF1 (Panel 6.1b), DoF2 (Panel 6.1c) and DoF3 (Panel 6.1d) using the same consTD method for subject 1.

Since the traditional NMF method does not identify each synergy to its respective movement, the same approach used in shared synergy studies of arranging synergies to maximise the correlation coefficient was used here. This was performed on the 27 subjects where the mean values for correlation coefficients were calculated across subjects.

6.2.2 Results

Muscle synergies of the three wrist DoFs were extracted using consTD applied to two 3^{rd}-order tensor setups. The first one is a 3-DoF tensor including the repetition of all six movements decomposed to $\{6, 9, 6\}$ components with 9 synergies (six task-specific and three shared) as shown in Figure 6.1a. The other approach uses a 1-DoF tensor including the repetition of two movements decomposed by consTD to $\{2, 3, 2\}$ components where two task-specific synergies and one shared are identified. This is done for each DoF separately as shown in Figure 6.1b, 6.1c and 6.1d for DoFs 1, 2 and 3 respectively.

The correlation coefficient and cosines of angles were computed between synergies extracted from 1-DoF tensor and their respective synergies estimated by the decomposition of 3-DoFs

tensors. The mean values of cosine similarity measures were> 0.88 as represented in Table 6.1. The correlation coefficients for the 27 subjects is represented as boxplots in Figure 6.2. The mean values for DoF1 were 0.899 and 0.968 for task-specific (*tsk-sp*) synergies and 0.936 for the shared synergy as shown in Figure 6.2a. On the other hand, 0.868 and 0.918 were the mean values of the correlation coefficient for DoF2 task-specific synergies and 0.854 for shared synergy (Figure 6.2b). Finally, 0.777, 0.783 and 0.723 were the mean values for DoF3 as shown in Figure 6.2c.

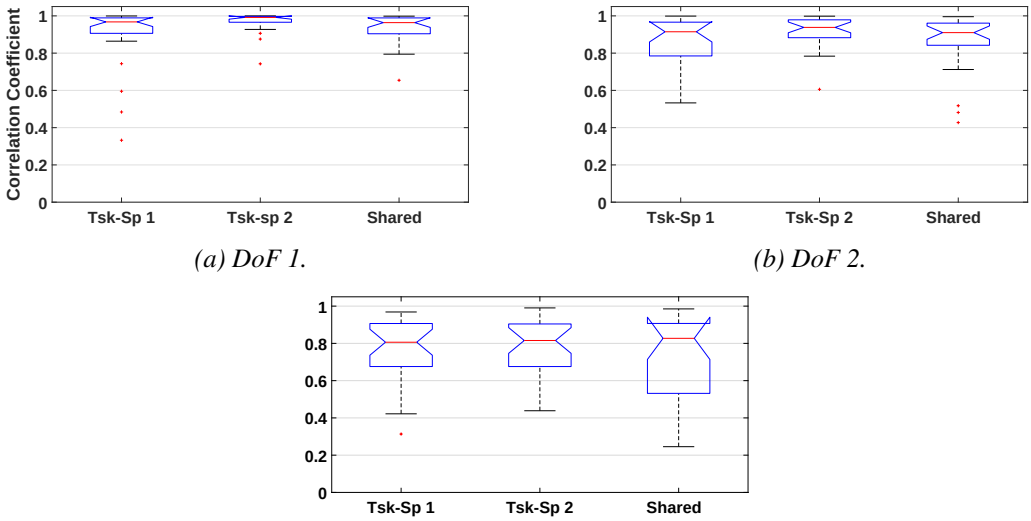

(a) DoF 1.

(b) DoF 2.

(c) DoF 3.

Figure 6.2: Boxplots for correlation coefficients between synergies extracted from the 3 DoFs tensor and from single DoF tensors for the 27 subjects. Each panel shows the correlation coefficients of the 3 synergies (2 task-specific and 1 shared) estimated from DoF1 (6.2a), DoF2 (6.2b) and DoF3 (6.2c) and their respective synergies estimated from the all 3 DoFs tensor.

Table 6.1: The mean of cosine angles between synergies extracted from 3-DoFs tensor and single DoF tensors across the 27 subjects.

	Task-sp. Synergy 1	Task-sp. Synergy 2	Shared Synergy
DoF1	0.963	0.986	0.979
DoF2	0.942	0.958	0.957
DoF3	0.881	0.887	0.909

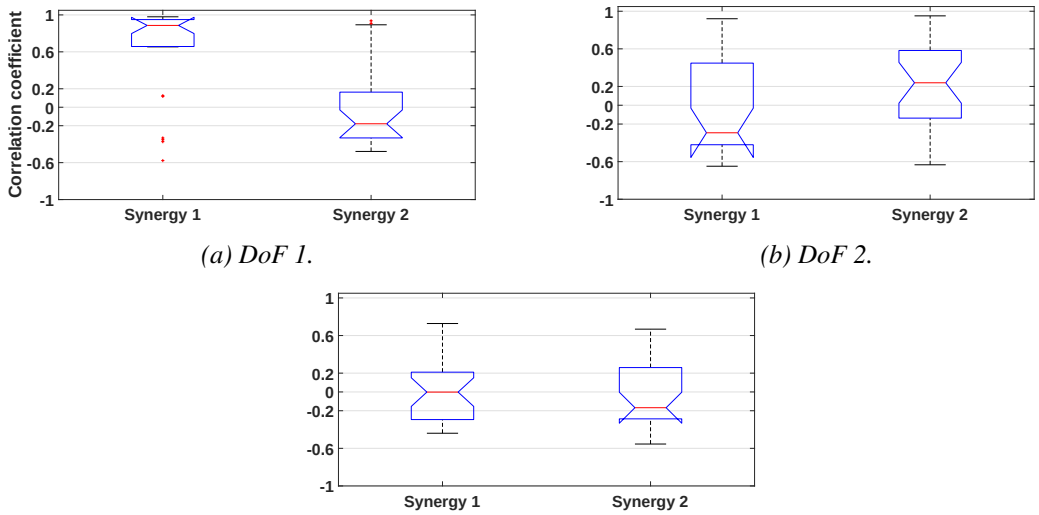

(a) DoF 1. *(b) DoF 2.*

(c) DoF 3.

Figure 6.3: Boxplots for correlation coefficients between the six synergies extracted via NMF from the EMG segment of all 3 DoFs and from single DoF segments for the 27 subjects.

6.2.3 Discussion

The ability of consTD to extract consistent muscle synergies with the increase of task dimensionality from one to three DoFs was investigated to assess the potential use of muscle synergies in proportional myoelectric control. Synergies extracted via consTD methods from 3-DoF tensor were similar to those extracted separately from 1-DoF tensors as shown in Figure 6.2 and Table 6.1. This supports the use of tensor factorisation to estimate synergies since the extracted profiles would not depend on the number of DoFs when considering the three DoFs of the wrist.

In the case of NMF, the results were notably worse than those of tensor synergies since the NMF approach cannot link the extracted synergies to their respective movements. Hence, studies utilised muscle synergies for myoelectric control [5, 119] used to divide the data into a 1-DoF segments and extract 2 task-specific synergies from each segment separately via NMF. Lin *et al.* [118] tried to solve this issue using SNMF to identify 4 task-specific synergies from a 2-DoFs segment. However, they need to label extracted synergies since NMF will not extract them in a fixed order. In contrast, the consTD approach can estimate consistent identified synergies directly from 3-DoFs data. Moreover, the Tucker model can extract three synergies for each DoF by incorporating additional shared synergy unlike NMF where only two synergies

are estimated for each DoF.

6.3 Tensor synergies for proportional myoelectric control

Given the consistency of the synergies extracted with consTD, in this section explore its potential use for proportional myoelectric control. The EMG data is tensorised by adding a $movements$ mode to the $spatial$ (channels) and $temporal$ (time) modes to create a 3rd-order tensor. Muscle synergies will be estimated from this tensor via consTD. Control signals for each DoF will be estimated through direct projection of the extracted synergies. In order to assess this approach, control signals will be compared against synergies extracted via NMF and SNMF using two publicly available datasets.

6.3.1 Methods

6.3.1.1 Data and tensor construction

Two datasets from the publicly available Ninapro [37,38] were used in this study (more details in Section 2.2.4). The data were divided into training and testing sets with 60% of the data assigned to training for each subject. In the case of dataset-1, the training consists of six repetitions while four repetitions are assigned for testing datasets. Four repetitions are assigned to training and two repetitions for testing in the case dataset-2. The wrist motion and its three DoFs are investigated. Therefore, six movements are selected to represent wrist's DoFs which are: the wrist radial and ulnar deviation that creates the horizontal Degree of freedom (DoF1); wrist extension and flexion movements which form the vertical DoF (DoF2); and finally wrist supination and pronation (DoF3).

3rd-order tensors were created in a similar way as discussed in Section 4.2.1. However, instead of stacking repetitions to form a $repetition$ mode, the whole training EMG segments of each movement are stacked to form a tensor with $temporal \times spatial \times movements$ modes as shown in Figure 6.4c.

In this study, the training tensor is designed to have four different movements where a pair of them make a wrist's DoF. This results in three training tensors for each subject where each one

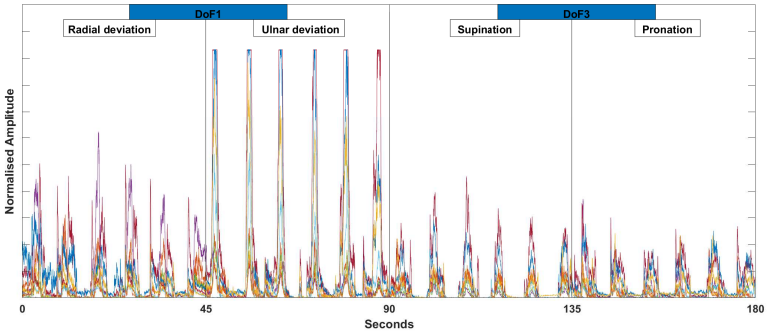

(a) An example of the 10-channels surface EMG training dataset for DoF1-3. It consists of 6 repetitions for the 4 wrist's movements forming DOF1-3 (radial/ulnar deviation and supination/pronation).

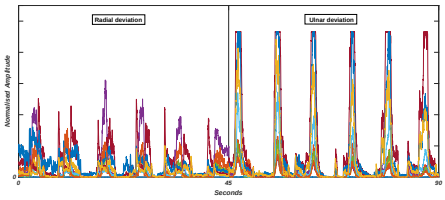

(b) The data preparation for NMF and SNMF to estimate the muscle synergies for DoF1.

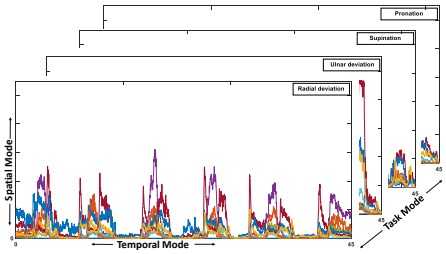

(c) 3^{rd}-order tensor for DoF1-3 with modes (time$\times$ Channels $\times$ movements).

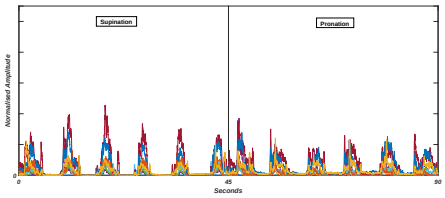

(d) The data preparation for NMF and SNMF to estimate the muscle synergies for DoF3.

Figure 6.4: An example for training data preparation and tensor construction for subject 6 and DoFs 1 and 3. Panel 6.4a shows the whole recorded segment for the 6 training repetitions of the 4 movements. Data preparation for both NMF and SNMF methods are illustrated in Panels 6.4b and 6.4d, The data is divided into two separate segments for each DoF and NMF is applied to estimate 2 muscle synergies from each segment (1 for each movement). Panel 6.4c shows the 3^{rd}-order tensor construction by stacking the 4 movements in panel 6.4a as separate slabs. Tensor decomposition is applied to directly estimate 6 synergies (4 task-specific and 2 shared).

consists of two wrist's DoF (4 movements). The three tensors are named DoF1-2 for horizontal and vertical DoFs; DoF1-3 for horizontal and inclination DoFs; and finally, DoF2-3 for vertical and inclination DoFs.

6.3.1.2 Constrained Tucker model

In this study, the same consTD presented in Section 6.2.1.2 was used to facilitate the extraction of muscle synergies (task-specific and shared) that could be utilised in myoelectric control. The only difference is the 3rd-order EMG tensor on which the consTD is applied. Here, the third additional mode to the $temporal$ and $spatial$ is $movements$ mode instead of $repetitions$ as described in Section 6.3.1.1. This change in tensor construction is due to few reasons. Firstly, it test the ability of the proposed consTD to work with different settings and data construction. Secondly, work on data structure similar to other synergy-based myoelectric control approaches under comparison, since NMF or SNMF are applied on EMG segments of several repetitions not on each repetition separately which will be discussed in details in Section 6.3.1.3.

The constraints are the same as the consTD in Section 6.2.1.2. Two constraints are imposed during the initialisation phase and one constraint in the iteration phase. For initialisation, the core tensor is initialised and fixed into a value of 1 between the interactions between components in the ($temporal \backslash movements$) modes and its respective spatial synergy and 0 otherwise as the following:

$$\begin{aligned} g_{n,n,n} &= 1 \quad n \in \{1,2,3,4\}, \\ g_{n,5,n} &= 1 \quad n \in \{1,2\}, \\ g_{n,6,n} &= 1 \quad n \in \{3,4\}, \\ g_{i,j,k} &= 0 \quad otherwise. \end{aligned}$$

The second initialisation constraint is fixing the $movements$ mode components since we have the information about each component and its corresponding movement. The non-negativity constraint on $temporal$ and $spatial$ modes is the only constraint in the iteration phase. Moreover, the algorithm would run for ten times to ensure that the model has not converged into local minima and the decomposition with the highest explained variance is chosen.

This consTD approach results in four task-specific synergies and two additional DoFs synergies in the spatial mode. The additional DoFs synergy are a shared synergy between the two movements (tasks) that form that DoF. This is determined by the set-up of the core tensor for the 5th and 6th factors (synergies) as shown above.

6.3.1.3 Matrix factorisation Models

In order to evaluate the tensor-based approach for proportional myoelectric control, we introduce NMF and SNMF as state of the art benchmarks to compare to.

In the recent years, NMF has been proposed for a proportional myoelectric control approach based on muscle synergies [5]. NMF processes the multi-channel EMG recording as a matrix $\mathbf{X} \in \mathbb{R}^{m \times n}$ with dimensions $(channel \times time)$. This matrix is factorised into two smaller matrices (factors) as

$$\mathbf{X}_{(m \times n)} = \mathbf{B}^{(1)}_{(m \times r)} \times \mathbf{B}^{(2)^T}_{(n \times r)} \tag{6.1}$$

where $\mathbf{B}^{(1)}$ holds the temporal information (known as weighting function) while the other factor $\mathbf{B}^{(2)}$ is the muscle synergy holding the spatial information and r is number of synergies where $r < m, n$ to achieve dimension reduction. The algorithm relies on a cost function where both factors are updated and optimised with respect to the non-negativity constraint to minimise the difference between the data matrix $\mathbf{X}$ and its approximation as the following:

$$\min_{\mathbf{B}^{(1)}, \mathbf{B}^{(2)}} \frac{1}{2} \|\mathbf{X} - \mathbf{B}^{(1)} \mathbf{B}^{(2)^T}\|_F^2 s.t. \mathbf{B}^{(1)}, \mathbf{B}^{(2)} \geq 0 \tag{6.2}$$

where $\|.\|_F^2$ is the Frobenius norm and both factors $\mathbf{B}^{(1)}$ and $\mathbf{B}^{(2)}$ are constrained to be non-negative. For more details see [145].

In order to use the NMF synergies for a simultaneous and proportional myoelectric control scheme, Jiang *et al.* [5, 95] proposed a "divide and conquer" approach. This is done by designing an experimental protocol to capture the EMG recording for a single DoF (2 tasks). Consequently, this approach would limit the factorisation into a few possible solutions. The result would be 2 muscle synergies and their respective weighting function (or control signal) for each DoF.

The SNMF approach is similar to the classic NMF method in many ways but it imposes sparseness on the factorisation outcome. Since lack of sparseness in the solution is one of the notable drawbacks for NMF [83, 150], SNMF would help to improve the muscle synergy estimation and simplify the training stage as demonstrated by Lin *et al.* [118]. This is done by imposing a sparseness constraint to the weighting functions (control signals) based on the

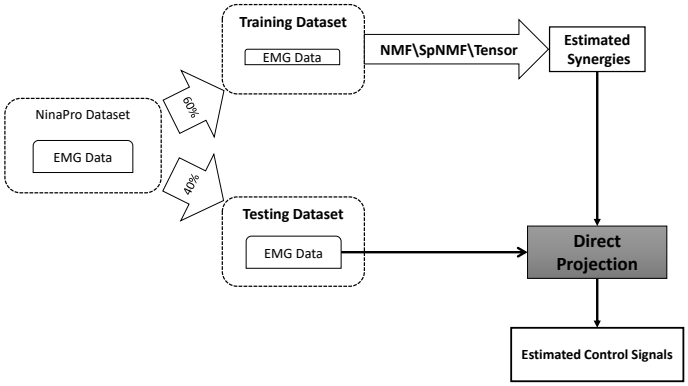

Figure 6.5: Block diagram for the use of extracted muscle synergies from the training dataset to estimate control signals.

SNMF scheme introduced in [151]. In the case of SNMF algorithm, the cost function of classic NMF shown in Equation 6.2 is modified to the following:

$$\min_{\mathbf{B}^{(1)},\mathbf{B}^{(2)}} \frac{1}{2}\|\mathbf{X}-\mathbf{B}^{(1)}\mathbf{B}^{(2)^T}\|_F^2+\lambda\sum_{n}^{j=1}\|\mathbf{B}^{(2)}(:,j)\|_1^2 \quad s.t.\mathbf{B}^{(1)},\mathbf{B}^{(2)}\geq 0 \tag{6.3}$$

where $\mathbf{B}^{(2)}(:,j)$ is the jth column vector of $\mathbf{B}^{(2)}$ and $\lambda > 0$ is a regularisation parameter to balance the trade-off between the accuracy of the approximation and the sparseness of $\mathbf{B}^{(2)}$ (control signals).

6.3.1.4 Direct projection of control signal

The muscle synergies extracted using consTD on the training tensors are utilised to estimate one control signal per movement (4 in total). This is done through direct projection of the testing data onto the fixed training components (core tensor and $spatial, movement$ modes) to estimate the $temporal$ mode components of the testing dataset. For the 3[rd]-order tensor in this study, the projection for training DoF tensor $\underline{\mathbf{X}}$ to the $temporal$ mode to estimate the control signals ($\mathbf{C}$) based on Equation 2.9 would be

$$\mathbf{C}^{(i_1\times j_1)}=\underline{\mathbf{X}}_{test}^{(i_1\times i_2 i_3)}[\underline{\mathbf{G}}^{(j_1\times j_3 j_2)}(\mathbf{B}^{(3)(i_3\times j_3)}\otimes\mathbf{B}^{(2)(i_2\times j_2)})^T]^+ \tag{6.4}$$

where $\mathbf{B}^{(2)}$ and $\mathbf{B}^{(3)}$ are the $spatial$ (synergy) and $movements$ modes calculated from the training dataset, while $\underline{\mathbf{G}}^{(j_1 \times j_3 j_2)}$ is the fixed core tensor unfolded across the temporal-mode (j_1). Therefore, Equation 6.4 can be used to project the testing dataset ($\underline{\mathbf{X}}_{test}$) to estimate the control signals ($temporal$ mode projection). The resulting projection consists of four control signals representing the projection of each movement for the input test dataset that can be used in real-time for myoelectric control.

In the case of matrix factorisation methods – either NMF or SNMF –, control signals for each movement are estimated using the the inverse model of the weighting functions. According to Equation 6.1, the control signal $\mathbf{C}$ would be

$$\mathbf{C} = \mathbf{X}_{test} \times \mathbf{B}^{(1)^+} \tag{6.5}$$

where $\mathbf{B}^{(1)^+}$ is the pseudo inverse of the synergy matrix $\mathbf{B}^{(1)^T}$ and $\mathbf{X}_{test}$ is the testing EMG dataset for one DoF. The resulting projection consists of two control signals representing the projection of both movements of the DoF test dataset.

For myoelectric control applications, the final control signal is calculated for each DoF in a similar approach to other synergy-based myoelectric control studies [5, 118]. It is deduced by taking the difference between the control signals of each movement and its antagonistic movement for each DoF. As a result, we estimate a final control signal for each wrist's DoF using NMF, SNMF and consTD methods.

6.3.2 Results

6.3.2.1 Constrained Tucker decomposition

The $\{4, 6, 4\}$ consTD decomposes the 3$^{\text{rd}}$-order tensors constructed for each pair of the wrist's DoFs. An example of the consTD for the EMG tensor (DoF1-3) of subject 6 is shown in Figure 6.6. The tensor is decomposed into $\{4, 6, 4\}$ components across its 3 modes ($temporal, spatial$ and $movements$) where the core tensor and movement mode are constrained to guide the decomposition into interpretable results as discussed in details in 6.2.1.2. Each component in the temporal mode is related to one movement of the four movements of DoFs 1 and 3. For the spatial mode, the first 4 components are task-specific

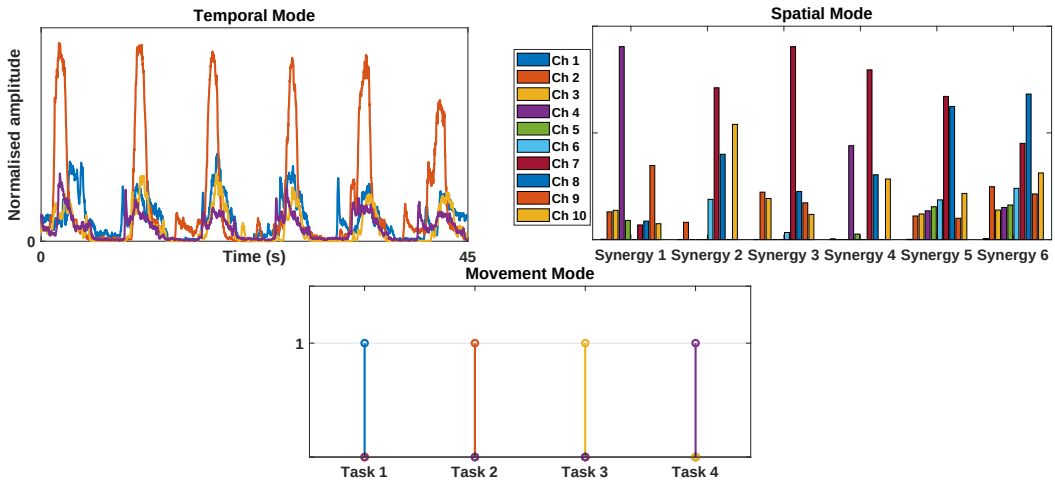

Figure 6.6: Constrained Tucker decomposition for DoF1-3 Tensor (shown 6.4c).

synergies for those four movements while the 5th and 6th are shared synergies for wrist's DoFs 1 and 3 respectively. Those synergies are then used to estimate the control signals for the testing dataset for proportional myoelectric control.

6.3.2.2 Matrix factorisation models

Both NMF and SNMF decompose a training EMG segment of one DoF (2 movements) into two synergies and their respective weighting functions. This was applied into the three main wrist's DoFs separately. Then the extracted synergies were used for estimating the testing glove dataset through direct projection of EMG data. SNMF was used to separate between movements directly by imposing sparseness on the weighting function. An example of NMF of DOF1 and DoF3 for subject 6 is shown in Figure 6.7. The same segments were decomposed by SNMF as illustrated in Figure 6.8.

6.3.2.3 Direct projection of control signal

Control signals for each movement are estimated using direct projection of matrix factorisation and consTD methods as discussed in Section 6.3.1.4. The final control signals are calculated via the difference between the control signals of each movement and its antagonistic movement for each DoF [146]. An example of the final control signals for DOF1 and DoF3 of subject 6 are illustrated in Figures 6.9 and 6.10 using NMF and SNMF respectively, while Figure 6.11

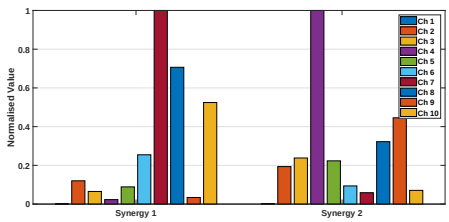

(a) NMF synergies for DoF1.

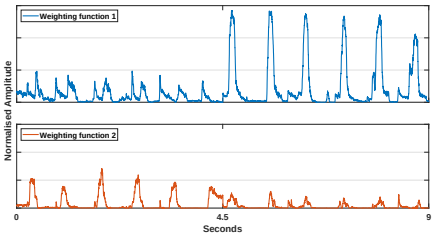

(b) Weighting Functions for DoF1.

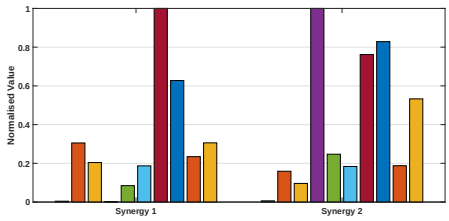

(c) NMF synergies for DoF3.

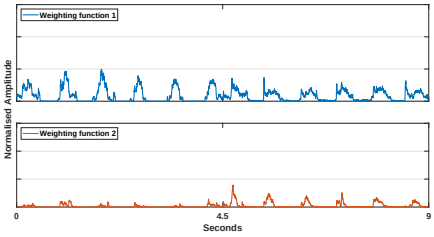

(d) Weighting Functions for DoF3.

Figure 6.7: The NMF of training EMG datasets for DoF1 (Panels 6.7a, 6.7b) and DoF3 (Panels 6.7c, 6.7d) recorded from subject 6.

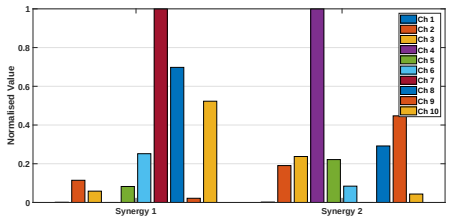

(a) Sparse NMF synergies for DoF1.

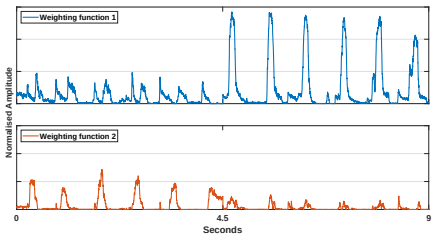

(b) Weighting Functions for DoF1.

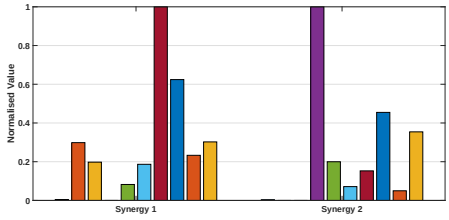

(c) Sparse NMF synergies for DoF3.

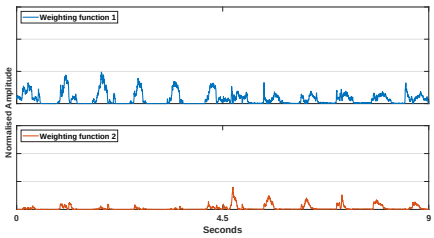

(d) Weighting Functions for DoF3.

Figure 6.8: The SNMF of training EMG datasets for DoF1 (Panels 6.8a, 6.8b) and DoF3 (Panels 6.8c, 6.8d) recorded from subject 6.

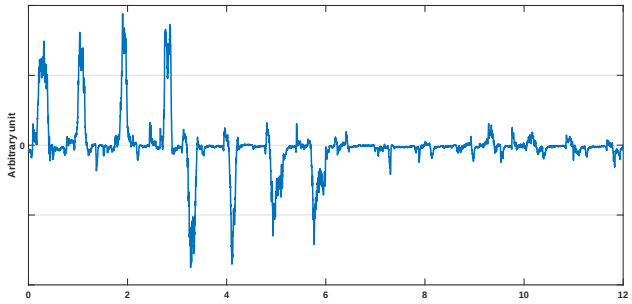

(a) Final control signal for DoF1.

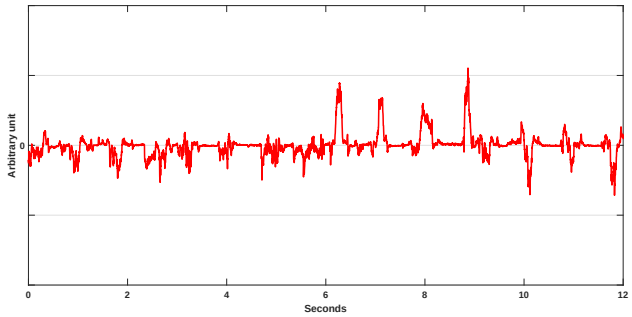

(b) Final control signal for DoF3.

Figure 6.9: Final control signal for DoF1 (Panel 6.9a) and DoF3 (6.9b) projected through direct projection of muscle synergies extracted via NMF recorded from subject 6.

shows the final control signals for the same segments using consTD approach.

6.3.3 Discussion

A consTD scheme was proposed to estimate muscle synergies from training data for proportional myoelectric control. Muscle synergies were extracted via both NMF and SNMF for comparison. The estimated synergies were used to deduce control signals for each DoF through direct projection of the EMG testing data.

The three methods were able to estimate control signals for each DoF that can be used in synergy-based myoelectric control systems. However, consTD was able to use all the data in one 3^{rd}-order tensor, unlike matrix factorisation models where data is segmented for each DoF as shown in Figure 6.4. Moreover, the consTD method provided more information by including additional shared synergies in comparison with matrix factorisation methods.

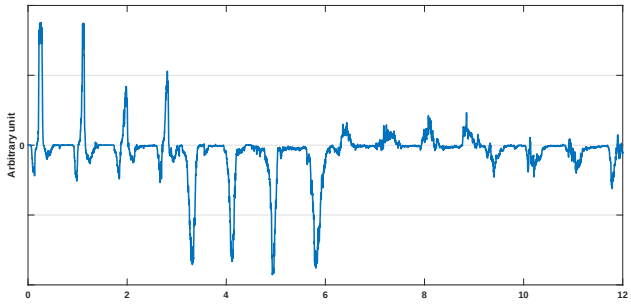

(a) Final control signal for DoF1.

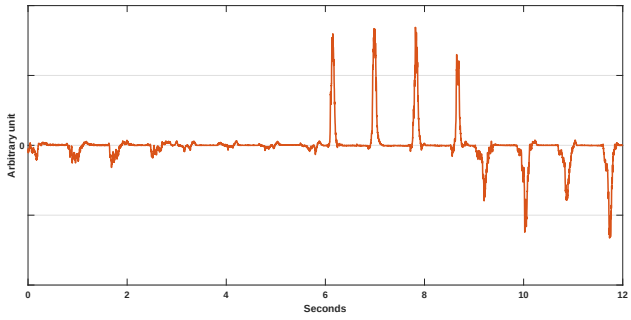

(b) Final control signal for DoF3.

Figure 6.10: Final control signal for DoF1 (Panel 6.10a) and DoF3 (6.10b) projected through direct projection of muscle synergies extracted via SNMF recorded from subject 6.

This study provides a proof of concept for the use of higher-order tensor decomposition in proportional myoelectric control. For this application, tensors provides an objective and direct approach to identify synergies since it does not require realignment of synergies as matrix factorisation methods often does. The information between each mode in the higher-order tensor for each DoF is included to the tensor construction and decomposition. On the other hand, NMF methods have to extract synergies separately through DoF-wise training [5, 119]. Sparse NMF was able to extract synergies from two DoFs datasets [118]. However, there was a need to identify synergies for each DoF after the factorisation process.

6.4 Conclusions

Currently, the state-of-the-art approach for upper-limb myoelectric control is the classic sequential control scheme of pattern recognition. Although it has been successful in recent years, the natural limb movements consist in the simultaneous activation of multiple DoFs.

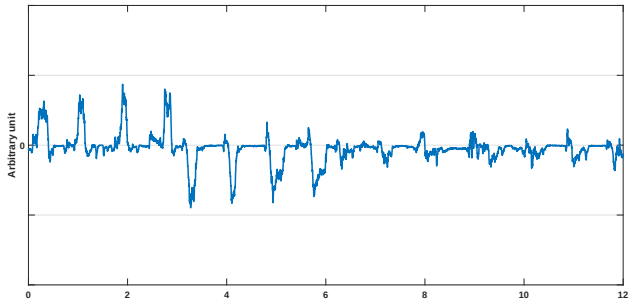

(a) Final control signal for DoF1.

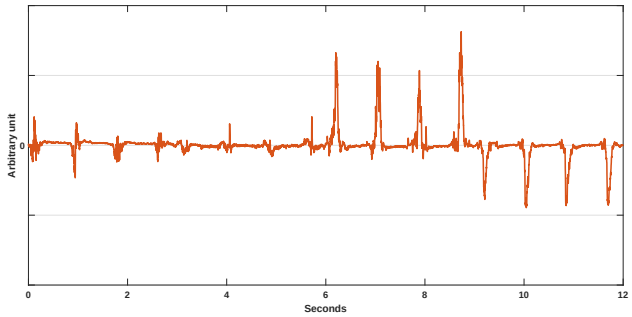

(b) Final control signal for DoF3.

Figure 6.11: Final control signal for DoF1 (Panel 6.11a) and DoF3 (6.11b) projected through direct projection of muscle synergies extracted via consTD recorded from subject 6.

Recently, several synergy-based systems have been proposed to achieve simultaneous and proportional myoelectric control [5, 118]. These approaches rely on matrix factorisation methods to extract muscle synergies which are utilised to provide continuous control signals. However, those approaches are still limited in terms of number of DoFs and task-dimensionality.

In this Chapter, the potential application of a higher-order tensor model in myoelectric control system were explored. We aim to improve the synergistic information extracted from the muscle activity datasets for synergy-based myoelectric control especially with the increase of task-dimensionality and number of DoFs.This was approached by using a consTD method for synergy extraction from 3rd-order EMG tensor and incorporating the shared synergy concept. In Section 6.2, we showed that consTD method is capable to estimate consistent synergies when the task dimensionality is increased up to 3-DoFs, while the traditional NMF was not able to extract consistent synergies when the EMG segments were expanded to include additional

DoFs. Finally, in Section 6.3, the consTD was proposed as a method to extract muscle synergies for proportional myoelectric control. It was compared against NMF and SNMF methods, the current synergy extraction methods used in synergy-based myoelectric control schemes. The methods were used to estimate control signal for each DoF to provide a proof of concept for the potential use of higher-order tensor decomposition in proportional myoelectric control.

Chapter 7

Discussion, Conclusions and Future Work

7.1 Discussion

In this thesis, we introduced muscle synergy extraction via higher-order tensor decomposition and developed different approaches for its potential applications in biomechanical analysis and myoelectric control.

In Chapter 3, the traditional methods for muscle synergy extraction were compared. The most common matrix factorisation techniques (PCA, ICA and NMF) for muscle synergy estimation alongside SOBI, which had not been applied for synergy extraction yet, were assessed under different settings and conditions [6]. It was found that the presence of sparse synergies and a higher number of channels would improve the quality of extracted synergies. This has been supported with a recent study [130] that found evidence of sparsity in grasping tasks. In addition, SNMF was introduced as a novel approach for a synergy-based myoelectric control system in a recent study [118]. Moreover, SOBI performed better than other methods the number of channels was equal to synergies although the performance was still poor in this case. Otherwise, NMF was found to be the best matrix factorisation method for robust synergy extraction. Therefore, it was used as a benchmark for the proposed higher-order tensor decomposition methods.

In Chapter 4, higher-order tensor decomposition for muscle synergy extraction was introduced. The first step was to construct a higher-order EMG tensor from a multichannel EMG dataset. Two potential models were proposed: a 3$^{\text{rd}}$-order tensor model with $spatial \times temporal \times repetition$ modes, and a 4$^{\text{th}}$-order tensor model that add a $spectral$

mode through time-frequency analysis to the other three modes. Moreover, we performed a preliminary study to extract muscle synergies from a 4^{th}-order EMG tensor using the Tucker decomposition model [9]. The extracted tensor synergies were compared to NMF synergies through simple movement classification. The results were encouraging and provided a proof-of-concept for higher-order tensor muscle synergy models. However, it was noticed that the unconstrained Tucker decomposition model cannot link its components to relevant and specific movements. Therefore, we concluded that imposing constraints on the Tucker model or using a less flexible model, such as PARAFAC, would help to improve the extracted synergistic information. Moreover, we found that the computational needs and execution time for 4^{th}-order tensor decomposition was very high due to the time-frequency analysis, which may not be suitable for some applications such as myoelectric control. Therefore, we turned our focus towards 3^{rd}-order EMG model aiming to extract more relevant and consistent muscle synergies.

In Chapter 5, we expanded our investigation on the higher-order tensor model for muscle activity analysis to highlight its potential in muscle synergy extraction. Benefiting from the knowledge gained from Chapter 4 and inspired by the shared synergy concept, a consTD method was proposed and compared to the most prominent tensor decomposition models (PARAFAC and Tucker) [10]. Both models were constrained to be non-negative because of the additive nature of muscle synergies. The results show that Tucker decomposition can provide a good fit for the data as shown by the high explained variance percentage. However, the estimated synergies were inconsistent as the decomposition solution is not unique. This problem had an effect on the execution time as well which increased since the algorithm could not converge easily. On the other hand, PARAFAC was significantly faster since it converged to the same local minima most of the time due to its extremely constrained structure. However, PARAFAC could not deal with larger tensors or a higher number of synergies as the decomposition deviates from the trilinear model, which was illustrated with the low CORCONDIA values. In comparison, the proposed consTD models were able to achieve over 70% explained variance but the execution time was shorter than the non-negative Tucker model by about 10-fold, while the extracted synergies were consistent as the solution the additional constraints help in the uniqueness of the solutions. Hence, the developed consTD method was selected for muscle synergy estimation by providing unique and interpretable synergies with

high explained variance and short execution time.

The proposed consTD model was utilised as a direct novel approach to identify shared and task-specific synergy. It was compared to the current standard approach of shared synergy identification [3, 72, 77, 78, 144] which requires repetitive application of NMF and relies on maximising a similarity metric through rearrangement of the estimated synergies. The consTD method was more suitable as the data is naturally in higher-order structure (space, time and movement) and it provided more direct and data-driven estimations of the synergies in comparison with NMF-based approaches. Furthermore, it was robust to disarrangement of repetitions and the loss of task-repetition information unlike, the NMF approach where rearrangement of synergies had a significant impact [3, 72, 77].

Finally in Chapter 6, the potential application of higher-order tensor decomposition models for myoelectric control is discussed and explored. We proposed a consTD model for muscle synergy extraction that can be used for simultaneous and proportional synergy-based myoelectric control and compare it to the current matrix factorisation models.

First, the consistency of tensor synergies were analysed when task dimensionality is increased from one to three DoFs (six movements). The results showed that tensor synergies extracted via consTD methods from 3-DoF tensors were similar to those extracted from 1-DoF tensors. In the case of NMF, the results were significantly worse as synergies extracted via NMF cannot be linked to their respective movements. Because of this downside, studies utilising NMF synergies for myoelectric control [5, 119] used 1-DoF segments and extracted the synergies for each DoF separately. Lin *et al.* [118] tried to solve this issue using SNMF to identify 4 task-specific synergies from 2-DoFs segments. However, the extracted synergies needed to be labelled after factorisation as SNMF cannot extract them in a fixed order. In contrast, the consTD approach was able to estimate consistent identified synergies directly from 3-DoFs data directly. Moreover, the Tucker model extracted three synergies for each DoF by incorporating additional shared synergy unlike NMF where only two synergies are estimated for each DoF.

Secondly, the use of the proposed consTD in synergy-based myoelectric control was demonstrated. Synergies extracted via consTD from training datasets were used to estimate control signal for each DoF through direct projection of the EMG testing data. The consTD

were compared against NMF and SNMF methods, the current state-of-the-art synergy extraction methods for proportional synergy-based myoelectric control schemes. This study demonstrated the potential use of higher-order tensor decomposition in proportional myoelectric control and provided a proof of concept for this application. In general, tensors provided an easier approach to identify synergies for each DoF by adding this information to the tensor construction and decomposition. While matrix factorisation methods have to extract synergies separately through a DoF-wise training approach.

Overall, this thesis explored the potential use of higher-order tensor decomposition in muscle synergy analysis. Higher-order tensor decomposition has been hardly used in EMG analysis [9], although EMG data are naturally structured in higher-order form in most EMG studies. We provided a framework for representing the EMG dataset in higher-order tensor form and extracting synergistic information using the consTD approach [10]. This approach incorporates the known information about repetitions, movement and synergies into the Tucker decomposition by imposing constraints that help in estimating meaningful muscle synergies and reduce the model complexity. Shared and task-specific synergies identification using consTD is introduced as an alternative to the current matrix factorisation methods. Moreover, the potential use of tensor synergies in proportional myoelectric control systems and its advantages over NMF and SNMF approaches are discussed.

Higher-order tensor decomposition models have been established as an advanced tool for signal analysis in vastly diverse branches of biomedical signal processing. Although, they have not been widely used in EMG analysis, a few studies [135, 152] employed a Tucker2 model for spatial and temporal concurrent analysis. Moreover, tensor decomposition models have been utilised frequently in brain activity analysis [131]. For instance, the Tucker model has been used to decompose 4^{th}-order EEG data tensor to classify epileptic patients [132]. In addition, a PARAFAC2 model has been utilised for the analysis of MEG activity to predict Alzheimer's disease [133], while a constrained PARAFAC model identified features from 3^{rd}-order EEG data to predict the developmental age of children [153]. Recently, higher order partial least squares (HOPLS) [154] has been introduced to analyse higher-order data sets with two modalities such as EEG and functional magnetic resonance imaging (fMRI) [154].

7.2 Limitations

In this section, certain limitations occurring in this thesis will be discussed. Firstly, EMG datasets are one of the limitations that affects most of the thesis experiments. For instance, only two datasets were used in our research and both of them were offline. Moreover, the datasets were recorded from healthy subjects and no amputee's data were included. In addition, only a selection of wrist's movements were under analysis as the thesis was motivated by upper-limb myoelectric control.

Regarding the matrix factorisation comparison, it might be biased towards NMF due to the non-negative nature of the simulated synergies. However, this choice is supported by previous studies [89] which suggested the usefulness of NMF due to the additive nature of the synergies. Further examination is needed if the setting of EMG acquisition changes dramatically (really bad SNR, much higher number of channels, etc.) to evaluate the validity of our conclusions in those settings.

In spite of the potential drawbacks of NMF shared synergies, we used NMF as benchmark to compare the proposed consTD method for shared and task-specific synergies identification since there is no ground truth for shared synergies to compare both methods against. Moreover, repetitive application of NMF has been the standard approach for shared and task-specific synergy identification [77, 144]. For these reasons, NMF has been included in the comparison against the proposed consTD method to show the advantages of higher-order tensor decomposition over the standard approach of NMF.

The simple k-NN classifier comparison in Chapters 3 and 4 was used in this paper as an example to guide synergy application and to support the synthetic results. Additional work is needed with more advanced techniques and variety of tasks and movements.

Finally, regarding the application of consTD synergies in myoelectric control, the resulting control signal for each DoF needs to be compared against dataset that capture the hand kinematics at the same time. This is has not been done because of the lack of the data that capture EMG and the hand kinematics especially the wrist's DoF simultaneously.

7.3 Future work

There are many routes for future work based on the contributions of this thesis owing to the introduction of various brand-new methods. Notably, the use of higher-order tensors in muscle activity analysis is a new topic that has been rarely investigated thoroughly in the literature before. Specifically, the potential and benefits of using higher-order tensor models in muscle synergy extraction have been presented in this thesis. Tensor synergies would be beneficial to several muscle synergy analysis applications when the EMG data is usually in a higher-order structure such as biomechanical analysis [155], myoelectric control [156] and rehabilitation [70]. I also hope these methods will inspire new ideas and further explorations into the use of higher order tensor in muscle activity analysis and we will explore some of these considerations in the rest of the Chapter.

The proposed consTD can be expanded and applied to many applications with the right set of constraints. The binary core tensor approach to control component interaction across modes would help to incorporate pre-decomposition information to improve tensor decomposition. For instance, the repetition mode information is used in the consTD for efficient muscle synergy extraction as shown in Chapter 4. Therefore, consTD can be useful for several applications including muscle synergy extraction. I have been already contacted by a group at University of Birmingham, UK for collaboration. We aim to apply consTD on EMG data recorded during cycling to extract shared and task-specific synergies. This would help assess the effect of back pain on the muscle synergies, and how effective is the rehabilitation process [157].

Moreover, investigating tensor synergies extracted via consTD or any other tensor decomposition method is a possible direction for future work. For example, the consistency comparison conducted in Section 6.2 could be expanded to examine other characterises of tensor synergies such as the effect of the number of channels or added noise on estimated synergies.

Finally, the use of tensor synergies in proportional myoelectric control needs further research to introduce a reliable synergy-based system. For instance, the muscle fatigue effect can be reduced by incorporating information since fatigue causes a spectral shift in the EMG signals

[158, 159]. One of the possible ideas worth exploring is data fusion of EMG and kinematic data. Higher-order tensor models can be exploited by including kinematic data such as inertial or glove datasets. The additional datasets will constrain and control the tensor decomposition for the training data. Hence, the outcome of the decomposition (tensor synergies) would be improved.

7.4 Conclusion

Overall, the developments in this thesis open up new ways to consider higher-order tensor decomposition for muscle activity analysis. Tensor decomposition methods are developed for effective muscle synergy extraction and compared the current matrix factorisation approaches. The proposed consTD method was utilised for shared and task-specific synergy identification and was successful in comparison with traditional methods which require repetitive application of NMF and rely on synergy arrangement and similarity metrics. Moreover, tensor synergies were used in synergy-based myoelectric control and showed promise for proportional and simultaneous myoelectric control. In general, higher-order tensor decomposition showed a potential for muscle synergy analysis and I hope this study will encourage others to explore this potential.

Appendices

Appendix A: Minimum description length

The MDL method for determining the number of synergies is performed by calculating the maximum likelihood estimates of factor loading matrix $\mathbf{A}$ and the unique variances diagonal matrix $\mathbf{\Psi}$ according to the factor analysis model

$$\mathbf{C} = \mathbf{A}\mathbf{A}^T + \mathbf{\Psi} \tag{1}$$

where $\mathbf{C}$ is the covariance matrix of $\mathbf{M}_{m\times n}$ the multi-channel EMG signal matrix with m channels and n samples.

This is done for different number of synergies (r) between $1 \leq r \leq \frac{1}{2}(2m+1-\sqrt{8m+1})$ in order to minimise the MDL. The boundary for r is set by comparing the number of equations with unknowns in order to have an algebraic solution for equation 2.

$$L(\mathbf{A}, \mathbf{\Psi}) = -\frac{1}{2}\left\{\mathtt{tr}(\mathbf{C}(\mathbf{\Psi} + \mathbf{A}\mathbf{A}^T)^{-1}) + \log(\det(\mathbf{\Psi} + \mathbf{A}\mathbf{A}^T)) + m\log 2\pi\right\} \tag{2}$$

The number of synergies r are selected to minimise the MDL value in equation 3.

$$\mathrm{MDL} = -L(\mathbf{A}, \mathbf{\Psi}) + \frac{\log n}{n}\left(m(r+1) - \frac{r(r-1)}{2}\right) \tag{3}$$

Appendix B: Comparison between $\{1, 3, 3\}$ and $\{2, 3, 2\}$ consTD models.

This is a comparison between the two $\{1, 3, 3\}$ and $\{2, 3, 2\}$ consTD models proposed in Chapter 4 and 6 respectively for 1-DoF tensors. The percentage of explained variance by the models and their execution time were recorded for the 27 subjects and the median values are shown in Table 1. An example of both methods is shown in Figure 1.

Table 1: The median explained variance and time for execution for the consTD approaches across the 27 Subjects.

consTD	$\{1, 3, 3\}$	$\{2, 3, 2\}$
Explained Variance	78.28%	80.21%
Time(s)	0.26	0.24

The modified consTD had better explained variance, mainly because of the additional component in the $temporal$ mode. Although the number of elements in $\{2, 3, 2\}$ consTD model is bigger than the other model, the execution time is slightly better, this is because the moving average in the additional repetition component for shared synergy identification in the $\{1, 3, 3\}$ is replaced by the core tensor binary setup as discussed in Section 6.2.1.2.

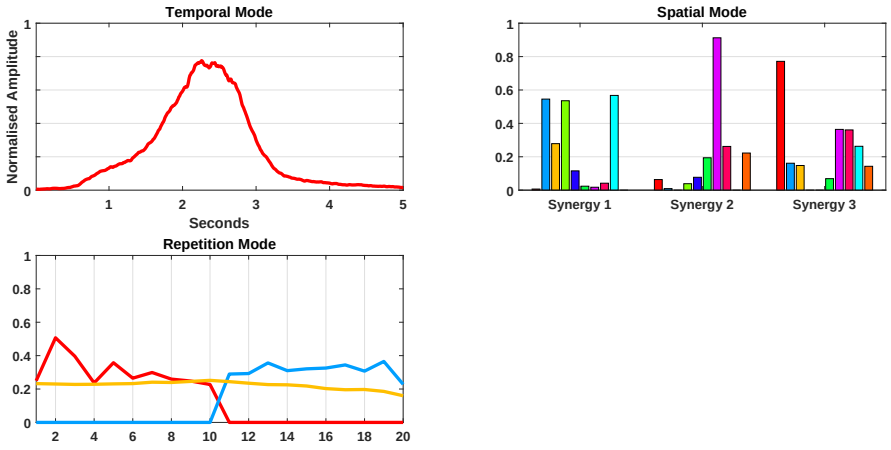

(a)

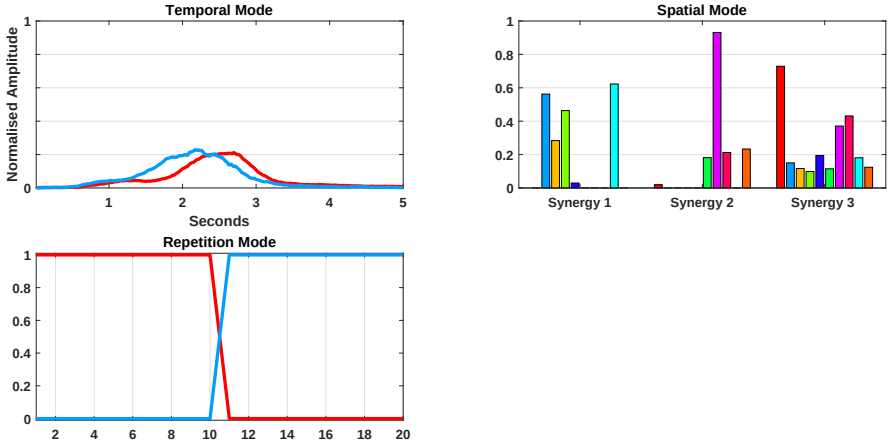

(b)

Figure 1: An example for the two consTD models $\{1, 3, 3\}$ *(Panel 1a)and* $\{2, 3, 2\}$ *(Panel 1b) applied on the same 1-DoF tensor.*

Bibliography

[1] M. C. Tresch, P. Saltiel, and E. Bizzi, "The construction of movement by the spinal cord." *Nature neuroscience*, vol. 2, no. 2, pp. 162–7, Feb. 1999.

[2] A. D'Avella, P. Saltiel, and E. Bizzi, "Combinations of muscle synergies in the construction of a natural motor behavior." *Nature neuroscience*, vol. 6, no. 3, pp. 300–308, Mar. 2003.

[3] M. M. Nazifi, H. U. Yoon, K. Beschorner, and P. Hur, "Shared and Task-Specific Muscle Synergies during Normal Walking and Slipping," *Frontiers in Human Neuroscience*, vol. 11, no. February, pp. 1–14, Feb. 2017.

[4] G. Rasool, K. Iqbal, N. Bouaynaya, and G. White, "Real-Time Task Discrimination for Myoelectric Control Employing Task-Specific Muscle Synergies." *IEEE transactions on neural systems and rehabilitation engineering*, vol. 24, no. 1, pp. 98–108, Jan. 2016.

[5] N. Jiang, H. Rehbaum, I. Vujaklija, B. Graimann, and D. Farina, "Intuitive, online, simultaneous, and proportional myoelectric control over two degrees-of-freedom in upper limb amputees." *IEEE transactions on neural systems and rehabilitation engineering*, vol. 22, no. 3, pp. 501–10, 2014.

[6] A. Ebied, E. Kinney-Lang, L. Spyrou, and J. Escudero, "Evaluation of matrix factorisation approaches for muscle synergy extraction," *Medical Engineering & Physics*, vol. 57, pp. 51–60, Jul. 2018.

[7] A. Cichocki, D. Mandic, A. H. Phan, C. Caiafa, G. Zhou, Q. Zhao, and L. De Lathauwer, "Tensor Decompositions for Signal Processing Applications From Two-way to Multiway Component Analysis," *IEEE Signal Processing Magazine*, vol. 32, no. 2, pp. 1–23, Mar. 2014.

[8] F. Cordella, A. L. Ciancio, R. Sacchetti, A. Davalli, A. G. Cutti, E. Guglielmelli, and L. Zollo, "Literature Review on Needs of Upper Limb Prosthesis Users," *Frontiers in Neuroscience*, vol. 10, p. 209, May 2016.

[9] A. Ebied, L. Spyrou, E. Kinney-Lang, and J. Escudero, "On the use of higher-order tensors to model muscle synergies," in *2017 39th Annual International Conference of the IEEE Engineering in Medicine and Biology Society (EMBC)*. IEEE, Jul. 2017, pp. 1792–1795.

[10] A. Ebied, E. Kinney-Lang, L. Spyrou, and J. Escudero, "Muscle activity analysis using higher-order tensor decomposition: Application to muscle synergy extraction," *IEEE Access*, vol. 7, pp. 27 257–27 271, Jan. 2019.

[11] A. Ebied, E. Kinney-Lang, and J. Escudero, "Consistency of Muscle Synergies Extracted via Higher-Order Tensor Decomposition Towards Myoelectric Control," in *9th International IEEE/EMBS Conference on Neural Engineering (NER2019)*. IEEE, Mar. 2019, pp. 315–318.

[12] ——, "Use of muscle synergies extracted via higher-order tensor decomposition for proportional myoelectric control," *ArXiv e-prints*, Nov. 2018.

[13] A. D'Avella, M. Giese, Y. P. Ivanenko, T. Schack, and T. Flash, "Editorial: Modularity in motor control: from muscle synergies to cognitive action representation." *Frontiers in computational neuroscience*, vol. 9, p. 126, Jan. 2015.

[14] C. S. Sherrington, "Flexion-reflex of the limb, crossed extension-reflex, and reflex stepping and standing," *The Journal of Physiology*, vol. 40, no. 1-2, pp. 28–121, Apr. 1910.

[15] E. Bizzi, F. A. Mussa-Ivaldi, and S. F. Giszter, "Computations underlying the execution of movement: a biological perspective." *Science (New York, N.Y.)*, vol. 253, no. 5017, pp. 287–91, Jul. 1991.

[16] S. F. Giszter, F. A. Mussa-Ivaldi, and E. Bizzi, "Convergent force fields organized in the frog's spinal cord." *The Journal of Neuroscience*, vol. 13, no. 2, pp. 467–491, Feb. 1993.

[17] F. A. Mussa-Ivaldi, S. F. Giszter, and E. Bizzi, "Linear combinations of primitives in vertebrate motor control." *Proceedings of the National Academy of Sciences of the United States of America*, vol. 91, no. 16, pp. 7534–7538, Aug. 1994.

[18] P. Saltiel, K. Wyler-Duda, A. D'Avella, M. C. Tresch, and E. Bizzi, "Muscle synergies encoded within the spinal cord: evidence from focal intraspinal NMDA iontophoresis in the frog." *Journal of neurophysiology*, vol. 85, no. 2, pp. 605–619, Feb. 2001.

[19] C. J. De Luca, "Electromyography," in *Encyclopedia of Medical Devices and Instrumentation*, J. G. Webster, Ed. Hoboken, NJ, USA: John Wiley & Sons, Inc., Apr. 2006, pp. 98–109.

[20] R. Merletti and D. Farina, *Surface Electromyography: Physiology, Engineering and Applications*, R. Merletti and D. Farina, Eds. Hoboken, New Jersey: John Wiley & Sons, Inc., Apr. 2016.

[21] E. G. T. Liddell and C. S. Sherrington, "Recruitment and some other Features of Reflex Inhibition," *Proceedings of the Royal Society of London. Series B, Containing Papers of a Biological Character*, vol. 97, no. 686, pp. 488–518, 1925.

[22] F. Buchthal, *An Introduction to Electromyography*. Gyldendal, 1957, vol. 1st.

[23] F. Buchthal, C. Guld, and Rosenfalck, "Action potential parameters in normal human muscle and their dependence on physical variables." *Acta physiologica Scandinavica*, vol. 32, no. 2-3, pp. 200–18, Nov. 1954.

[24] P. Konrad, "The abc of emg," *A practical introduction to kinesiological electromyography*, vol. 1, pp. 30–35, 2005.

[25] J. Duchateau and R. M. Enoka, "Human motor unit recordings: Origins and insight into the integrated motor system," *Brain Research*, vol. 1409, pp. 42–61, Aug. 2011.

[26] C. J. De Luca, A. Adam, R. Wotiz, L. Donald Gilmore, S. Hamid Nawab, and D. Luca, "Decomposition of Surface EMG Signals," *J Neurophysiol*, vol. 96, no. 3, pp. 1646–1657, Sep. 2006.

[27] E. a. Clancy, E. L. Morin, and R. Merletti, "Sampling, noise-reduction and amplitude estimation issues in surface electromyography," *Journal of Electromyography and Kinesiology*, vol. 12, no. 1, pp. 1–16, Feb. 2002.

[28] M. A. Oskoei and H. Hu, "Myoelectric Control Systems - A Survey," *Biomedical Signal Processing and Control*, vol. 2, no. 4, pp. 275–294, 2007.

[29] F. Hug, "Can muscle coordination be precisely studied by surface electromyography?" *Journal of electromyography and kinesiology : official journal of the International Society of Electrophysiological Kinesiology*, vol. 21, no. 1, pp. 1–12, Feb. 2011.

[30] C. J. De Luca, "cc," *DelSys Incorporated*, vol. 10, no. 2, pp. 1–10, 2002.

[31] O. Fukuda, T. Tsuji, M. Kaneko, and A. Otsuka, "A human-assisting manipulator teleoperated by EMG signals and arm motions," *IEEE Transactions on Robotics and Automation*, vol. 19, no. 2, pp. 210–222, Apr. 2003.

[32] C. J. De Luca, "The use of surface electromyography in biomechanics," *Journal of Applied Biomechanics*, vol. 13, no. 2, pp. 135–163, 1997.

[33] R. Merletti, D. Farina, and M. Gazzoni, "The linear electrode array: A useful tool with many applications," *Journal of Electromyography and Kinesiology*, vol. 13, no. 1, pp. 37–47, Feb. 2003.

[34] G. Drost, D. F. Stegeman, B. G. van Engelen, and M. J. Zwarts, "Clinical applications of high-density surface EMG: A systematic review," *Journal of Electromyography and Kinesiology*, vol. 16, no. 6, pp. 586–602, Dec. 2006.

[35] D. Farina, N. Jiang, H. Rehbaum, A. Holobar, B. Graimann, H. Dietl, and O. C. Aszmann, "The extraction of neural information from the surface EMG for the control of upper-limb prostheses: Emerging avenues and challenges," *IEEE Transactions on Neural Systems and Rehabilitation Engineering*, vol. 22, no. 4, pp. 797–809, 2014.

[36] M. Ison, I. Vujaklija, B. Whitsell, D. Farina, and P. Artemiadis, "High-Density Electromyography and Motor Skill Learning for Robust Long-Term Control of a 7-DoF Robot Arm," *IEEE Transactions on Neural Systems and Rehabilitation Engineering*, vol. 24, no. 4, pp. 424–433, Apr. 2016.

[37] M. Atzori, A. Gijsberts, C. Castellini, B. Caputo, A.-G. M. Hager, S. Elsig, G. Giatsidis, F. Bassetto, and H. Müller, "Electromyography data for non-invasive naturally-controlled robotic hand prostheses." *Scientific data*, vol. 1, p. 140053, Jan. 2014.

[38] M. Atzori, A. Gijsberts, I. Kuzborskij, S. Elsig, A.-G. Mittaz Hager, O. Deriaz, C. Castellini, H. Muller, and B. Caputo, "Characterization of a Benchmark Database for Myoelectric Movement Classification," *IEEE Transactions on Neural Systems and Rehabilitation Engineering*, vol. 23, no. 1, pp. 73–83, Jan. 2015.

[39] M. Atzori, A. Gijsberts, S. Heynen, A.-G. M. Hager, O. Deriaz, P. van der Smagt, C. Castellini, B. Caputo, and H. Muller, "Building the Ninapro database: A resource for the biorobotics community," *Proceedings of the IEEE RAS and EMBS International Conference on Biomedical Robotics and Biomechatronics*, pp. 1258–1265, Jun. 2012.

[40] A. Gijsberts, M. Atzori, C. Castellini, H. Müller, and B. Caputo, "Movement error rate for evaluation of machine learning methods for sEMG-based hand movement classification," *IEEE Transactions on Neural Systems and Rehabilitation Engineering*, vol. 22, no. 4, pp. 735–744, Jul. 2014.

[41] V. C.-K. K. Cheung, A. Turolla, M. Agostini, S. Silvoni, C. Bennis, P. Kasi, S. Paganoni, P. Bonato, and E. Bizzi, "Muscle synergy patterns as physiological markers of motor cortical damage," *Proceedings of the National Academy of Sciences*, vol. 109, no. 36, pp. 14 652–14 656, Sep. 2012.

[42] M. C. Tresch and A. Jarc, "The case for and against muscle synergies," *Current Opinion in Neurobiology*, vol. 19, no. 6, pp. 601–607, Dec. 2009.

[43] W. J. Kargo and S. F. Giszter, "Individual Premotor Drive Pulses, Not Time-Varying Synergies, Are the Units of Adjustment for Limb Trajectories Constructed in Spinal Cord," *Journal of Neuroscience*, vol. 28, no. 10, pp. 2409–2425, Mar. 2008.

[44] C. B. Hart and S. F. Giszter, "Modular premotor drives and unit bursts as primitives for frog motor behaviors." *The Journal of neuroscience : the official journal of the Society for Neuroscience*, vol. 24, no. 22, pp. 5269–82, Jun. 2004.

[45] M. C. Tresch and E. Bizzi, "Responses to spinal microstimulation in the chronically spinalized rat and their relationship to spinal systems activated by low threshold cutaneous stimulation," *Experimental Brain Research*, vol. 129, no. 3, pp. 0401–0416, Nov. 1999.

[46] M. A. Lemay and W. M. Grill, "Modularity of motor output evoked by intraspinal microstimulation in cats." *Journal of neurophysiology*, vol. 91, no. 1, pp. 502–14, Jan. 2004.

[47] F. Haiss and C. Schwarz, "Spatial segregation of different modes of movement control in the whisker representation of rat primary motor cortex." *The Journal of neuroscience : the official journal of the Society for Neuroscience*, vol. 25, no. 6, pp. 1579–87, Feb. 2005.

[48] I. Stepniewska, P.-C. Fang, and J. H. Kaas, "Microstimulation reveals specialized subregions for different complex movements in posterior parietal cortex of prosimian galagos." *Proceedings of the National Academy of Sciences of the United States of America*, vol. 102, no. 13, pp. 4878–83, Mar. 2005.

[49] S. A. Overduin, A. D'Avella, J. Roh, and E. Bizzi, "Modulation of Muscle Synergy Recruitment in Primate Grasping," *Journal of Neuroscience*, vol. 28, no. 4, pp. 880–892, Jan. 2008.

[50] S. a. Overduin, A. D'Avella, J. M. Carmena, and E. Bizzi, "Muscle synergies evoked by microstimulation are preferentially encoded during behavior." *Frontiers in computational neuroscience*, vol. 8, no. March, p. 20, Nov. 2014.

[51] L. H. Ting and J. M. Macpherson, "A limited set of muscle synergies for force control during a postural task." *Journal of neurophysiology*, vol. 93, no. 1, pp. 609–13, Jan. 2005.

[52] G. Torres-Oviedo, J. M. Macpherson, and L. H. Ting, "Muscle synergy organization is robust across a variety of postural perturbations." *Journal of neurophysiology*, vol. 96, no. 3, pp. 1530–1546, Jan. 2006.

[53] V. C.-K. K. Cheung, "Central and Sensory Contributions to the Activation and Organization of Muscle Synergies during Natural Motor Behaviors," *Journal of Neuroscience*, vol. 25, no. 27, pp. 6419–6434, Jul. 2005.

[54] E. J. Weiss and M. Flanders, "Muscular and postural synergies of the human hand." *Journal of neurophysiology*, vol. 92, no. 1, pp. 523–35, Jul. 2004.

[55] A. D'Avella, A. Portone, L. Fernandez, and F. Lacquaniti, "Control of Fast-Reaching Movements by Muscle Synergy Combinations," *Journal of Neuroscience*, vol. 26, no. 30, pp. 7791–7810, Jul. 2006.

[56] J. M. Wakeling and T. Horn, "Neuromechanics of muscle synergies during cycling," *Journal of neurophysiology*, vol. 101, no. 2, pp. 843–54, Feb. 2009.

[57] F. Hug, N. a. Turpin, A. Couturier, and S. Dorel, "Consistency of muscle synergies during pedaling across different mechanical constraints." *Journal of neurophysiology*, vol. 106, no. 1, pp. 91–103, Jul. 2011.

[58] L. H. Ting and J. L. McKay, "Neuromechanics of muscle synergies for posture and movement." *Current opinion in neurobiology*, vol. 17, no. 6, pp. 622–8, Dec. 2007.

[59] C. J. De Luca and Z. Erim, "Common drive of motor units in regulation of muscle force." *Trends in neurosciences*, vol. 17, no. 7, pp. 299–305, Jul. 1994.

[60] ——, "Common drive in motor units of a synergistic muscle pair." *Journal of neurophysiology*, vol. 87, no. 4, pp. 2200–2204, apr 2002.

[61] K. Nazarpour, A. Barnard, and A. Jackson, "Flexible Cortical Control of Task-Specific Muscle Synergies," *Journal of Neuroscience*, vol. 32, no. 36, pp. 12 349–12 360, sep 2012.

[62] J. P. Scholz and G. Schöner, "The uncontrolled manifold concept: Identifying control variables for a functional task," *Experimental Brain Research*, vol. 126, no. 3, pp. 289–306, May 1999.

[63] M. L. Latash, J. P. Scholz, and G. Schöner, "Toward a new theory of motor synergies." in *Motor control*, jul 2007, vol. 11, no. 3, pp. 276–308.

[64] E. Todorov and M. I. Jordan, "Optimal feedback control as a theory of motor coordination." *Nature neuroscience*, vol. 5, no. 11, pp. 1226–1235, Nov. 2002.

[65] T. Pistohl, C. Cipriani, A. Jackson, and K. Nazarpour, "Abstract and proportional myoelectric control for multi-fingered hand prostheses," *Annals of Biomedical Engineering*, vol. 41, no. 12, pp. 2687–2698, Dec. 2013.

[66] M. Ison and P. Artemiadis, "Proportional Myoelectric Control of Robots: Muscle Synergy Development Drives Performance Enhancement, Retainment, and Generalization," *IEEE Transactions on Robotics*, vol. 31, no. 2, pp. 259–268, Apr. 2015.

[67] J. J. Kutch and F. J. Valero-Cuevas, "Challenges and new approaches to proving the existence of muscle synergies of neural origin." *PLoS computational biology*, vol. 8, no. 5, p. e1002434, Jan. 2012.

[68] E. Bizzi and V. C.-K. K. Cheung, "The neural origin of muscle synergies." *Frontiers in computational neuroscience*, vol. 7, no. April, p. 51, Feb. 2013.

[69] D. Torricelli, F. Barroso, M. Coscia, C. Alessandro, F. Lunardini, E. Bravo Esteban, and A. D'Avella, "Muscle Synergies in Clinical Practice: Theoretical and Practical Implications," in *Emerging Therapies in Neurorehabilitation II*, ser. Biosystems & Biorobotics, J. L. Pons, R. Raya, and J. González, Eds. Cham: Springer International Publishing, 2016, vol. 10, pp. 251–272.

[70] M. Coscia, P. Tropea, V. Monaco, and S. Micera, "Muscle synergies approach and perspective on application to robot-assisted rehabilitation," in *Rehabilitation Robotics*, R. Colombo and V. Sanguineti, Eds. Elsevier, 2018, ch. 23, pp. 319–331.

[71] G. C. Matrone, C. Cipriani, M. C. Carrozza, and G. Magenes, "Real-time myoelectric control of a multi-fingered hand prosthesis using Principal Components Analysis," *Journal of NeuroEngineering and Rehabilitation*, vol. 9, no. 1, p. 40, Jan. 2012.

[72] G. Martino, Y. P. Ivanenko, A. D'Avella, M. Serrao, A. Ranavolo, F. Draicchio, G. Cappellini, C. Casali, and F. Lacquaniti, "Neuromuscular adjustments of gait associated with unstable conditions," *Journal of Neurophysiology*, vol. 114, no. 2011, p. jn.00029.2015, Sep. 2015.

[73] A. Danna-Dos-Santos, E. Y. Shapkova, A. L. Shapkova, A. M. Degani, and M. L. Latash, "Postural control during upper body locomotor-like movements: similar synergies based on dissimilar muscle modes." *Experimental brain research*, vol. 193, no. 4, pp. 565–79, Mar. 2009.

[74] V. Krishnamoorthy, M. L. Latash, J. P. Scholz, and V. M. Zatsiorsky, "Muscle modes during shifts of the center of pressure by standing persons: Effect of instability and additional support," *Experimental Brain Research*, vol. 157, no. 1, pp. 18–31, Oct. 2004.

[75] G. Torres-Oviedo and L. H. Ting, "Subject-Specific Muscle Synergies in Human Balance Control Are Consistent Across Different Biomechanical Contexts," *Journal of Neurophysiology*, vol. 103, no. 6, pp. 3084–3098, Jun. 2010.

[76] A. D'Avella and E. Bizzi, "Shared and specific muscle synergies in natural motor behaviors." *Proceedings of the National Academy of Sciences of the United States of America*, vol. 102, no. 8, pp. 3076–81, Feb. 2005.

[77] F. O. Barroso, D. Torricelli, J. C. Moreno, J. Taylor, J. Gomez-Soriano, E. Bravo-Esteban, S. Piazza, C. Santos, and J. L. Pons, "Shared muscle synergies in human walking and cycling," *Journal of Neurophysiology*, vol. 112, no. 8, pp. 1984–1998, 2014.

[78] S. A. Chvatal, G. Torres-Oviedo, S. A. Safavynia, and L. H. Ting, "Common muscle synergies for control of center of mass and force in nonstepping and stepping postural behaviors," *Journal of Neurophysiology*, vol. 106, no. 2, pp. 999–1015, Aug. 2011.

[79] A. D'Avella and M. C. Tresch, "Modularity in the motor system: decomposition of muscle patterns as combinations of time-varying synergies," in *Advances in Neural Information Processing Systems 14*, vol. 3. Neural information processing systems foundation, 2002, pp. 141–148.

[80] C. B. Hart and S. F. Giszter, "Distinguishing synchronous and time-varying synergies using point process interval statistics: motor primitives in frog and rat." *Frontiers in computational neuroscience*, vol. 7, no. May, p. 52, Jan. 2013.

[81] J. E. Jackson, *A User's Guide to Principal Components*, ser. Wiley Series in Probability and Statistics. Hoboken, NJ, USA: John Wiley & Sons, Inc., Mar. 1991.

[82] A. Hyvärinen and E. Oja, "Independent component analysis: algorithms and applications," *Neural Networks*, vol. 13, no. 4-5, pp. 411–430, Jun. 2000.

[83] D. D. Lee and H. S. Seung, "Learning the parts of objects by non-negative matrix factorization." *Nature*, vol. 401, no. 6755, pp. 788–91, Oct. 1999.

[84] H. Abdi and L. J. Williams, "Principal component analysis," *Wiley Interdisciplinary Reviews: Computational Statistics*, vol. 2, no. 4, pp. 433–459, Jul. 2010.

[85] P. K. Artemiadis and K. J. Kyriakopoulos, "EMG-based control of a robot arm using low-dimensional embeddings," *IEEE Transactions on Robotics*, vol. 26, no. 2, pp. 393–398, Apr. 2010.

[86] C. Castellini and P. Van Der Smagt, "Evidence of muscle synergies during human grasping," *Biological Cybernetics*, vol. 107, no. 2, pp. 233–245, Apr. 2013.

[87] R. Ranganathan and C. Krishnan, "Extracting synergies in gait: using EMG variability to evaluate control strategies." *Journal of neurophysiology*, vol. 108, no. 5, pp. 1537–44, Sep. 2012.

[88] W. J. Kargo and D. A. Nitz, "Early skill learning is expressed through selection and tuning of cortically represented muscle synergies." *The Journal of Neuroscience*, vol. 23, no. 35, pp. 11 255–69, Dec. 2003.

[89] C. Choi and J. Kim, "Synergy matrices to estimate fluid wrist movements by surface electromyography," *Medical Engineering and Physics*, vol. 33, no. 8, pp. 916–923, Oct. 2011.

[90] D. J. Berger and A. D'Avella, "Effective force control by muscle synergies." *Frontiers in computational neuroscience*, vol. 8, no. April, p. 46, Jan. 2014.

[91] F. Artoni, V. Monaco, and S. Micera, "Selecting the best number of synergies in gait: Preliminary results on young and elderly people," in *IEEE International Conference on Rehabilitation Robotics*. IEEE, Jun. 2013, pp. 1–5.

[92] S. Ikeda and K. Toyama, "Independent component analysis for noisy data - MEG data analysis," *Neural Networks*, vol. 13, no. 10, pp. 1063–1074, 2000.

[93] J. T. Kent, "Information gain and a general measure of correlation," *Biometrika*, vol. 70, no. 1, pp. 163–173, Apr. 1983.

[94] S. Muceli and D. Farina, "Simultaneous and proportional estimation of hand kinematics from EMG during mirrored movements at multiple degrees-of-freedom," *IEEE Transactions on Neural Systems and Rehabilitation Engineering*, vol. 20, no. 3, pp. 371–378, May 2012.

[95] N. Jiang, K. B. Englehart, and P. a. Parker, "Extracting simultaneous and proportional neural control information for multiple-dof prostheses from the surface electromyographic signal," *IEEE Transactions on Biomedical Engineering*, vol. 56, no. 4, pp. 1070–1080, Apr. 2009.

[96] P. Comon, "Tensors : A brief introduction," *IEEE Signal Processing Magazine*, vol. 31, no. 3, pp. 44–53, May 2014.

[97] S. Liu and G. Trenkler, "Hadamard, Khatri-Rao, Kronecker and other matrix products," *Int. J. Inf. Syst. Sci*, vol. 4, no. 1, pp. 160–177, 2008.

[98] R. a. Harshman, "Foundations of the PARAFAC procedure: Models and conditions for an "explanatory" multimodal factor analysis," *UCLA Working Papers in Phonetics*, vol. 16, no. 10, pp. 1–84, 1970.

[99] F. L. Hitchcock, "The Expression of a Tensor or a Polyadic as a Sum of Products," *Journal of Mathematics and Physics*, vol. 6, no. 1-4, pp. 164–189, Apr. 1927.

[100] T. G. Kolda and B. W. Bader, "Tensor Decompositions and Applications," *SIAM Review*, vol. 51, no. 3, pp. 455–500, Aug. 2008.

[101] A. Smilde, R. Bro, and P. Geladi, *Multi-Way Analysis with Applications in the Chemical Sciences*. Chichester, UK: John Wiley & Sons, Ltd, Aug. 2004.

[102] A. Cichocki, R. Zdunek, A. H. Phan, and S.-I. Amari, *Nonnegative Matrix and Tensor Factorizations: Applications to Exploratory Multi-Way Data Analysis and Blind Source Separation*. John Wiley & Sons, 2009, vol. 1.

[103] R. Bro and H. A. L. Kiers, "A new efficient method for determining the number of components in PARAFAC models," *Journal of Chemometrics*, vol. 17, no. 5, pp. 274–286, Jun. 2003.

[104] L. R. Tucker, "Implications of factor analysis of three-way matrices for measurement of change," *Problems in measuring change*, vol. 15, pp. 122–137, 1963.

[105] M. Mørup, "Applications of tensor (multiway array) factorizations and decompositions in data mining," *Wiley Interdisciplinary Reviews: Data Mining and Knowledge Discovery*, vol. 1, no. 1, pp. 24–40, Jan. 2011.

[106] G. Zhou and A. Cichocki, "Fast and unique Tucker decompositions via multiway blind source separation," *Bulletin of the Polish Academy of Sciences: Technical Sciences*, vol. 60, no. 3, pp. 389–405, Jan. 2012.

[107] R. A. Harshman and M. E. Lundy, "PARAFAC: Parallel factor analysis," *Computational Statistics & Data Analysis*, vol. 18, no. 1, pp. 39–72, Aug. 1994.

[108] R. Sands and F. W. Young, "Component models for three-way data: An alternating least squares algorithm with optimal scaling features," *Psychometrika*, vol. 45, no. 1, pp. 39–67, Mar. 1980.

[109] P. Comon, X. Luciani, and A. L. F. de Almeida, "Tensor decompositions, alternating least squares and other tales," *Journal of Chemometrics*, vol. 23, no. 7-8, pp. 393–405, Jul. 2009.

[110] C. K. Battye, A. Nightingale, and J. Whillis, "The use of myo-electric currents in the operation of prostheses." *The Journal of bone and joint surgery. British volume*, vol. 37-B, no. 3, pp. 506–510, Aug. 1955.

[111] D. S. Dorcas and R. N. Scott, "A three-state myo-electric control," *Medical & Biological Engineering*, vol. 4, no. 4, pp. 367–370, Jul. 1966.

[112] P. A. Parker, J. Stuller, and R. Scott, "Signal processing for the multistate myoelectric channel," *Proceedings of the IEEE*, vol. 65, no. 5, pp. 662–674, May 1977.

[113] K. Englehart and B. S. Hudgins, "A robust, real-time control scheme for multifunction myoelectric control." *IEEE Transactions on Biomedical Engineering*, vol. 50, no. 7, pp. 848–854, 2003.

[114] F. Sebelius, L. Eriksson, C. Balkenius, and T. Laurell, "Myoelectric control of a computer animated hand: a new concept based on the combined use of a tree-structured artificial neural network and a data glove." *Journal of medical engineering & technology*, vol. 30, no. 1, pp. 2–10, Jul. 2006.

[115] L. J. Hargrove, E. J. Scheme, K. B. Englehart, and B. S. Hudgins, "Multiple binary classifications via linear discriminant analysis for improved controllability of a powered prosthesis," *IEEE Transactions on Neural Systems and Rehabilitation Engineering*, vol. 18, no. 1, pp. 49–57, Feb. 2010.

[116] A. J. Young, L. J. Hargrove, and T. a. Kuiken, "The effects of electrode size and orientation on the sensitivity of myoelectric pattern recognition systems to electrode shift," *IEEE Transactions on Biomedical Engineering*, vol. 58, no. 9, pp. 2537–2544, Sep. 2011.

[117] L. J. Hargrove, K. Englehart, and B. S. Hudgins, "A training strategy to reduce classification degradation due to electrode displacements in pattern recognition based myoelectric control," *Biomedical Signal Processing and Control*, vol. 3, no. 2, pp. 175–180, Apr. 2008.

[118] C. Lin, B. Wang, N. Jiang, and D. Farina, "Robust extraction of basis functions for simultaneous and proportional myoelectric control via sparse non-negative matrix factorization," *Journal of Neural Engineering*, vol. 15, no. 2, p. 026017, Apr. 2018.

[119] J. Ma, N. V. Thakor, and F. Matsuno, "Hand and Wrist Movement Control of Myoelectric Prosthesis Based on Synergy," *IEEE Transactions on Human-Machine Systems*, vol. 45, no. 1, pp. 74–83, Feb. 2015.

[120] A. Belouchrani, K. Abed-Meraim, J.-F. J. Cardoso, and E. Moulines, "A blind source separation technique using second-order statistics," *IEEE Transactions on Signal Processing*, vol. 45, no. 2, pp. 434–444, 1997.

[121] M. C. Tresch, V. C.-K. K. Cheung, and A. D'Avella, "Matrix factorization algorithms for the identification of muscle synergies: evaluation on simulated and experimental data sets." *Journal of neurophysiology*, vol. 95, no. 4, pp. 2199–2212, Apr. 2006.

[122] N. Lambert-Shirzad and H. F. M. Van der Loos, "On identifying kinematic and muscle synergies: a comparison of matrix factorization methods using experimental data from the healthy population," *Journal of Neurophysiology*, vol. 117, no. 1, pp. 290–302, 2017.

[123] A. Hyvärinen, "A family of fixed-point algorithms for independent component analysis," in *IEEE 5th Int. Conf. on Acoustics, Speech and Signal Processing (ICASSP)*, 1997, pp. 3917–3920.

[124] M. W. Berry, M. Browne, A. N. Langville, V. P. Pauca, and R. J. Plemmons, "Algorithms and applications for approximate nonnegative matrix factorization," *Computational Statistics and Data Analysis*, vol. 52, no. 1, pp. 155–173, Sep. 2007.

[125] A. Cichocki, S. Amari, K. Siwek, T. Tanaka, and A. H. Phan, *ICALAB Toolboxes*, http://www.bsp.brain.riken.jp/ICALAB, Brain science institute RIKEN Std.

[126] G. Torres-Oviedo and L. H. Ting, "Muscle synergies characterizing human postural responses." *Journal of neurophysiology*, vol. 98, no. 4, pp. 2144–56, Oct. 2007.

[127] N. Jiang, J. L. G. Vest-Nielsen, S. Muceli, and D. Farina, "EMG-based simultaneous and proportional estimation of wrist/hand kinematics in uni-lateral trans-radial amputees." *Journal of neuroengineering and rehabilitation*, vol. 9, no. 1, p. 42, Jan. 2012.

[128] E. A. Clancy, C. Martinez-Luna, M. Wartenberg, C. Dai, and T. R. Farrell, "Two degrees of freedom quasi-static EMG-force at the wrist using a minimum number of electrodes," *Journal of Electromyography and Kinesiology*, vol. 34, pp. 24–36, 2017.

[129] S. Muceli, N. Jiang, and D. Farina, "Extracting Signals Robust to Electrode Number and Shift for Online Simultaneous and Proportional Myoelectric Control by Factorization Algorithms," *IEEE Transactions on Neural Systems and Rehabilitation Engineering*, vol. 22, no. 3, pp. 623–633, May 2014.

[130] R. Prevete, F. Donnarumma, A. D'Avella, and G. Pezzulo, "Evidence for sparse synergies in grasping actions," *Scientific Reports*, vol. 8, no. 1, p. 616, Dec. 2018.

[131] F. Cong, Q.-H. Lin, L.-D. Kuang, X.-F. Gong, P. Astikainen, and T. Ristaniemi, "Tensor decomposition of EEG signals: A brief review," *Journal of Neuroscience Methods*, vol. 248, pp. 59–69, Jun. 2015.

[132] L. Spyrou, S. Kouchaki, and S. Sanei, "Multiview Classification and Dimensionality Reduction of Scalp and Intracranial EEG Data through Tensor Factorisation," pp. 1–12, Aug. 2016.

[133] J. Escudero, E. Acar, A. Fernández, and R. Bro, "Multiscale entropy analysis of resting-state magnetoencephalogram with tensor factorisations in Alzheimer's disease," *Brain Research Bulletin*, vol. 119, pp. 136–144, 2015.

[134] P. Xie and Y. Song, "Multi-domain feature extraction from surface EMG signals using nonnegative tensor factorization," in *2013 IEEE International Conference on Bioinformatics and Biomedicine*. IEEE, Dec. 2013, pp. 322–325.

[135] I. Delis, S. Panzeri, T. Pozzo, and B. Berret, "A unifying model of concurrent spatial and temporal modularity in muscle activity," *Journal of Neurophysiology*, vol. 111, no. 3, pp. 675–693, 2014.

[136] L. R. Tucker, "Some mathematical notes on three-mode factor analysis," *Psychometrika*, vol. 31, no. 3, pp. 279–311, Sep. 1966.

[137] I. Delis, S. Panzeri, T. Pozzo, and B. Berret, "Task-discriminative space-by-time factorization of muscle activity," *Frontiers in Human Neuroscience*, vol. 9, p. 399, Jul. 2015.

[138] O. Debals and L. De Lathauwer, "Stochastic and Deterministic Tensorization for Blind Signal Separation," in *Latent Variable Analysis and Signal Separation*. Springer, Cham, 2015, pp. 3–13.

[139] C. G. Kukulka and H. P. Clamann, "Comparison of the recruitment and discharge properties of motor units in human brachial biceps and adductor pollicis during isometric contractions," *Brain Research*, vol. 219, no. 1, pp. 45–55, 1981.

[140] D. Iatsenko, P. V. E. McClintock, and A. Stefanovska, "Linear and synchrosqueezed time-frequency representations revisited: Overview, standards of use, resolution, reconstruction, concentration, and algorithms," *Digital Signal Processing: A Review Journal*, vol. 42, pp. 1–26, 2015.

[141] A. Cichocki, Y. Washizawa, T. Rutkowski, H. Bakardjian, A. H. Phan, S. Choi, H. Lee, Q. Zhao, L. Zhang, and Y. Li, "Noninvasive BCIs: Multiway signal-processing array decompositions," *Computer*, vol. 41, no. 10, pp. 34–42, Oct. 2008.

[142] A. de Rugy, G. E. Loeb, and T. J. Carroll, "Are muscle synergies useful for neural control?" *Frontiers in computational neuroscience*, vol. 7, no. March, p. 19, Jan. 2013.

[143] F. Nie, S. Xiang, Y. Song, and C. Zhang, "Extracting the optimal dimensionality for local tensor discriminant analysis," *Pattern Recognition*, vol. 42, no. 1, pp. 105–114, 2009.

[144] S. A. Chvatal and L. H. Ting, "Common muscle synergies for balance and walking." *Frontiers in computational neuroscience*, vol. 7, no. May, p. 48, Jan. 2013.

[145] K. Devarajan, "Nonnegative matrix factorization: an analytical and interpretive tool in computational biology." *PLoS computational biology*, vol. 4, no. 7, p. e1000029, Jan. 2008.

[146] N. Jiang, T. Lorrain, and D. Farina, "A state-based, proportional myoelectric control method: online validation and comparison with the clinical state-of-the-art." *Journal of neuroengineering and rehabilitation*, vol. 11, no. 1, p. 110, Jul. 2014.

[147] E. Biddiss, D. Beaton, and T. Chau, "Consumer design priorities for upper limb prosthetics," *Disability and rehabilitation. Assistive technology*, vol. 2, no. 6, pp. 346–357, Jul. 2007.

[148] P. Geethanjali, "Myoelectric control of prosthetic hands: state-of-the-art review." *Medical devices (Auckland, N.Z.)*, vol. 9, pp. 247–55, 2016.

[149] N. Jiang, S. Dosen, K.-r. Muller, and D. Farina, "Myoelectric Control of Artificial Limbs: Is There a Need to Change Focus? [In the Spotlight]," *IEEE Signal Processing Magazine*, vol. 29, no. 5, pp. 150–152, 2012.

[150] D. D. Lee and H. S. Seung, "Algorithms for Non-negative Matrix Factorization," in *Advances in Neural Information Processing Systems*, 2001, pp. 556–562.

[151] H. Kim and H. Park, "Sparse non-negative matrix factorizations via alternating non-negativity-constrained least squares for microarray data analysis," *Bioinformatics*, vol. 23, no. 12, pp. 1495–1502, Jun. 2007.

[152] A. Onken, J. K. Liu, P. P. R. Karunasekara, I. Delis, T. Gollisch, and S. Panzeri, "Using Matrix and Tensor Factorizations for the Single-Trial Analysis of Population Spike Trains," *PLoS Computational Biology*, vol. 12, no. 11, p. e1005189, Nov. 2016.

[153] E. Kinney-Lang, L. Spyrou, A. Ebied, R. F. Chin, and J. Escudero, "Tensor-driven extraction of developmental features from varying paediatric EEG datasets," *Journal of Neural Engineering*, vol. 15, no. 4, p. 046024, Aug. 2018.

[154] Q. Zhao, C. F. Caiafa, D. P. Mandic, Z. C. Chao, Y. Nagasaka, N. Fujii, L. Zhang, and A. Cichocki, "Higher order partial least squares (HOPLS): A generalized multilinear regression method," *IEEE Transactions on Pattern Analysis and Machine Intelligence*, vol. 35, no. 7, pp. 1660–1673, Jul. 2013.

[155] S. Aoi and T. Funato, "Neuromusculoskeletal models based on the muscle synergy hypothesis for the investigation of adaptive motor control in locomotion via sensory-motor coordination," *Neuroscience Research*, vol. 104, pp. 88–95, Mar. 2016.

[156] M. Ison and P. Artemiadis, "The role of muscle synergies in myoelectric control: trends and challenges for simultaneous multifunction control." *Journal of neural engineering*, vol. 11, no. 5, p. 051001, Oct. 2014.

[157] A. Santuz, A. Ekizos, L. Janshen, F. Mersmann, S. Bohm, V. Baltzopoulos, and A. Arampatzis, "Modular control of human movement during running: An open access data set," *Frontiers in Physiology*, vol. 9, no. Oct., p. 1509, 2018.

[158] P. Bonato, S. H. Roy, M. Knaflitz, and C. J. De Luca, "Time frequency parameters of the surface myoelectric signal for assessing muscle fatigue during cyclic dynamic contractions," *IEEE Transactions on Biomedical Engineering*, vol. 48, no. 7, pp. 745–753, Jul. 2001.

[159] A. Ebied, "Biceps Brachii Muscle Fatigue Assessment Through EMG Median Frequency Analysis," in *Proceedings of the 9th ICEENG Conference*, vol. 1, 2014, pp. EE1–EE12.